Journal of Medicinal Chemistry

Perspective

pubs.acs.org/jmc

Recent Advances in Structure-Based Drug Design Targeting Class A G Protein-Coupled Receptors Utilizing Crystal Structures and Computational Simulations

Yoonji Lee,[†] Shaherin Basith,[†] and Sun Choi*

National Leading Research Laboratory (NLRL) of Molecular Modeling & Drug Design, College of Pharmacy and Graduate School of Pharmaceutical Sciences, Ewha Womans University, Seoul 03760, Republic of Korea

ABSTRACT: G protein-coupled receptors (GPCRs) represent the largest and most physiologically important integral membrane protein family, and these receptors respond to a wide variety of physiological and environmental stimuli. GPCRs are among the most critical therapeutic targets for numerous human diseases, and approximately one-third of the currently marketed drugs target this receptor family. The recent breakthroughs in GPCR structural biology have significantly contributed to our understanding of GPCR function, ligand binding, and pharmacological action as well as to the design of new drugs. This perspective highlights the latest advances in GPCR structures with a focus on the receptor−ligand interactions of each receptor family in class A nonrhodopsin GPCRs as well as the structural features for their activation, biased signaling, and allosteric mechanisms. The current state-of-the-art methodologies of structure-based drug design (SBDD) approaches in the GPCR research field are also discussed.

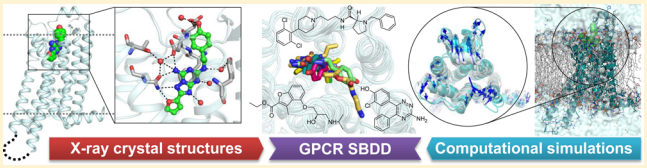

1. INTRODUCTION

G protein-coupled receptors (GPCRs), also known as seven transmembrane (7TM) receptors, represent the largest and most physiologically important integral membrane protein family. GPCRs are activated by a wide variety of physiological and environmental stimuli including subatomic particles (photons), ions, small organic molecules, and macromolecules (peptides or proteins). The GPCR protein family is composed of approximately 800 genes in the human genome that regulate signaling pathways involved in several physiological roles, such as behavior, cognition, immune response, mood, olfaction, blood pressure regulation, and taste.[1] Many GPCRs are important therapeutic targets for numerous human diseases, including cancer, cardiac disorders, central nervous system (CNS) disorders, inflammatory disorders, metabolic imbalances, and monogenic diseases.[2] Approximately one-third of the currently marketed drugs target this receptor family by turning them "on" or "off".

Evolutionary studies suggest that the occurrence of GPCRs and G protein signaling dates back approximately 1.2 billion years, prior to fungi, plants, and animals, emerging from a common ancestor.[3] On the basis of sequence and functional similarities, GPCRs are categorized into six classes: Class A (rhodopsin-like receptors), Class B (the secretin family), Class C (metabotropic glutamate receptors), Class D (fungal mating pheromone receptors), Class E (cyclic adenosine monophosphate (cAMP) receptors), and Class F (Frizzled and Smoothened receptors).[4,5] The class A rhodopsin-like receptors can be further subdivided into "rhodopsin GPCRs" and "nonrhodopsin GPCRs".[6] On the basis of the roles they play in diseases and their relative ease of accessibility, class A GPCRs are well characterized within the drug market and development pipeline.

All class A GPCRs share a common structural organization with 7TM helices (TM1−TM7) that are connected by three extracellular loops (ECL1−3) and three intracellular loops (ICL1−3) (Figure 1). The 7TM bundle can be divided into two modules, including extracellular (EC) and intracellular (IC) modules. The N-terminus (located on the extracellular side) and the ECLs are responsible for the recognition of a wide variety of ligands and the modulation of ligand entry. ECLs often contain disulfide bridges that are essential for maintaining loop stability and for preventing GPCR promiscuity.[7] The 7TM bundle forms the main structural core that undergoes conformational changes upon ligand binding, and it transduces signals from the extracellular to the intracellular region. The C-terminus and the ICLs interact with G proteins, arrestins, GPCR kinases (GRKs), and other downstream signaling effectors, which are essential for signal transduction and other receptor modulatory functions. Due to the limited types of downstream signaling effectors, the IC region is relatively conserved. The C-terminal portion generally contains a 3−4 turn α-helix, commonly known as helix 8, which is positioned parallel to the membrane. This helix is characterized by the presence of a common [F(RK)xx-(FL)xxx] amphiphilic motif.[8] Despite sharing a common 7TM-architecture, GPCRs represent a captivating model of fine-tuned recognition modules. This fact is due to the recognition of a wide range of ligands with strikingly different physicochemical and structural properties, thus showing a remarkable convergence in the signaling and regulatory processes.

Received: September 30, 2016
Published: June 28, 2017

DOI: 10.1021/acs.jmedchem.6b01453
J. Med. Chem. 2018, 61, 1−46

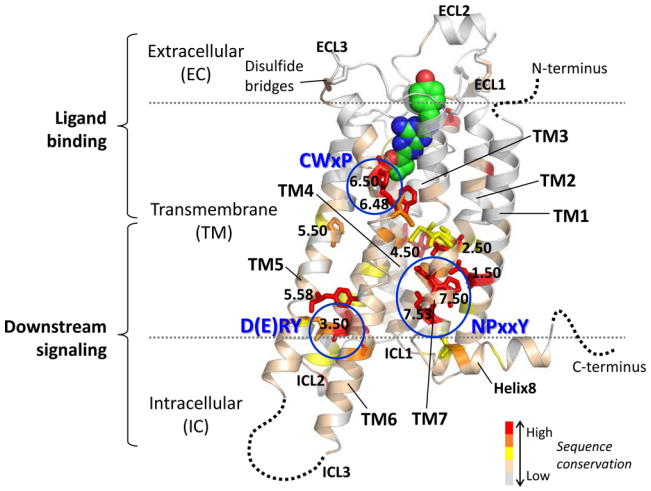

Figure 1. General architecture and structural features of GPCRs. All GPCRs represent a common seven transmembrane (7TM) α-helical bundle characteristic, which are connected by three extracellular loops (ECL1−3) and three intracellular loops (ICL1−3). The heptahelical bundle (TM1−7) and key structural features are shown on an example of the A_{2A}AR crystal structure (PDB ID: 4EIY) bound to ligand **28** (depicted with spheres with their carbons in green). The structure is displayed and colored by the sequence conservation level of class A GPCR family. In addition to the ECLs, the EC module responsible for ligand binding consists of an N-terminal region that can range from a short unstructured region (observed in class A GPCRs) to long, globular structured domains (observed in classes B, C, and F). Besides ICLs, the IC module responsible for interacting with downstream effectors consists of an intrinsically disordered C-terminal tail that is not readily accessible for crystallographic studies. The C-terminal region of most GPCRs also comprises an amphipathic helix 8 and carries a palmitoylation site (not shown) that is responsible for anchoring helix 8 to the membrane. The TM module (considered as the highly conserved component of GPCRs) shows characteristic hydrophobic patterns and several functionally potent signature sequence motifs, including the D(E)RY motif in helix 3, the CWxP motif in helix 6, and the NPxxY motif in helix 7, which are highlighted in blue circles. The important microswitch residues (labeled according to Ballesteros−Weinstein numbering scheme) and disulfide bridges that connect the ECLs are represented as sticks.

GPCR signaling is initiated with the binding of an agonist to the receptor. Ligand-induced GPCR signaling is based on conformational changes that occur in the 7TM structure, which alter the cytoplasmic surface of the receptor to allow the binding of signaling of effectors. Upon agonist binding, GPCRs couple with specific G protein families, including $G\alpha_s$, $G\alpha_{i/o}$, $G\alpha_{q/11}$, and others followed by the generation of second messengers and the initiation of downstream signaling events. Receptor coupling via $G\alpha_s$ leads to the stimulation of adenylyl cyclase followed by an increase in the production of cAMP. Conversely, coupling to $G\alpha_{i/o}$ inhibits adenylyl cyclase but activates mitogen-activated protein kinase (MAPK). Coupling through $G\alpha_{q/11}$ activates phospholipase C (PLC) enzymes, which hydrolyze membrane phospholipids to release second messengers, such as inositol 1,4,5-triphosphate (IP_3) and diacylglycerols (DAGs). These releases further lead to an increase in the intracellular Ca^{2+} levels and the stimulation of protein kinase C (PKC) and protein kinase D1 (PKD1). $G\alpha_{q/11}$ activation can lead to increased phosphoinositide 3-kinase (PI3K) and Akt stimulations.[9] However, GRKs regulate the activity of GPCRs, which trigger the recruitment of multifunctional proteins, namely β-arrestins, leading to the desensitization of the phosphorylated receptor via steric hindrance. Simultaneously, β-arrestins can also facilitate clathrin-mediated endocytosis, which promotes GPCR internalization and initiates G protein-independent downstream signaling events, thus mediating distinct biological effects.

The latest revolution in the investigation of GPCRs using advanced structural and computational methods has overturned its research paradigm. Recent developments in the area of protein engineering and the crystallography of membrane proteins, such as the formation of receptor complexes with antibody fragments, the engineering of chimera proteins using fusion proteins, and thermostabilization of the receptor via systematic scanning mutagenesis, are considered major breakthroughs in GPCR research, all of which assisted in the determination of numerous crystal structures. However, the limitations involved in the structural determination of GPCRs have been overcome by using these sophisticated protocols. Additionally, the abundance of ligand-bound GPCR structures provides invaluable insights into the structure, function, and pharmacology of the receptors, which enables the application of structure-based drug design (SBDD) approaches to aid in the discovery of potent candidates with improved pharmacological profiles. In addition to the simple two-state receptor models ("on" (activation) and "off" (inactivation)), the unveiling of new types of ligand−receptor−effector relationships, such as inverse agonism, positive and negative allosterism, multimeric receptor pharmacology, and ligand-biased signaling, have broadened our knowledge of GPCR biology and introduced novel mechanistic methods for manipulating its therapeutic potential.[10]

In this perspective, we will discuss the recent advances in SBDD approaches targeting GPCRs, especially studies involving protein crystallography and computational simulations. To narrow the scope, which is too broad to cover well, the discussion is focused on class A nonrhodopsin GPCRs including those receptors activated by biogenic amines, catecholamines, glycoproteins, lipids, nucleotides, and peptides.[10] First, the status of the structural studies of class A nonrhodopsin GPCRs determined via the X-ray crystallography technique is summarized, highlighting key receptor−ligand interactions and orthosteric binding sites for the design of novel molecules. Sodium (Na^+) allosteric modulation, biased signaling, and the importance of highly conserved structural motifs and the TM-helical core in GPCR signaling are also discussed. Second, the latest advances in the working principles of SBDD in relation to GPCR studies are reviewed. Furthermore, the structural and mechanistic principles of the GPCR signaling complexes supported by molecular dynamics or multiscale simulation studies are presented. All of the residues mentioned in this perspective are numbered according to the Ballesteros−Weinstein numbering scheme,[11] which enumerates GPCR TM residues in the X.YY format in superscript where X represents the helix number and YY represents the residue position related to the most conserved residue in the helix (note that the most conserved residue in each helix is marked as X.50, see Figure 1).

2. PROGRESS IN STRUCTURAL STUDIES OF CLASS A NONRHODOPSIN GPCRS

2.1. Methodological Advances in the Visualization of GPCRs and Signaling Complexes. Due to the limitations in the expression and crystallization of GPCRs, this family has remained the largest "terra incognita" of structural biology for decades, delaying the molecular interpretation of biophysical and biochemical findings as well as rational drug discovery applications.[12] After the structural elucidation of bovine

DOI: 10.1021/acs.jmedchem.6b01453
J. Med. Chem. 2018, 61, 1−46

Table 1. List of Available X-ray Crystal Structures of G Protein-Coupled Receptors (GPCRs) Released Until December of 2016

class type, classification	receptor type	species	ligand	ligand type	released year	resolution (Å)	PDB ID
A, rhodopsin	rho	bovine	11-*cis*-retinal	inverse agonist	2000	2.8	1F88
	rho	bovine	11-*cis*-retinal	inverse agonist	2001	2.8	1HZX
	rho	bovine	11-*cis*-retinal	inverse agonist	2002	2.6	1L9H
	rho	bovine	11-*cis*-retinal	inverse agonist	2003	2.65	1GZM
	rho	bovine	11-*cis*-retinal	inverse agonist	2004	2.2	1U19
	rho	bovine	all-*trans*-retinal	agonist	2006	2.8	2HPY
	rho	bovine	11-*cis*-retinal	inverse agonist	2006	2.6	2G87
	rho	bovine	11-*cis*-retinal	inverse agonist	2006	3.8	2I35
	rho	bovine	11-*cis*-retinal	inverse agonist	2006	4.1	2I36
	rho	bovine	all-*trans*-retinylidene	agonist	2006	4.15	2I37
	rho	bovine	11-*cis*-retinal	inverse agonist	2007	3.4	2J4Y
	rho	bovine	9-*cis*-retinal	inverse agonist	2007	2.95	2PED
	rho[a]	bovine	N/A	N/A	2008	2.9	3CAP
	rho	bovine	11-*cis*-retinal	inverse agonist	2008	2.65	3C9L
	rho	bovine	11-*cis*-retinal	inverse agonist	2008	3.4	3C9M
	rho[a]	bovine	N/A	N/A	2008	3.2	3DQB
	rho	squid	11-*cis*-retinal	inverse agonist	2008	3.7	2ZIY
	rho	squid	11-*cis*-retinal	inverse agonist	2008	2.5	2Z73
	rho	bovine	all-*trans*-retinal	agonist	2011	3	3PXO
	rho	bovine	all-*trans*-retinal	agonist	2011	2.85	3PQR
	rho	bovine	all-*trans*-retinal	agonist	2011	3	2X72
	rho	squid	all-*trans*-retinal	agonist	2011	2.8	3AYM
	rho	squid	9-*cis*-retinal	inverse agonist	2011	2.7	3AYN
	rho	bovine	11-*cis*-retinal	inverse agonist	2011	2.6	3OAX
	rho	bovine	All-*trans*-retinal	agonist	2012	3.3	4A4M
	rho	bovine	11-*cis*-retinal	inverse agonist	2013	2.9	4BEY
	rho	bovine	11-*cis*-retinal	inverse agonist	2013	3.3	4BEZ
	rho[a]	bovine	N/A	N/A	2013	2.65	4J4Q
	rho[a]	bovine	N/A	N/A	2014	2.75	4PXF
	rho	squid	all-*trans*-retinal	agonist	2015	2.8	4WW3
	rho	bovine	nonyl β-D-glucopyranoside	inverse agonist	2015	2.29	4X1H
	rho[a]	human	N/A	N/A	2015	3.3	4ZWJ
	rho[a]	human	N/A	N/A	2016	7.7	5DGY
	rho	bovine	all-*trans*-retinal	agonist	2016	2.81	5EN0
	rho	bovine	all-*trans*-retinal	agonist	2016	2.3	5DYS
A, nonrhodopsin (aminergic receptors)	β_1AR	turkey	**11**	antagonist	2008	2.7	2VT4
	β_1AR	turkey	**1**	inverse agonist	2011	3	2YCW
	β_1AR	turkey	**11**	antagonist	2011	3.25	2YCX
	β_1AR	turkey	**12**	antagonist	2011	3.65	2YCZ
	β_1AR	turkey	**11**	antagonist	2011	3.15	2YCY
	β_1AR	turkey	**9** (dobutamine)	partial agonist	2011	2.5	2Y00
	β_1AR	turkey	**9**	partial agonist	2011	2.6	2Y01
	β_1AR	turkey	salbutamol	partial agonist	2011	3.05	2Y04
	β_1AR	turkey	carmoterol	full agonist	2011	2.6	2Y02
	β_1AR	turkey	(*R*)-isoprenaline	full agonist	2011	2.85	2Y03
	β_1AR	turkey	**16**	biased agonist	2012	3.2	4AMI
	β_1AR	turkey	**17**	biased agonist	2012	2.3	4AMJ
	β_1AR[a]	turkey	N/A	N/A	2013	3.5	4GPO
	β_1AR	turkey	**13**	antagonist	2013	2.7	3ZPR
	β_1AR	turkey	**14**	antagonist	2013	2.8	3ZPQ
	β_1AR	turkey	**11**	antagonist	2014	2.1	4BVN
	β_1AR	turkey	**11**	antagonist	2015	3.35	5F8U
	β_1AR	turkey	**15**	inverse agonist	2015	2.4	5A8E
	β_2AR	human	**1**	inverse agonist	2007	2.4	2RH1
	β_2AR	human	**1**[b]	inverse agonist	2007	3.4	2R4R
	β_2AR	human	**1**[b]	inverse agonist	2007	3.4	2R4S
	β_2AR	human	**2**	inverse agonist	2008	2.8	3D4S
	β_2AR	human	**1**[b]	inverse agonist	2010	3.4	3KJ6
	β_2AR	human	**3**	inverse agonist	2010	2.84	3NY8
	β_2AR	human	**4**	inverse agonist	2010	2.84	3NY9

DOI: 10.1021/acs.jmedchem.6b01453
J. Med. Chem. 2018, 61, 1−46

Table 1. continued

class type, classification	receptor type	species	ligand	ligand type	released year	resolution (Å)	PDB ID
	β_2AR	human	**5**	antagonist	2010	3.16	3NYA
	β_2AR[c]	human	**8**	agonist	2011	3.5	3P0G
	β_2AR[d]	human	**8**	agonist	2011	3.2	3SN6
	β_2AR	human	**6**	covalent agonist	2011	3.5	3PDS
	β_2AR	human	**1**	inverse agonist	2012	3.99	4GBR
	β_2AR[c]	human	**8**	agonist	2013	2.79	4LDE
	β_2AR[c]	human	**10**	agonist	2013	3.1	4LDL
	β_2AR[c]	human	adrenaline	agonist	2013	3.2	4LDO
	β_2AR[c]	human	**7**	covalent agonist	2014	3.3	4QKX
	β_2AR	human	**1**	inverse agonist	2016	3.2	5D6L
	β_2AR	human	**1**	inverse agonist	2016	2.48	5D5A
	β_2AR	human	**1**	inverse agonist	2016	3.8	5D5B
	β_2AR	human	**1**	inverse agonist	2016	3.2	5JQH
	D_3R	human	**18**	antagonist	2010	2.89	3PBL
	H_1R	human	**19**	antagonist	2011	3.1	3RZE
	M_1R	human	**21**	inverse agonist	2016	2.7	5CXV
	M_2R	human	**20**	inverse agonist	2012	3	3UON
	M_2R[c]	human	**22**	agonist	2013	3.5	4MQS
	M_2R[c]	human	**22, 23**	agonist, allosteric	2013	3.7	4MQT
	M_3R	rat	**21**	inverse agonist	2012	3.4	4DAJ
	M_3R	rat	**21**	inverse agonist	2014	3.57	4U14
	M_3R	rat	**21**	inverse agonist	2014	2.8	4U15
	M_3R	rat	*N*-methylscopolamine	antagonist	2014	3.7	4U16
	M_4R	human	**21**	inverse agonist	2016	2.6	5DSG
	5-HT_{1B}	human	**25**	agonist	2013	2.8	4IAQ
	5-HT_{1B}	human	**24**	agonist	2013	2.7	4IAR
	5-HT_{2B}	human	**24**	agonist	2013	2.7	4IB4
	5-HT_{2B}	human	**24**	agonist	2013	2.8	4NC3
A, nonrhodopsin (nucleotide-like receptors)	A_{2A}AR	human	**28**	inverse agonist	2008	2.6	3EML
	A_{2A}AR	human	**28**	inverse agonist	2011	3.3	3PWH
	A_{2A}AR	human	**27**	neutral antagonist	2011	3.31	3REY
	A_{2A}AR	human	**26**	neutral antagonist	2011	3.6	3RFM
	A_{2A}AR	human	**36**	full agonist	2011	2.71	3QAK
	A_{2A}AR	human	adenosine	full agonist	2011	3	2YDO
	A_{2A}AR	human	**35**	full agonist	2011	2.6	2YDV
	A_{2A}AR	human	**28**	inverse agonist	2012	2.7	3VG9
	A_{2A}AR	human	**28**	inverse agonist	2012	3.1	3VGA
	A_{2A}AR	human	**33**	antagonist	2012	3.34	3UZC
	A_{2A}AR	human	**34**	antagonist	2012	3.27	3UZA
	A_{2A}AR	human	**28**	inverse agonist	2012	1.8	4EIY
	A_{2A}AR	human	**37**	agonist	2015	2.6	4UG2
	A_{2A}AR	human	**37**	agonist	2015	2.6	4UHR
	A_{2A}AR	human	**28**	inverse agonist	2016	2.5	5K2A
	A_{2A}AR	human	**28**	inverse agonist	2016	2.5	5K2B
	A_{2A}AR	human	**28**	inverse agonist	2016	1.9	5K2C
	A_{2A}AR	human	**28**	inverse agonist	2016	1.9	5K2D
	A_{2A}AR	human	**28**	inverse agonist	2016	1.7	5IU4
	A_{2A}AR	human	**29**	antagonist	2016	2.2	5IUA
	A_{2A}AR	human	**32**	antagonist	2016	2.1	5IUB
	A_{2A}AR	human	**30**	antagonist	2016	1.9	5IU7
	A_{2A}AR	human	**31**	antagonist	2016	2.0	5IU8
	A_{2A}AR[d]	human	**35**	full agonist	2016	3.4	5G53
	$P2Y_1$	human	**42**	allosteric antagonist	2015	2.2	4XNV
	$P2Y_1$	human	**41**	antagonist	2015	2.7	4XNW
	$P2Y_{12}$	human	**40**	antagonist	2014	2.62	4NTJ
	$P2Y_{12}$	human	**38**	agonist	2014	2.5	4PXZ
	$P2Y_{12}$	human	**39**	agonist	2014	3.1	4PY0
A, nonrhodopsin (peptide-like receptors)	CXCR4	human	CVX15 (cyclic peptide)	antagonist	2010	2.9	3OE0
	CXCR4	human	**43**	antagonist	2010	2.5	3ODU
	CXCR4	human	**43**	antagonist	2010	3.2	3OE6

DOI: 10.1021/acs.jmedchem.6b01453
J. Med. Chem. 2018, 61, 1−46

Table 1. continued

class type, classification	receptor type	species	ligand	ligand type	released year	resolution (Å)	PDB ID
	CXCR4	human	**43**	antagonist	2010	3.1	3OE8
	CXCR4	human	**43**	antagonist	2010	3.1	3OE9
	CXCR4	human	vMIP-II	antagonist	2015	3.1	4RWS
	CCR5	human	**44**	inverse agonist	2013	2.71	4MBS
	δ-OR	mouse	**49**	antagonist	2012	3.4	4EJ4
	δ-OR	human	**49**	antagonist	2013	1.8	4N6H
	δ-OR	human	DIPP-NH_2 (bifunctional tetrapeptide)	antagonist	2015	3.28	4RWA
	δ-OR	human	DIPP-NH_2 (bifunctional tetrapeptide)	antagonist	2015	2.7	4RWD
	κ-OR	human	**50**	antagonist	2012	2.9	4DJH
	μ-OR	mouse	**47**	covalent antagonist	2012	2.8	4DKL
	μ-OR	mouse	**48**	agonist	2015	2.1	5C1M
	NOP	human	**51**	antagonist	2012	3.01	4EA3
	NOP	human	**53**	antagonist	2015	3.0	5DHH
	NOP	human	**52**	antagonist	2015	3.0	5DHG
	NTSR1	rat	NTS_{8-13}	agonist	2012	2.8	4GRV
	NTSR1	rat	NTS_{8-13}	agonist	2014	3.0	3ZEV
	NTSR1	rat	NTS_{8-13}	agonist	2014	2.75	4BUO
	NTSR1	rat	NTS_{8-13}	agonist	2014	3.1	4BV0
	NTSR1	rat	NTS_{8-13}	agonist	2014	3.57	4BWB
	NTSR1	rat	NTS_{8-13}	agonist	2015	2.6	4XES
	NTSR1	rat	NTS_{8-13}	agonist	2015	2.9	4XEE
	PAR1	human	**54**	antagonist	2012	2.2	3VW7
	AT_1R	human	**55**	antagonist	2015	2.9	4YAY
	AT_1R	human	olmesartan	inverse agonist	2015	2.8	4ZUD
	OX_1R	human	**56**	antagonist	2016	2.75	4ZJ8
	OX_1R	human	**57**	antagonist	2016	2.83	4ZJC
	OX_2R	human	**56**	antagonist	2015	2.5	4S0V
	ET_B	human	endothelin-1	agonist	2016	2.8	5GLH
	ET_B[a]	human	N/A	N/A	2016	2.5	5GLI
A, nonrhodopsin (lipid-like receptors)	$S1P_1$	human	**58**	antagonist	2012	2.8	3V2Y
	$S1P_1$	human	**58**	antagonist	2012	3.35	3V2W
	FFAR1	human	**62**	partial agonist	2014	2.33	4PHU
	LPA_1	human	**59**	antagonist	2015	3.0	4Z34
	LPA_1	human	**60**	antagonist	2015	2.9	4Z35
	LPA_1	human	**61**	antagonist	2015	2.9	4Z36
	CB_1	human	**63**	antagonist	2016	2.8	5TGZ
A, nonrhodopsin (unclassified)	US28[e]	hCMV	CX3CL1	inverse agonist	2015	2.89	4XT1
	US28[e]	hCMV	CX3CL1	inverse agonist	2015	3.8	4XT3
B, secretin-like receptors	CRF_1	human	CP-376395	antagonist	2013	2.98	4K5Y
	CRF_1	human	CP-376395	antagonist	2016	3.18	4Z9G
	GCGR[a]	human	N/A	N/A	2013	3.3	4L6R
	GCGR	human	MK-0893	antagonist	2016	2.5	5EE7
C, metabotropic glutamate receptors	$mGlu_1R$	human	FITM	negative allosteric modulator	2014	2.8	4OR2
	$mGlu_5R$	human	mavoglurant	negative allosteric modulator	2014	2.6	4OO9
	$mGlu_5R$	human	HTL14242	negative allosteric modulator	2015	2.6	5CGD
	$mGlu_5R$	human	3-chloro-4-fluoro-5-[6-(1*H*-pyrazol-1-yl) pyrimidin-4-yl]benzonitrile	negative allosteric modulator	2015	3.1	5CGC
F, frizzled and smoothened receptors	SMO	human	LY2940680	antagonist	2013	2.45	4JKV
	SMO	human	SANT-1	antagonist	2014	2.8	4N4W
	SMO	human	cyclopamine	antagonist	2014	3.2	4O9R
	SMO	human	SAG1.5	agonist	2014	2.6	4QIN
	SMO	human	Anta XV	antagonist	2014	2.61	4QIM
	SMO	human	vismodegib	antagonist	2016	3.3	5L7I
	SMO	human	cholesterol	agonist	2016	3.2	5L7D

[a]Ligand-free basal state of the receptor. [b]Electron density of the bound ligand was not resolved. [c]Active-state conformation stabilized by a G protein mimicking nanobody. [d]Fully active structure complexed with a G protein. [e]Unique GPCR encoded by human cytomegalovirus (hCMV).

DOI: 10.1021/acs.jmedchem.6b01453
J. Med. Chem. 2018, 61, 1−46

rhodopsin, an additional seven years of extensive research and technological developments were required to solve the structure of the first human GPCR with a diffusible ligand, namely, β_2-adrenergic receptor (β_2AR).[13] Crystallizing membrane proteins such as GPCRs presents numerous challenges, including the minimal availability of a polar surface area of receptors for crystal contacts, difficulties in obtaining substantial amounts of functional protein, low expression levels of recombinant receptors in hosts, and the inherent conformational flexibility of receptors that is essential for their functional diversity.[5] However, through technological innovations over the last ten years, considerable progress has been made in the visualization of GPCRs and their signaling complexes at the structural level. The advances in GPCR biochemistry and X-ray crystallography, such as protein engineering, lipidic cubic phase (LCP) crystallization methods, new detergents, and microfocus synchrotron beamlines, have tremendously increased the success rate of obtaining GPCR structures.[5]

GPCRs exhibit a high degree of structural and conformational flexibility that is essential for receptor coupling to different effectors and diverse signaling mechanisms. Additionally, these receptors are embedded in lipid membranes in such a manner that their exposed hydrophilic surface area, which is important for making crystal lattice contacts, is relatively small. This inherent structural flexibility and the lack of a polar surface area are considered as major obstacles in GPCR crystallization.[14] If the highly flexible loop regions are simply truncated, the polar surface contacts could also be decreased. Therefore, small, stable, and well-crystallizable protein domains have been added to replace these flexible regions and improve the crystal contacts. T4 lysozyme (T4L) and b_{562}RIL (BRIL) are predominantly used as fusion proteins. Rubredoxin and the catalytic domain of *P. abyssi* glycogen synthase have also been used.[14] Initial attempts at designing fusion proteins were focused on the replacement of the highly flexible ICL3 region, but currently, the N-terminus and ICL2 regions are also considered to be amenable to the insertion of these fusions. In addition to the fusion strategy, introduction of antibody fragments or nanobodies (single-domain antibodies) have also been utilized during GPCR crystallization to improve receptor conformational stability and increase their polar surface area. By using this approach, it became possible to develop antibodies or nanobodies that preferentially bind to distinct GPCR states and capture such active-like or fully activated receptor conformations.[14] Another technique to reduce the conformational flexibility of GPCRs is thermostabilization, which is referred to as the StaR (stabilized receptor) approach.[15] This method is used not only for increasing the thermostability of the receptor in a particular conformation but also for enhancing protein expression levels.[14] The StaR approach can also be combined with the two aforementioned techniques, i.e., fusion protein and antibodies/nanobodies, which is currently trending for solving new structures.

Since GPCRs are integral membrane proteins, it is essential to extract them from the lipid membrane environment before purification. Therefore, it is necessary to select a suitable mild detergent that can efficiently extract the protein from the membrane and maintain its stability. The mixed micelle system of *N*-dodecyl-β-D-maltoside (DDM) and cholesteryl hemisuccinate (CHS) are the most frequently used combined detergent to extract GPCRs from the membrane.[14] The nature of the bound ligand also plays a crucial role in trapping a receptor at a specific conformation and maintaining its functional stability. In general, GPCRs tend to exist in multiple conformations in the ligand-free state, thus showing a higher degree of heterogeneity that reduces the likelihood of successful crystallization. On the other hand, ligand binding drives GPCRs to adopt one major population, thereby promoting nucleation, which is the initial step in protein crystallization, and proper crystal packing.[5] To date, most of the crystallized GPCR structures are in complex with a high-affinity ligand. In particular, covalent ligands often have been used to assist in the crystallization of agonist-bound active conformations, which are less stable, as they cannot diffuse away from the protein sample. However, StaRs do not require such potent ligands because the protein conformations can be trapped by mutagenesis.

Membrane proteins can be crystallized using either vapor diffusion, which is the most commonly used crystallization technique for proteins, or lipid-based crystallization approaches such as bicelles and lipidic cubic phase (LCP). Compared to the vapor diffusion method in which the large size of the detergent micelle could occlude the relatively small hydrophilic surface area of GPCRs and prohibit the formation of crystal lattice contacts, the lipid-based methods can provide crystals of ligand−GPCR complexes in a more amenable, well-crystallizable conformation.[14] In particular, in the LCP (also known as *meso*-crystallization) methods, membrane proteins are embedded in a membrane-mimetic lipid environment and interact with each other, improving crystal contacts with both hydrophilic and hydrophobic regions of the receptor.[14] Because LCP mimics native lipid bilayers, protein stability can be maintained compared to using detergent micelles. Although lipid-based approaches are more commonly used nowadays for GPCR crystallization, it is also important to note that thermostabilized GPCRs can also be crystallized in detergent micelles using the conventional vapor diffusion method.[5]

The latest advanced method implemented in GPCR crystallography is X-ray free electron laser (xFEL), also known as serial femtosecond crystallography.[5] High-quality single crystals of a GPCR are sometimes hard to obtain, hence working with microcrystals can be used to overcome this limitation. Although the microcrystals are sensitive to radiation, several advanced synchrotron sources with functional and tailored microfocus beamlines in place are currently available. When using xFEL, microcrystals are exposed to highly intense and ultrashort X-ray pulses, thereby enabling the collection of diffraction data from a single point on the microcrystal.[5] The primary advantages of this method include the ability of the microcrystals to escape radiation damage and the performance of data collection at room temperature, which mimics the native-state conditions.

Because of these methodological improvements in crystallography, experimental structures are available for more than 30 different GPCRs, encompassing the four major classes (class A, B, C, and F; Table 1).[16] Moreover, since 2007, class A nonrhodopsin GPCR structures have been continually elucidated, resulting in the identification of more than 120 crystal structures to date, thus providing insights into the mechanistic understandings of the receptor. These methodological advances in GPCR crystallography suggest that an unprecedented amount of structural data will become available in the field of GPCR biology in the near future.

2.2. Solved Structures of Class A Nonrhodopsin GPCRs.

In the past few years, technological advancements in both membrane protein engineering and crystallography have led to an exponential growth in the determination of GPCR structures. To date, more than 120 crystal structures have been solved for

DOI: 10.1021/acs.jmedchem.6b01453
J. Med. Chem. 2018, 61, 1−46

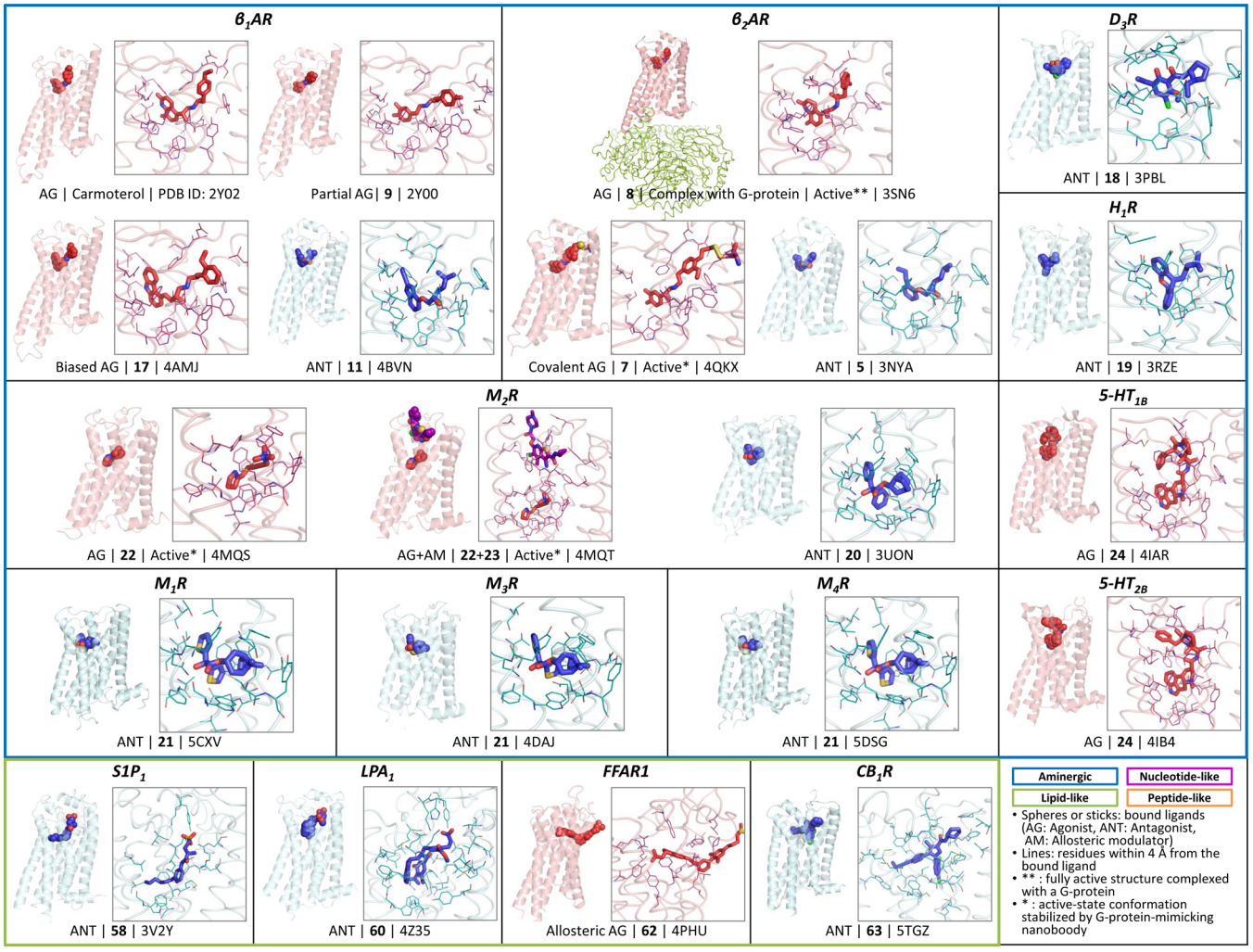

Figure 2. continued

DOI: 10.1021/acs.jmedchem.6b01453
J. Med. Chem. 2018, 61, 1−46

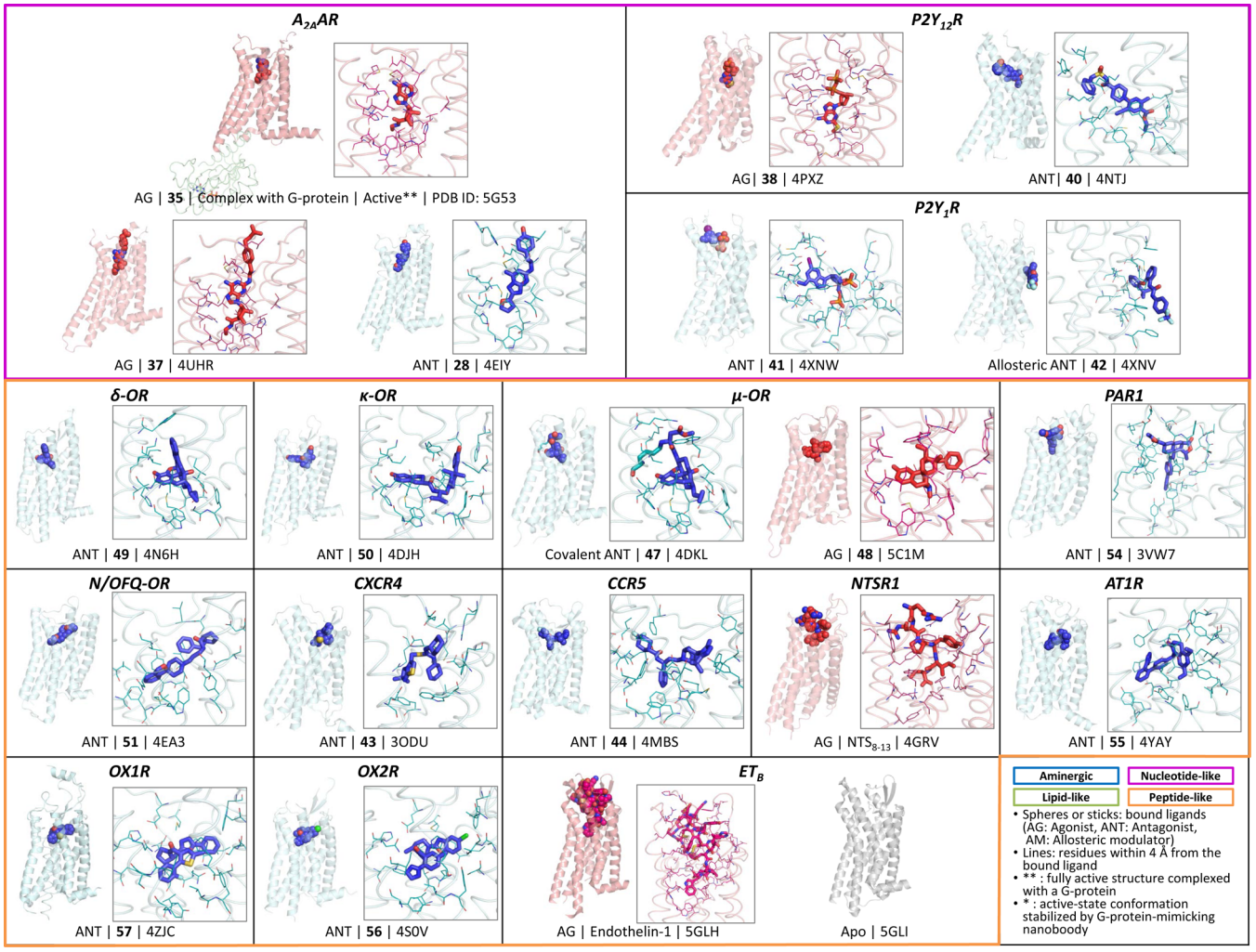

Figure 2. Ligand binding pockets of the nonrhodopsin class A GPCRs. The agonist- and antagonist-bound structures are displayed in pink and cyan ribbons, respectively, and the bound ligands are represented in spheres or sticks. In the closed view on the right, the residues within 4 Å from the bound ligand are also depicted with lines. The active-state conformations stabilized by a G protein or a G protein mimicking nanobody are marked with double asterisks and an asterisk, respectively.

class A GPCRs as follows: (1) rhodopsin (bovine and squid rhodopsin), (2) aminergic receptors (β_1- and β_2-adrenergic receptors (β_1AR and β_2AR), dopamine D_3 receptor (D_3R), histamine H_1 receptor (H_1R), muscarinic acetylcholine receptors (M_1R, M_2R, M_3R, and M_4R), and serotonin 1B and 2B receptors ($5HT_{1B}R$ and $5HT_{2B}R$)), (3) nucleotide-like receptors (A_{2A} adenosine receptor ($A_{2A}AR$), $P2Y_1$ purinergic receptor ($P2Y_1R$), and $P2Y_{12}$ purinergic receptor ($P2Y_{12}R$)), (4) peptide-like receptors (chemokine receptors (CXCR4 and CCR5), opioid receptors (δ-opioid receptor (δ-OR), κ-opioid receptor (κ-OR), μ-opioid receptor (μ-OR), and nociceptin/orphanin FQ peptide receptor (NOP)), neurotensin receptor 1 ($NTSR_1$), protease-activated receptor 1 (PAR1), angiotensin II type-1 receptor (AT_1R), orexin receptors (OX_1R, OX_2R), and endothelin receptor (ET_B)), (5) lipid-like receptors (free fatty acid receptor 1 (FFAR1), sphingosine 1-phosphate receptor 1 ($S1P_1$), lysophosphatidic acid receptor 1 (LPA_1), and cannabinoid receptor (CB_1)), and (6) unclassified receptor (US28). The solved structures include receptors in both energetically stable inactive and active conformations that are stabilized by either a heterotrimeric G protein or a G protein mimetic nanobody. These structures not only provide molecular details of the ligand binding mechanism, activation mechanism, allosteric modulation, and receptor dimerization but also present novel opportunities for SBDD. In the following section, we discuss the structural features of each class A nonrhodopsin GPCR receptor family. In Figure 2, the ligand binding position and receptor−ligand interactions are represented in a table-like view for efficient comparison.

2.2.1. Aminergic Receptors. Aminergic receptors belong to the level 1 subfamily of the class A rhodopsin-like family and act as a target for approximately 25% of currently available drugs. Depending on the recognition of specific biogenic amines as their endogenous activators, the 42 human aminergic GPCRs can be classified into six level 2 subfamilies, including adrenergic, dopaminergic, histaminergic, muscarinic, serotoninergic, and trace amine receptors. Each level 2 subfamily can be further subdivided into several subgroups that consist of closely related subtypes. To date, more than 50 crystal structures have been solved for ten of the 42 aminergic GPCRs, including β_1- and β_2-adrenergic receptors (β_1AR and β_2AR), dopamine D_3 receptor (D_3R), histamine H_1 receptor (H_1R), muscarinic acetylcholine receptors (M_1R, M_2R, M_3R, and M_4R), and serotonin 1B and 2B receptors ($5HT_{1B}R$ and $5HT_{2B}R$) in several active, intermediate-active, and inactive conformational states.

DOI: 10.1021/acs.jmedchem.6b01453
J. Med. Chem. 2018, 61, 1−46

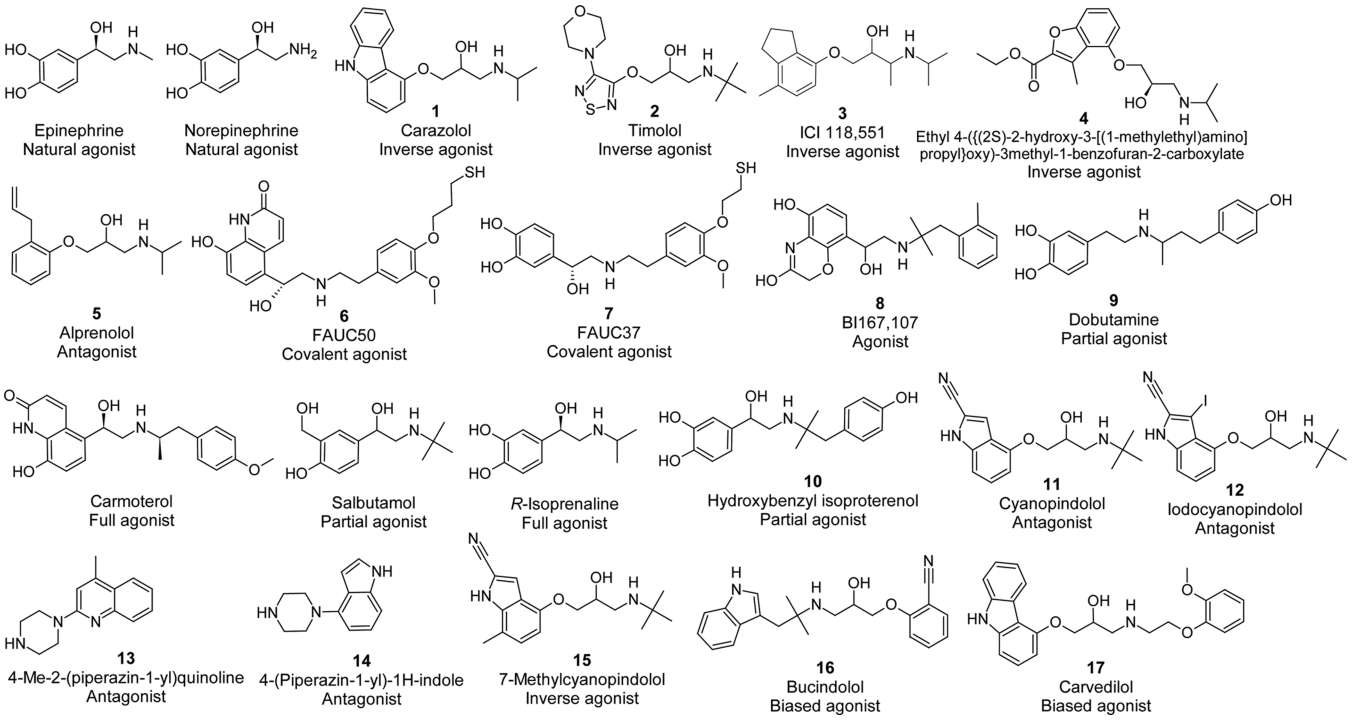

Figure 3. Chemical structures of the endogenous ligands and drug molecules of β-adrenergic receptors reported in this perspective.

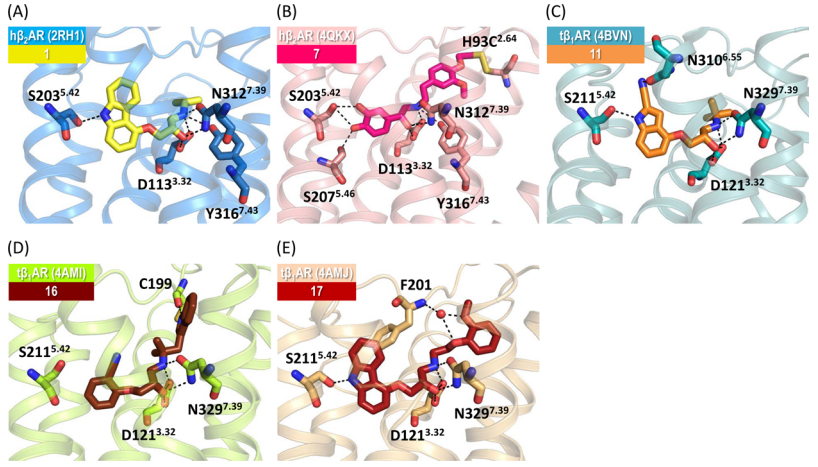

Figure 4. Ligand–receptor interactions observed in the crystal structures of β-adrenergic receptors. Key residues involved in the ligand–receptor interactions are represented as sticks, and the hydrogen bonds are marked with black dashed lines. Water oxygens mediating ligand–receptor interactions are depicted as small red spheres. The displayed receptor–ligand complexes correspond to (A) human β_2AR-**1**, (B) human $_{\beta 2}$AR-7, (C) turkey β_1AR-**11**, (D) turkey β_1AR-**16**, and (E) turkey β_1AR-**17**.

2.2.1.1. β-Adrenergic Receptors (β_1AR and β_2AR). Adrenergic receptors (adrenoceptors) are activated by endogenous catecholamines, especially epinephrine (adrenaline) and norepinephrine (noradrenaline),[17] resulting in the stimulation of intracellular G proteins. These receptors are classified into two main classes, α and β, and each group has its own subgroups, including α_1, α_2, β_1, β_2, and β_3. The β-adrenoceptor was the first GPCR to be sequenced, cloned, and structurally determined after rhodopsin, thus playing an important role in the investigation of GPCRs to date. More than four decades of research have resulted in the identification of several clinically important ligands targeting this receptor family. Therapeutically, β-adrenergic receptor antagonists, also known as "β-blockers", are applied in cardiovascular medicine as well as in migraine and anxiety treatments, and the agonists are utilized for the treatment of respiratory-related diseases. To date, more than 35 crystal structures of β-adrenoceptors have been reported, providing rich structural insights into their ligand–receptor interactions, which impart full agonist, partial agonist, or antagonist pharmacologies.[18] The chemical structures of the β-adrenergic receptor ligands, including their natural substrates, are shown in Figure 3.

Among the aminergic GPCRs, β_2AR is the most well-studied GPCR from a structural perspective due to the availability of structures in the inactive, partially active, and fully active state with a G protein. Initially, the structure of β_2AR bound to an inverse agonist **1** (carazolol)[19] and in complex with Fab5 that binds to ICL3 was solved at 3.4 Å; however, the EC domains with the ligand binding pocket were not observed in the solved inactive structure of the β_2AR-Fab5 complex. For these missing portions to be solved, a high-resolution crystal structure of the

DOI: 10.1021/acs.jmedchem.6b01453
J. Med. Chem. 2018, 61, 1–46

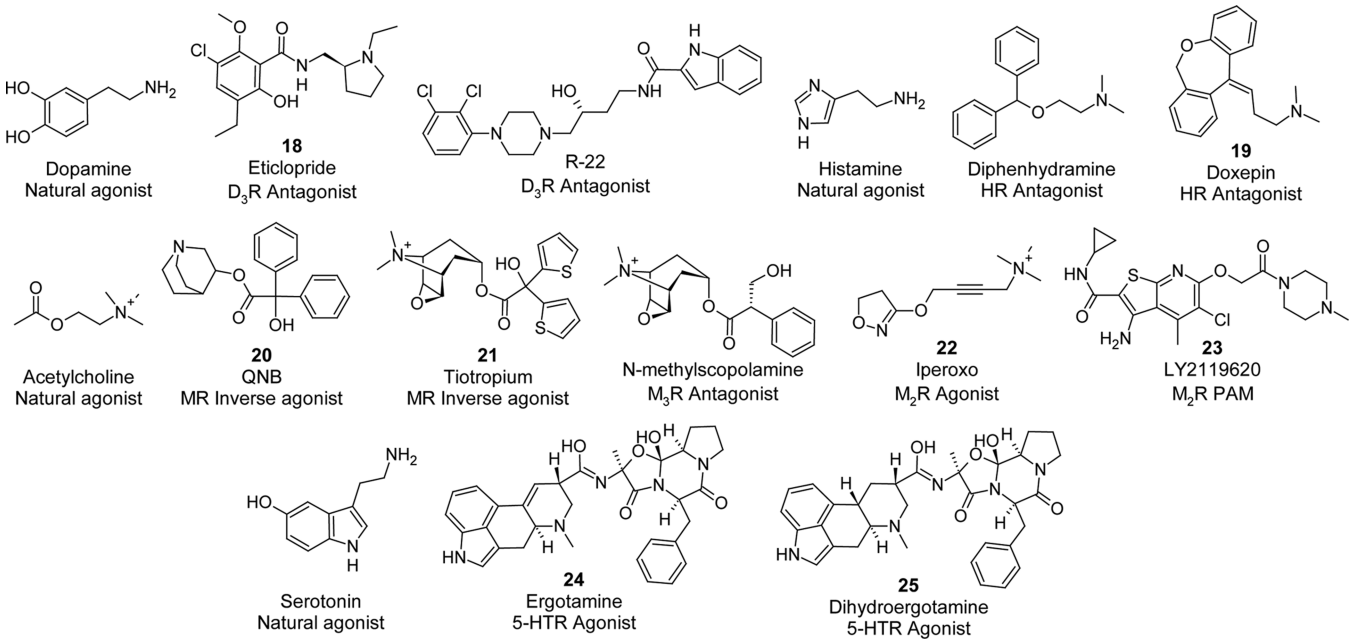

Figure 5. Chemical structures of the endogenous ligands and drug molecules of dopamine, muscarinic acetylcholine, and serotonin receptors reported in this perspective.

β_2AR-T4L fusion protein bound to high-affinity inverse agonist **1** was determined at 2.4 Å.[13] At the ligand binding site, this inverse agonist forms hydrogen bonds with S203$^{5.42}$, D113$^{3.32}$, N312$^{7.39}$, and Y316$^{7.43}$ and also has hydrophobic interactions with V114$^{3.33}$, F290$^{6.52}$, and F193$^{5.32}$ (Figure 4A). Crystal structures of the inactive state of human β_2AR in complex with other inverse agonists, including **1**, **2** (timolol), **3** (ICI 118,551), and **4** (ethyl 4-({(2S)-2-hydroxy-3-[(1-methylethyl)amino]propyl}oxy)-3-methyl-1-benzofuran-2-carboxylate),[13,19−22] and in complex with neutral antagonist **5** (alprenolol)[21] were also elucidated. Only minor structural rearrangements of the ligand binding site have been observed to accommodate different chemical properties of ligands, whereas their overall structural folds are preserved. The hydrogen bonding network with D113$^{3.32}$, N312$^{7.39}$, and Y316$^{7.43}$ is sustained in the interactions of **5**, **1**, and **2**; however, additional hydrogen bonding and hydrophobic interactions vary depending on each ligand, which may relate to the strength of inverse agonism. Recently, two structures of **1**-bound β_2AR were solved using crystals grown by the in meso method,[23] but the overall structures and key ligand−receptor interactions are the same as the previously reported ones.

In 2011, the first agonist-bound structure of β_2AR was released in complex with covalent agonist **6** (FAUC50).[24] Although it provides a significant breakthrough in the structural understanding of the GPCR activation mechanism, this structure did not represent the fully active state of the receptor due to the absence of G protein binding partners. Upon comparison with the previously solved inactive β_2AR structures, a few subtle differences were present in the active state. For example, hydrogen bonds were formed between serine residues S$^{5.42}$ and S$^{5.46}$ with the catechol replacing the ring of **6**, thus altering the conformation of both residues. Later, a complex structure of β_2AR with another covalent agonist **7** (FAUC37)[25] was determined in the active state, which is stabilized by G protein mimicking nanobody. Similar to **6**, **7** forms the hydrogen bonding interaction with both serine residues and covalently links to the mutated H93C$^{2.64}$ (Figure 4B). Active structures of human β_2AR in complex with noncovalent agonists (adrenaline, **8** (BI167,107), and **10** (hydroxybenzyl isoproterenol))[24,26−28] were also determined. Strikingly, the structure bound with **8** forms a signaling complex with the heterotrimeric G protein, which is in the fully active state. This finding is one of the most important breakthroughs in the history of GPCR crystallography. In 2014, the visualization of β_2AR with β-arrestin 1 was also enabled via electron microscopy studies.[29] Details of these signaling complexes will be discussed later (in section 3).

In the case of β_1AR, the inactive structure of turkey β_1AR in complex with antagonist **11** (cyanopindolol)[30] was determined in 2008 (Figure 4C). Other inactive crystal structures of turkey β_1AR bound to antagonists (**11**, **12** (iodocyanopindolol), arylpiperazine derivatives **13** (4-methyl-2-(piperazin-1-yl)-quinoline) and **14** (4-(piperazin-1-yl)-1*H*-indole),[18,31] and inverse agonists **1** and **15** (7-methylcyanopindolol)[31,32] were reported. The agonist-bound structures of turkey β_1AR in complex with several partial and full agonists were also released but all showed inactive state-like receptor conformations.[33] In the active state, a significant outward movement of TM5 and -6 was observed in β_2AR, whereas this movement was absent in β_1AR. This finding may be due to the agonist binding in β_2AR, which imparts 1 Å contraction in the orthosteric binding pocket associated with rotamer conformational changes of S212$^{5.43}$ and S215$^{5.46}$. This rotamer conformation strengthens the TM5-TM6 interaction but weakens the TM4-TM5 interaction, which may have led to the outward shift of TM5 and -6 helices in β_2AR. The extracellular side of the receptors, including the three ECLs, are almost identical, which provides access for the diffusible ligands to the ligand binding pocket that is composed of residues from TM3, -5, -6, and -7 and ECL2.

Interestingly, the thermostabilized structure of turkey β_1AR was determined in the presence of the biased agonists **16** (bucindolol) and **17** (carvedilol).[34] The head groups of the biased agonists were found to adopt a similar conformation to that of the antagonist-bound β-AR structures. Both compounds form additional contacts with residues lining the extended ligand

DOI: 10.1021/acs.jmedchem.6b01453
J. Med. Chem. 2018, 61, 1−46

binding pocket, which is composed of TM2, -3, and -7 and ECL2, thus elucidating the structural requirements of biased ligands (Figure 4D, E). One more interesting thing is the identification of a ligand-free basal state of β_1AR, which was reported by Huang et al. in 2013.[35] This structure was represented as the only class A nonrhodopsin structure crystallized in the ligand-free state; however, it still remains controversial after Leslie et al. repeated the structure determination using the deposited structure factors and identified substantial unmodeled electron density for a ligand in the orthosteric pocket.[36,37]

The sequence identity between β_1AR and β_2AR is approximately 67% in the TM regions. Because of the high sequence identity, the overall structures of the two receptor subtypes in their inactive states are similar. Although the receptor subtypes exhibit different ligand specificities and functions, a high similarity has been observed in the orthosteric binding pockets of both β_1AR and β_2AR. The ligand binding modes of **1** and **11** at β_1AR and β_2AR revealed common structural characteristics of ligand binding, including a salt bridge formation between the ammonium moiety of the ligand and $D^{3.32}$, and two hydrogen bonds: one between the aromatic head groups of the ligands and $S^{5.42}$ and another between the aliphatic OH-group of the ligands and $N^{7.39}$ (Figure 4A, C). This conserved ligand binding mode was also observed with other cocrystallized ligands, including **3** and **5**, thus demonstrating the highly conserved orthosteric binding pockets of the receptors. However, the ECL1−3 regions exhibit high variability in the amino acid sequences. The differences in the amino acid residues in ECL2 have been suggested to play a vital role in imparting ligand specificity.

Furthermore, structural comparisons of the intracellular parts of β_1AR and β_2AR revealed similar conformations of ICL1 but exhibited differences at ICL2 and ICL3. However, the difference observed in ICL3 is due to the introduction of stabilizing mutations and insertions. A secondary α-helical structure was observed in the ICL2 region of β_1AR, whereas a loop was seen in β_2AR due to the different lattice crystal contacts in ICL2. In both receptor subtypes, a noninteracting, open conformation of the "ionic lock" was detected. On the basis of the structure of rhodopsin, the ionic interaction between $R^{3.50}$ of the highly conserved D(E)RY motif at the bottom of TM3 and $E^{6.30}$ at the bottom of TM6 has been hypothesized to stabilize the inactive conformation of the GPCR. However, the structural data of β_1AR and β_2AR dispute this hypothesis because the ionic lock is absent in the inverse-agonist-bound inactive state of β_2AR and in a few antagonist-bound β_1ARs but is present in ligand-free basal state conformations.

2.2.1.2. Dopamine D_3 Receptor (D_3R). Similar to epinephrine and norepinephrine, dopamine also acts as an essential neurotransmitter and belongs to catecholamines (Figure 5); however, it binds to different receptor types.[38] By activating the distinct dopamine receptor subtypes in the brain, the essential neurotransmitter dopamine modulates our movements, memories, and emotions. Dopamine receptors are subdivided into two groups: the D1 group consisting of D_1 and D_5 subtypes and the D2 group composed of D_2, D_3, and D_4 subtypes.[39] Among these subtypes, D_3R was the first to be characterized and was found to share high sequence homology with the TM region of D_2R, particularly in the dopamine binding site. Therefore, most dopaminergic compounds are not subtype-selective, and the discovery of D_2- or D_3-selective ligands has been an especially challenging task.

Dopaminergic dysfunction leads to numerous CNS disorders, particularly schizophrenia, Parkinson's disease, and drug addiction.[38] Antipsychotic drugs that inhibit both D_2R and D_3R were used clinically to treat schizophrenia. However, these compounds produced multiple adverse effects, thus limiting their tolerability. It has been suggested that selective targeting of the individual D_2-like receptor subtypes might produce fewer side effects.[40] Therefore, via extensive medicinal chemistry efforts, D_3R-preferential antagonists and partial agonists were developed, which were shown to attenuate drug-seeking behavior in animal models without the associated motor effects. However, these compounds displayed high lipophilicity, poor bioavailability, and toxicity, which hampered the probability of these drugs entering preclinical studies.[41,42] Moreover, as previously mentioned, the high sequence identity observed between D_2R and D_3R ligand binding pockets makes the discovery of highly selective D_3R ligands even more difficult.

To overcome these limitations and to better understand the dopamine receptor, the crystal structure of hD_3R in complex with the D_2/D_3R-specific inhibitor **18** (eticlopride)[43] was determined in 2010. As expected, the ligand binding site was found to be similar to that of β_2AR due to the closely related catecholamine-based natural substrates, whereas the ECL2 region of D_3R was much shorter than that in β_2AR and lacked the secondary helical structure. The aromatic ring of **18** binds to the hydrophobic cavity formed by the extracellular half of TM5−7, and the ionizable tertiary amine interacts via a salt bridge with $D110^{3.32}$. Most of the D_3R residues directly in contact with **18** are identical to the D_2R binding site; therefore, D_3R selectivity has been proposed to require ligand extension toward the extracellular opening of the binding pocket. Molecules with extended flexible linkers connecting the tertiary amine to an extended aryl amide structure are thought to have the potential to achieve subtype selectivity.[44,45] Additionally, docking studies of the selective antagonist (*R*)-*N*-(4-(4-(2,3-dichloro-phenyl)piperazin-1-yl)-3-hydroxybutyl)-1*H*-indole-2-carboxamide (R-22) onto D_3R showed that the core amine-containing substituent binds in a similar pocket as **18**, whereas the indole-2-carboxamide terminus is oriented toward the extracellular binding pocket, which is formed by ECL2/ECL1 and the junction of TM1, -2, and -7, thus defining a second binding pocket.[43] This ligand−receptor interaction observed in the extracellular region defines the D_3R selectivity and can be utilized in the design of D_3R-selective ligands for treating drug addiction and other neuropsychiatric disorders.

2.2.1.3. Histamine H_1 Receptor (H_1R). Histamine is a biogenic amine that is involved in various physiological processes, such as allergic and inflammatory reactions, gastric acid secretion, and neurotransmission in the CNS.[46] Histamine exerts its effects via the activation of four receptor subtypes, H_1−H_4, where H_1R is the most validated drug target.[47] Several studies have developed H_1R antagonists (antihistamines) to alleviate the symptoms of allergic reactions. However, first-generation drugs, such as diphenhydramine and **19** (doxepin) (Figure 5),[48,49] have poor receptor selectivity and significant blood-brain barrier (BBB) penetration profiles that result in considerable side effects, including dry mouth, sedation, and arrhythmia. For example, tricyclic antidepressant (TCA) **19** has exhibited antagonist activity with H_2R, serotonin 5-HT_2R, α_1-adrenergic receptor, and muscarinic acetylcholine receptors (mAChRs) in addition to the reuptake inhibition of serotonin and norepinephrine.[48,49]

In an attempt to elucidate the structure of H_1R and to guide the design of H_1R-selective ligands, the X-ray crystallographic structure of the H_1R-T4L fusion protein in complex with first-generation antagonist **19** was determined in 2011.[48] H_1R shares

DOI: 10.1021/acs.jmedchem.6b01453
J. Med. Chem. 2018, 61, 1−46

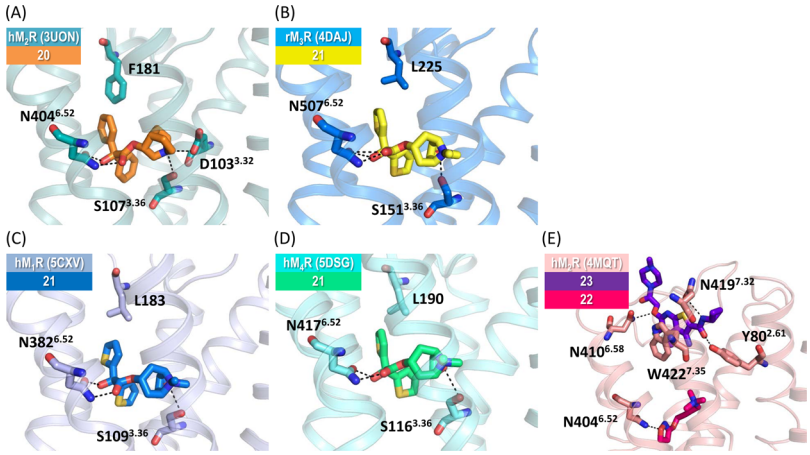

Figure 6. Ligand–receptor interactions observed at the orthosteric and allosteric sites of muscarinic receptors. Key residues are represented as sticks, and the hydrogen bonds are marked with black dashed lines. The displayed receptor–ligand complexes correspond to (A) human M_2R in complex with **20**, (B) rat M_3R in complex with **21**, (C) human M_1R in complex with **21**, (D) human M_4R in complex with **21**, and (E) human M_2R in complex with orthosteric agonist **22** and allosteric modulator **23**, which are shown in magenta and purple sticks, respectively.

relatively high overall structural similarity with other receptors, including β_1AR, β_2AR, and D_3R but largely deviates from the rhodopsin, A_{2A}AR, and CXCR4 structures. The tricyclic ring of **19** sits deeply in the orthosteric site, which is surrounded by highly conserved hydrophobic residues that contribute to the low selectivity of the first-generation ligands. Interestingly, an anion binding site has been observed in the entrance of the binding pocket occupied by a phosphate ion, forming ionic interactions with the protonated tertiary amine. Compared to first-generation antihistamines, the structures of second-generation drugs generally possess zwitterionic properties, making them too polar to cross the BBB, thus rendering them more selective for peripheral H_1R, which leads to reduced side effects.[50] The docking study of the second-generation H_1R-selective antagonists, which contain an additional carboxylic group, revealed that the selective compounds interact with nonconserved anion binding site residues including $K191^{5.39}$ and $K179^{ECL2}$, elucidating the molecular basis for histamine receptor subtype selectivity.

2.2.1.4. Muscarinic Receptors (M_1R–M_4R). Acetylcholine is an essential neurotransmitter found in the brain, neuromuscular junctions, and the autonomic ganglia.[51] The muscarinic acetylcholine receptor (mAChR), which is more sensitive to muscarine than to nicotine, acts as the main end-receptor stimulated by acetylcholine released from postganglionic fibers in the parasympathetic nervous system. Its counterpart receptor, nicotinic acetylcholine receptor (nAChR), is a receptor ion channel that is also important in the autonomic nervous system. Widely distributed in tissues, mAChRs are subdivided into five subtypes, M_1–M_5, and are classified into two major classes based on their G protein coupling: (1) M_1, M_3, and M_5 coupled to $G_{q/11}$ and (2) M_2 and M_4 coupled to $G_{i/o}$. mAChRs are involved in a variety of physiological functions and are utilized as therapeutic targets in the treatment of several neurodegenerative disorders, such as Alzheimer's disease, schizophrenia, Parkinson's disease, and chronic obstructive pulmonary disease (COPD).[51] Except M_5R, three-dimensional (3D) structures of all other mAChR subtypes (M_1R–M_4R) have been elucidated to date. M_2R structures were elucidated for both active and inactive states, whereas M_1R, M_3R, and M_4R structures were solved for the inactive state only. These structures provide extensive structural details for the ligand-induced activation and inhibition processes, receptor subtype selectivity, and binding of ligands to an allosteric site.

Similar to several other GPCR subfamilies, mAChRs also showed high sequence conservation in their acetylcholine binding sites, especially between M_2R and M_3R, thus making the discovery of highly subtype-selective orthosteric ligands a highly difficult task. In 2012, the X-ray crystal structures of T4L-modified human M_2R[52] and rat M_3R[53] were identified in complex with the inverse agonists, **20** (3-quinuclidinyl-benzilate, QNB)[52] and **21** (tiotropium),[53] respectively. In the case of hM_1R and hM_4R, the structures were recently determined in complex with **21**.[54] The overall structural topology of muscarinic receptor subtypes is similar to that of other aminergic receptors with the orthosteric binding pockets deeply buried within the TM core.[51] However, subtle differences have been observed between receptor subtypes in the less conserved regions, i.e., extra- and intracellular portions.

Because both ligands (**20** and **21**) are chemically similar (Figure 5), they display similar binding poses with extensive hydrophobic contacts with the receptor, and their structural comparisons provide insights into the subtle differences observed between the M_2R and M_3R binding sites. The orthosteric sites of M_2R and M_3R are highly homologous, and the only significant difference is F181 of M_2R and L225 of M_3R in ECL2, which creates an enlarged binding pocket in M_3R (Figure 6A, B). There is also a significant difference at the cytoplasmic end of the TM domains, particularly the interhelical distance between TM5 and -6. In addition, MD simulation studies indicated that **21** dissociates from M_3R at a much slower rate compared with its dissociation from M_2R, which may be due to the different flexibilities observed in the ECL2 region of the two subtypes.[53] Recent MD and site-directed mutagenesis studies have explained the long duration of action for **21** that has been observed in COPD therapy.[55] Interestingly, the ligand binding pocket of both receptors is almost completely occluded from the solvent with a tyrosine "lid-like" structure that is located directly above the pocket. This lid-like structure divides the large solvent-accessible binding pocket into two distinct sites, and antagonists were found to only bind one site. The upper portion of the pocket (extracellular vestibule) is lined with amino acids that have been implicated in the binding of allosteric modulators (discussed in the following section).[56] The recently solved

DOI: 10.1021/acs.jmedchem.6b01453
J. Med. Chem. 2018, 61, 1–46

inactive structures of M_1R and M_4R showed a similar binding pose of **21** with that of the inactive M_3R structure (Figure 6C, D).[54] Interestingly, the inactive M_4R structure was crystallized with an intact ionic lock that seems to be missing in other mAChR structures. Another unique feature of the M_4R structure is a rotameric change of $D112^{3.32}$ that points away from the ligand followed by the slight movements of $Y439^{7.39}$ and $Y443^{7.43}$, thereby forming a network of hydrogen bonds.

In the case of M_2R, the active form structures were also determined. In 2013, Kobilka's group solved two crystal structures of M_2R in complex with high-affinity agonist **22** (iperoxo)[57] alone and in combination with a positive allosteric modulator (PAM) **23** (LY2119620).[57] The selection of an appropriate G protein mimetic camelid antibody enabled stabilization of the receptor in the active state. Compared with the inactive structures, the cytoplasmic end of the **22**-bound M_2R shows helical rearrangement in combination with the outward displacement and inward movement of TM6, which creates a cavity for G protein binding. In addition, conserved motifs such as DR(E)Y and NPxxY showed conformational changes similar to those seen in β_2AR or rhodopsin. In the orthosteric binding site, the most pronounced change is the inward movement of TM6, which creates a hydrogen bond interaction between **22** and $N404^{6.52}$. The authors claim that this interaction is possibly involved in the activation of M_2R. Both structures of M_2R complexed with agonist **22** alone and those with **22** and PAM **23** reveal the location of an allosteric binding site situated in the extracellular vestibule (Figure 6E). The latter structure is largely congruous with that of the receptor conformation of the former; however, PAM **23** induces a slight contraction around the allosteric binding site.[53] Remarkably, the conformational change of $W422^{7.35}$ allows aromatic stacking interactions with the ligand. It may be assumed that the binding of **22** preforms the allosteric binding site in the extracellular vestibule that can be selectively addressed by **23**. This aspect may be utilized in the development of subtype-selective ligands for mAChRs that interact with the nonconserved residues in the allosteric site.

2.2.1.5. Serotonin receptors (5-HT$_{1B}$ and 5-HT$_{2B}$). Serotonin, or 5-hydroxytryptamine (5-HT), is a neurotransmitter that exerts its effect via the activation of a large family of 5-HT receptor proteins, which are grouped into seven subfamilies, 5-HT$_{1-7}$.[58] With the exception of 5-HT$_3$ (ion channel), the other 5-HT subtypes belong to the GPCR family. These GPCRs act as important drug targets in the treatment of several psychiatric and neurological disorders, such as depression, anxiety, migraine, nausea, and vomiting. To date, only two human crystal structures of 5-HT$_{1B}$ in complex with the full agonists **24** (ergotamine) and **25** (dihydroergotamine) (antimigraine medications; Figure 5)[59] have been reported. Stevens et al. elucidated the crystal structure of the human 5-HT$_{2B}$ receptor in complex with **24** to investigate the structural basis for biased signaling.[60] Furthermore, Cherezov et al. used LCP-derived microcrystals in combination with an xFEL with individual 50 fs duration X-ray pulses to obtain a high-resolution room temperature 5-HT$_{2B}$ structure that represents the real receptor conformation more precisely.[61]

As expected from the high sequence homology, a structural comparison of 5-HT$_{1B}$ and 5-HT$_{2B}$ bound to **24** reveals that their orthosteric binding pockets are highly similar. The binding modes of the ergoline moiety of **24** in both subtypes were almost identical, and the only substantial difference was observed in the benzyl group because of the differences in the extended ligand binding pockets (Figure 7). Key differences between the two subtypes include (i) an outward shift of the EC portion of TM5

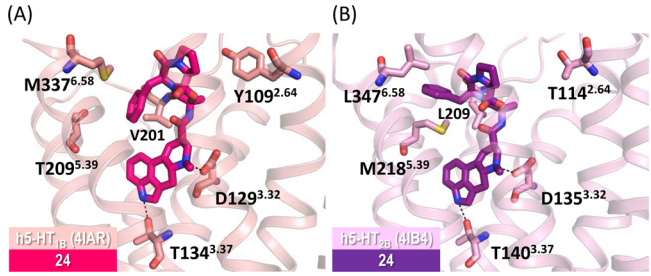

Figure 7. Ligand–receptor interactions observed in the crystal structures of serotonin receptors. Key residues are represented as sticks, and the hydrogen bonds are marked with black dashed lines. Compound **24** in complex with (A) human 5-HT$_{1B}$ and (B) human 5-HT$_{2B}$ display identical binding modes of the ergoline moiety.

in 5-HT$_{1B}$ by 3 Å relative to that of 5-HT$_{2B}$, which creates a broadened accessory binding pocket, (ii) the difference between $Y^{2.64}$ (5-HT$_{1B}$) and $T^{2.64}$ (5-HT$_{2B}$), resulting in a larger cavity in 5-HT$_{2B}$ due to the smaller residue size, and (iii) the substantial differences in the intracellular regions, which could explain the fact that ergoline moieties show biased signaling in favor of the β-arrestin pathway at 5-HT$_{2B}$, whereas signaling at 5-HT$_{1B}$ appears to be nonbiased. Moreover, the **24**-bound structure of 5-HT$_{1B}$ is in an active-like conformation, whereas the same ligand-bound 5-HT$_{2B}$ structure shows conformational aspects of both active and inactive states. Hence, it has been hypothesized that **24** stabilizes the 5-HT$_{2B}$ receptor conformation, which does not allow G protein signaling. These structural insights gleaned from the 5-HT crystal structures could aid in understanding ligand-induced differential signaling and the design of novel subtype selective and biased ligands.

2.2.2. Nucleotide-like Receptors. Purinergic receptors, one of the evolutionarily oldest receptors, are divided into P1 and P2 receptors and are preferentially activated by adenosine and a variety of other nucleotides, respectively. P2 receptors are subdivided into two types: ionotropic P2X receptors, which are activated by ATP, and G protein-coupled P2Y receptors, which are stimulated by nucleotides, di- or triphosphates, purines, or pyrimidines.[62] These receptors participate in short-term signaling functions, such as neurotransmission, neuromodulation, and secretion as well as in long-term signaling processes including cell proliferation, differentiation, and death.[62] Currently, more than 20 crystal structures have been solved for one of the subtypes of the P1 receptor, adenosine A_{2A} receptor (A_{2A}AR), in both agonist- and antagonist-bound states, whereas less than 10 crystal structures have been determined for two of the subtypes of P2Y receptors, including $P2Y_1R$ and $P2Y_{12}R$.

2.2.2.1. Adenosine A_{2A} Receptor (A_{2A}AR). The purine nucleoside adenosine is a ubiquitous neuromodulator that exerts its effects through the activation of four distinct subtypes of P1 purinoceptors: A_1, A_{2A}, A_{2B}, and A_3. A_1 and A_3 receptors generally couple with $G_{i/o}$ (sometimes A_3 may also couple with $G_{q/11}$), whereas A_{2A} and A_{2B} couple with G_s proteins.[63] In response to adenosine, all four adenosine receptor subtypes play vital roles in the CNS for the regulation of sleep, arousal, epilepsy, and neuroprotection.[63] Currently, structural studies for only one of the subtypes, A_{2A}AR, have been elucidated, thereby providing structural insights into its activation, inhibition, and allosteric modulatory mechanisms. Crystal structures of A_{2A}AR have been determined for both the active and inactive conformations in complex with various ligands (Figure 8). Inactive structures of A_{2A}AR bound to neutral antagonists (**26** (caffeine) and **27**

DOI: 10.1021/acs.jmedchem.6b01453
J. Med. Chem. 2018, 61, 1–46

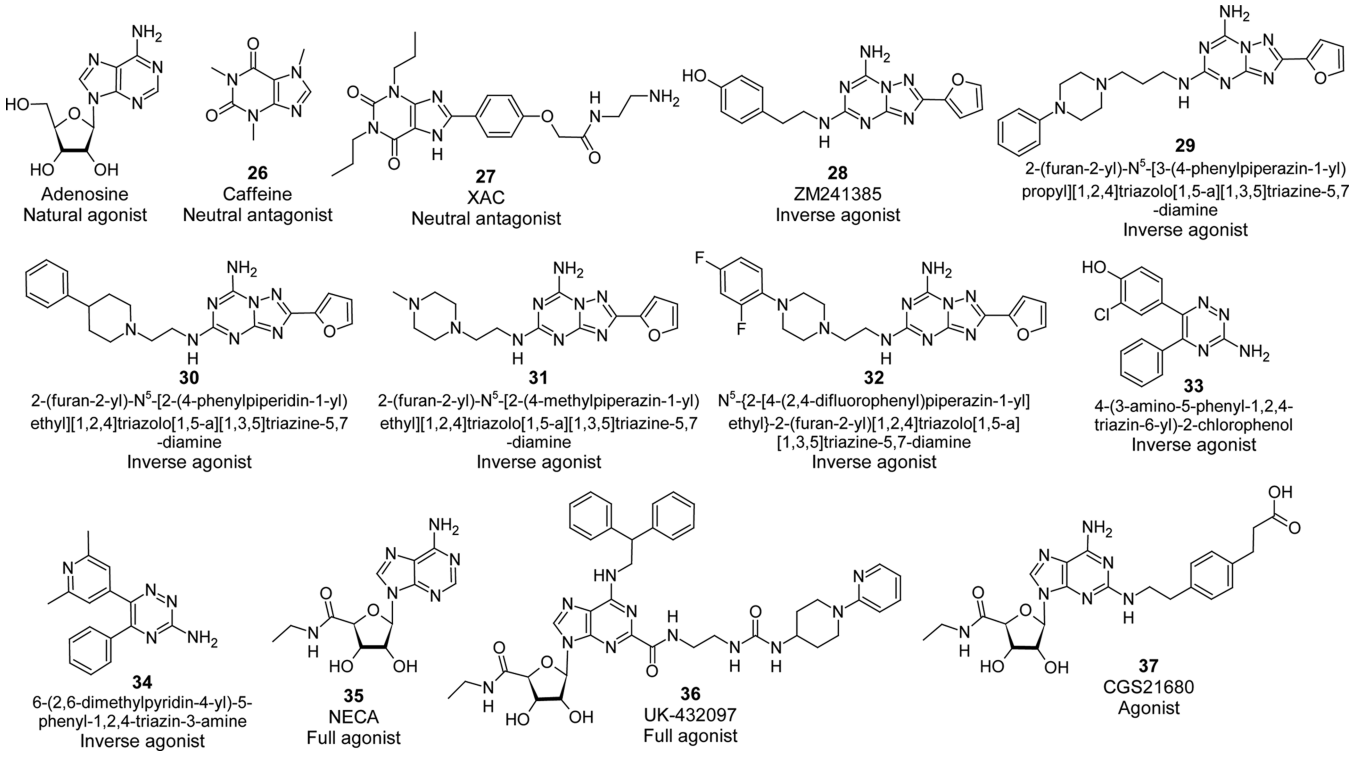

Figure 8. Chemical structures of the endogenous ligands and drug molecules of $A_{2A}AR$ reported in this perspective.

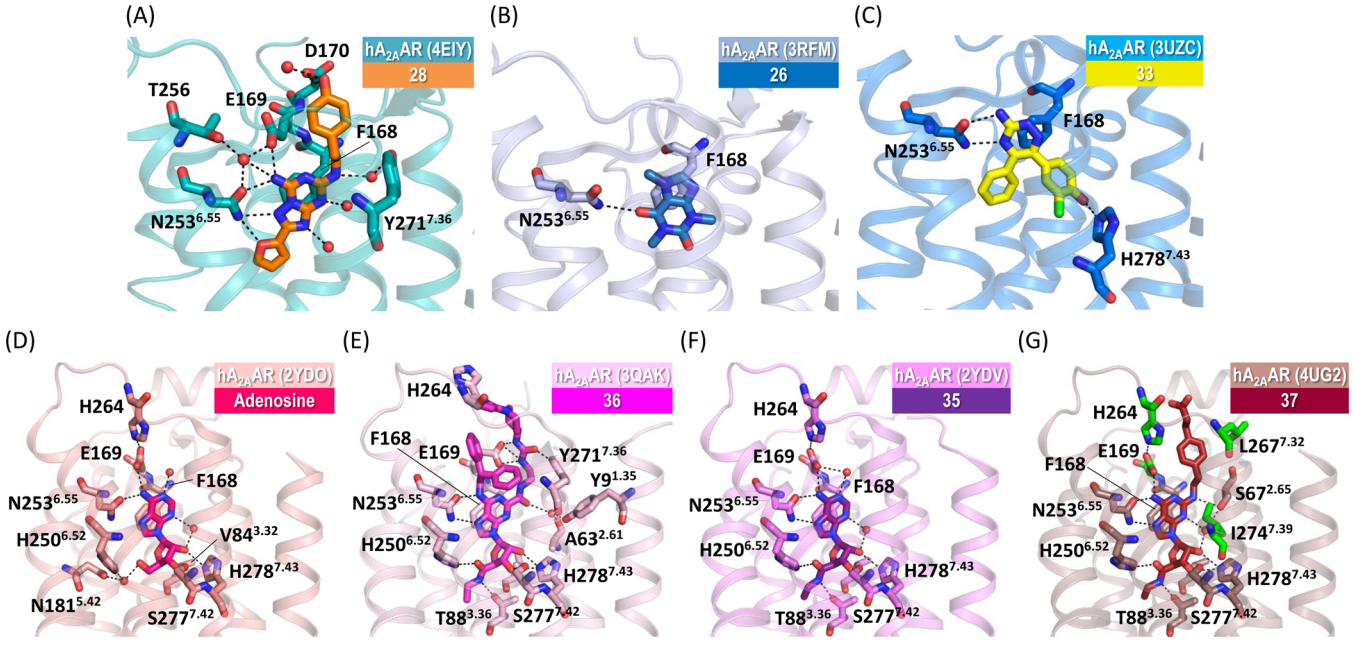

Figure 9. Ligand−receptor interactions observed in the crystal structures of the human $A_{2A}AR$. Key residues are represented as sticks, and the hydrogen bonds are marked with black dashed lines. Two important residues $N253^{6.55}$ and $F168^{ECL2}$, which are critical in both agonist and antagonist binding, are also highlighted. Water oxygens mediating ligand−receptor interactions are depicted as small red spheres. Human $A_{2A}AR$ in complex with different ligands corresponds to (A) **28**, (B) **26**, (C) **33**, (D) adenosine, (E) **36**, (F) **35**, and (G) **37**.

(xanthine amine congener (XAC)))[64] and inverse agonists (**28** (ZM241385)[64−67] and its related compounds (**29** (2-(furan-2-yl)-N^5-[3-(4-phenylpiperazin-1-yl)propyl][1,2,4]triazolo[1,5-*a*][1,3,5]triazine-5,7-diamine), **30** (2-(furan-2-yl)-N^5-[2-(4-phenylpiperidin-1-yl)ethyl][1,2,4]triazolo[1,5-*a*][1,3,5]triazine-5,7-diamine), **31** (2-(furan-2-yl)-N^5-[2-(4-methylpiperazin-1-yl)-ethyl][1,2,4]triazolo[1,5-*a*][1,3,5]triazine-5,7-diamine), and **32** (N^5-{2-[4-(2,4-difluorophenyl)piperazin-1-yl]ethyl}-2-(furan-2-yl)[1,2,4]triazolo[1,5- a][1,3,5]triazine-5,7-diamine)),[68] and 1,2,4-triazine derivatives (**33** (4-(3-amino-5-phenyl-1,2,4-triazin-6-yl)-2-chlorophenol) and **34** (6-(2,6-dimethylpyridin-4-yl)-5-phenyl-1,2,4-triazin-3-amine))[69] were solved. Active structures of $A_{2A}AR$ have also been determined after cocrystallization with either full agonists (adenosine,[70] **35** (NECA),[70] and **36** (UK-432097)[71]) or highly selective agonist **37** (CGS21680).[72] The binding modes of these ligands are shown in Figure 9. It has been

DOI: 10.1021/acs.jmedchem.6b01453
J. Med. Chem. 2018, 61, 1−46

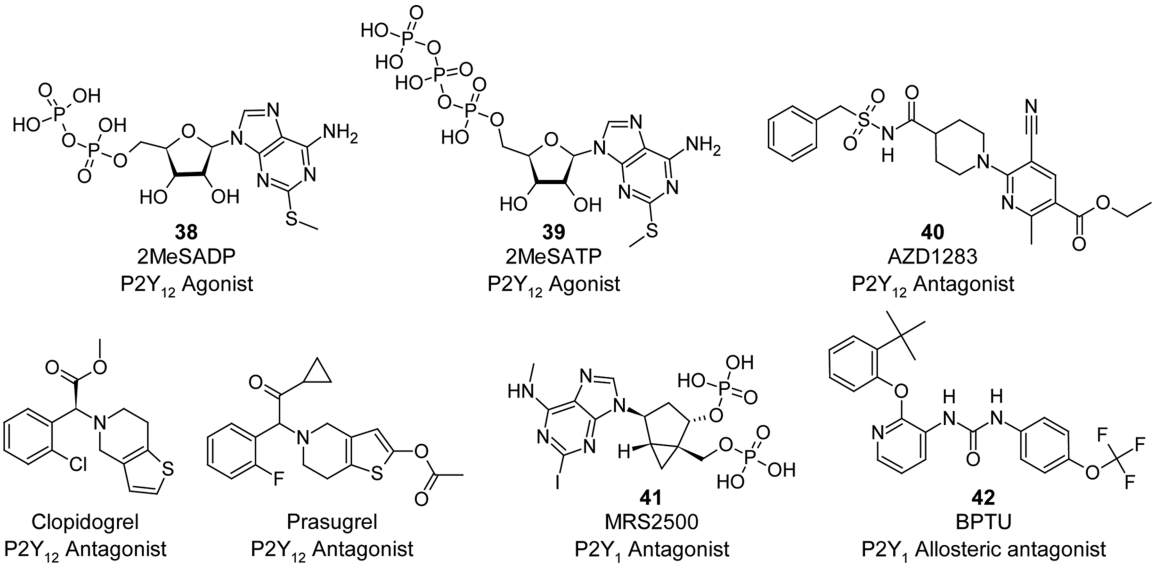

Figure 10. Chemical structures of the endogenous ligands and drug molecules of P2Y purinergic receptors reported in this perspective.

proposed that all the identified active crystal structures of $A_{2A}AR$ represent the active-intermediate conformation of the receptor and not the fully active one. This notion is supported by the data that include the presence of rotamer changes in the highly conserved residues linked with the activation of other GPCRs[73] and the absence of a large scale movement of TM6 away from the receptor bundle core.[74] Hence, for the fully activated state of $A_{2A}AR$ to be elucidated, the receptor structure in complex with a high-affinity agonist and an engineered G protein were recently determined (discussed in detail later).[75]

The first $hA_{2A}AR$ structure was solved in complex with **28** after engineering a T4L fusion and crystallizing it in LCP.[65] The inactive structure $A_{2A}AR$-**28** revealed unique features, such as a distinct organization of ECLs, an extended conformation of the ligand in the binding pocket toward extracellular space, and divergences in the helical positions, all of which were distinct from rhodopsin and adrenergic structures. This finding suggested that the ligand binding pocket was placed in a different location and orientation, which may be essential for achieving ligand selectivity. Subsequently, the thermostabilized version of the $A_{2A}AR$ structure that is also in complex with **28** was determined.[64] The high similarity observed between these two structures suggested that neither the T4L fusion nor the thermostabilizing mutations had any significant effect on the receptor structure.[76] Interestingly, the mechanism of the allosteric modulation of $A_{2A}AR$ by the Na^+ ion for antagonistic activity was elucidated following the determination of the highest 1.8 Å resolution structure of the $A_{2A}AR$-**28** complex.[77] A homologous Na^+ ion at an identical position has been subsequently identified in other class A GPCR structures.[78−80] Furthermore, advancements in structural biology have led to the development of novel $A_{2A}AR$ antagonists (triazine derivatives) using SBDD by Heptares Therapeutics.[69] Remarkably, all the inactive $A_{2A}AR$ structures show high similarity in their conformations despite being bound to different antagonists.[75]

The active structures of $A_{2A}AR$ bound to either endogenous agonist adenosine or full agonists, **35**[70] and **36**,[71] were determined following the elucidation of the $A_{2A}AR$ inactive structure. The majority of the $A_{2A}AR$ agonists were designed based on the structure of adenosine, which requires a bicyclic adenine core and a ribose ring for receptor stimulation. These active structures revealed the presence of hydrogen bonds between the ribose and side chains of $S277^{7.42}$ and $H278^{7.43}$ in TM7. Furthermore, TM3 residues ($V84^{3.32}$ and $T88^{3.36}$) were also found to be important for agonist binding and receptor activation. In the $A_{2A}AR$-adenosine/**35** structures, ECL2 and ECL3 are in close proximity with a hydrogen bond between $H264^{EL3}$ and $E169^{EL2}$. However, different conformations of ECL2 and ECL3 are observed in the $A_{2A}AR$-**36** structure in which the bulky extensions from position 2 on the adenosine ring sterically hinder close interactions between ECL2 and ECL3, resulting in a larger distance than that observed in the structures bound to adenosine or **35**. Recently, another active structure of the thermostabilized human $A_{2A}AR$-GL31 bound to selective agonist **37** ($hA_{2A}AR$-GL31-**37**)[72] was elucidated to understand the molecular determinants of agonist binding and subtype selectivity. Comparisons of all active structures of $A_{2A}AR$ show that the adenosine moiety binds to the receptor in a similar manner. However, the extension observed in **37** is due to the (2-carboxyethyl)phenylethylamino group that binds in an extended vestibule formed through contacts with TM2 and -7, and ECL2 and -3. Additionally, this group forms van derWaals (vdW) interactions with $E169^{EL2}$, $H264^{EL3}$, $L267^{7.32}$, and $I274^{7.39}$ residues, and the amine group forms a hydrogen bond with the $S67^{2.65}$ residue. Among these residues, $I274^{7.39}$ is the most highly conserved across the adenosine receptor subfamily.

The crystal structures of $A_{2A}AR$ have revealed a common set of residue interactions with ligands, including $L85^{3.33}$, $F168^{EL2}$, $E169^{EL2}$, $M177^{5.38}$, $W246^{6.48}$, $L249^{6.51}$, $N253^{6.55}$, and $I274^{7.39}$.[72] Among these residues, $N253^{6.55}$ and $F168^{EL2}$ have strong interactions with the adenine moiety in active structures and the corresponding triazolotriazine moiety in inverse agonists through two hydrogen bonds and π-electron stacking, respectively. Despite the overall structural similarity in the binding mode of the adenosine moieties in all active structures of $A_{2A}ARs$, the shape of the binding pocket in the extracellular surface differs significantly. Compared with the $hA_{2A}AR$-adenosine structure, the binding pocket of the $hA_{2A}AR$-GL31-**37** structure appears to be narrow at the extracellular surface due to an inward shift of TM2. This conformation is stabilized via a direct single hydrogen bond or through an ordered water molecule. However, in the $hA_{2A}AR$-**35** structure, an extensive

DOI: 10.1021/acs.jmedchem.6b01453
J. Med. Chem. 2018, 61, 1−46

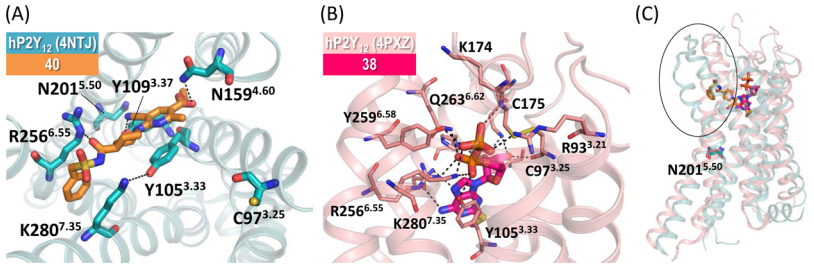

Figure 11. Ligand−receptor interactions observed in the crystal structures of the human $P2Y_{12}$ receptor bound to (A) **40** (in the extracellular view) and (B) **38**. Key residues are represented as sticks, and the hydrogen bonds are marked with black dashed lines. (C) Aligned structures of the antagonist (**40**)-bound and the agonist (**38**)-bound states. Both ligands bind to the same binding pocket; however, their orientations are completely different. In the antagonist-bound state, the presence of $N201^{5.50}$ residue (represented as a stick and labeled) in TM5 results in the lack of a helical bend. Large conformational changes in the TM region of agonist-bound receptor lead to the shift of TM6 and -7 helices toward the helical axis (highlighted in the black circle).

hydrogen bond network is formed through the seven ordered water molecules, resulting in a wider extracellular opening to the binding pocket. In the $hA_{2A}AR$-**36** structure, the bulky extensions to the adenosine moiety result in a wider extracellular opening to the binding pocket compared with that of the **35**-bound structure.

2.2.2.2. P2Y Receptors ($P2Y_1R$ and $P2Y_{12}R$). To date, eight different subtypes of human P2Y receptors, including $P2Y_1$, $P2Y_2$, $P2Y_4$, $P2Y_6$, $P2Y_{11}$, $P2Y_{12}$, $P2Y_{13}$, and $P2Y_{14}$, have been cloned and isolated. However, only two P2Y receptor subtypes, namely, Gq-coupled $P2Y_1R$[81] and Gi-coupled $P2Y_{12}R$,[82,83] have been structurally elucidated. Both of these receptors are stimulated by ADP to induce platelet activation, which plays a vital role in thrombosis formation, and the inhibition of either receptor leads to a decrease in platelet aggregation.[84,85]

X-ray crystal structures of $hP2Y_{12}R$ in both the active and inactive states have been solved: one in complex with the agonists **38** (2MeSADP) and **39** (2MeSATP),[83] and another in complex with antagonist **40** (AZD1283)[82] (Figure 10). The introduction of a 2′-methylthio group into ATP and ADP, which results in **38** and **39**, respectively, was shown to increase the ligand potency for $P2Y_{12}R$, resulting in full agonism.[86] Antagonist **40** serves as a potent antagonist of $P2Y_{12}R$ and shows a dose-dependent increase in blood flow and a blockade of ADP-induced platelet aggregation with antithrombotic effects in vivo. This compound progressed to human clinical trials as a candidate drug.[87] Although both the agonist and antagonist bind to the same binding pocket, their occupancy and orientations are completely distinct (Figure 11A, B). Unlike other class A GPCRs, which have highly conserved $P^{5.50}$ in TM5 causing a twist in the helix structure, this receptor has an $N^{5.50}$ residue in TM5 and lacks a helical bend (Figure 11C). In addition, at the orthosteric site, it has a bridge-like segment formed by residues $Y^{3.33}$ and $K^{7.35}$ that separates the pocket into two sites with only one pocket occupied by the antagonist (Figure 11A). Presumably, the other pocket is involved in the covalent binding of the active metabolites of drugs, such as Clopidogrel and Prasugrel,[88] to the conserved residue $C97^{3.25}$, thereby defining a unique labile disulfide bond.

In the agonist-bound state, the receptor undergoes large conformational changes in the TM helices, where the extracellular regions of TM6 and -7 shift above 10 and 5 Å, respectively, toward the helical bundle axis (highlighted in a black circle in Figure 11C). These movements result in the extensive formation of polar and ionic interactions with the phosphate groups of **38** (Figure 11B) compared with the antagonist-bound structure. Additional key interactions include the movement of the N-terminus toward the helical bundle axis and the change in the position of ECL2, where the presence of a disulfide bond results in the unwinding of the helical bulge, leading to the subsequent relocation of the residues in this region. Because of the observed large scale movements in the helical bundle, the receptor has a tighter conformation than that of other class A GPCRs, and agonist **38** seems to be fully enclosed within the receptor. The negatively charged phosphate groups of agonists form a key interaction with the receptor by closing the lid-like structure formed by the highly cationic ECLs and the N-terminus, thus enhancing the receptor agonistic activity. Because of its high structural complexity, the identification of $P2Y_{12}R$ ligands continues to be challenging and controversial. However, the recently solved ligand-bound $P2Y_{12}R$ structures are expected to facilitate the discovery of antithrombotic drugs using SBDD approaches.

The structure of another P2Y receptor subtype, $P2Y_1R$, was recently elucidated in complex with nucleotide and non-nucleotide antagonists, **41** (MRS2500) and **42** (BPTU),[81] respectively. The structure of $P2Y_1R$ is unique among class A GPCRs due to the presence of two disparate ligand binding pockets with chemically and structurally contrasting aspects. The hydrophilic and charged ligand binding pocket for **41** is located within the 7TM helical bundle, which is different in shape and location than those of the $P2Y_{12}R$-**40** crystal binding pocket. Antagonist **42** binds to a shallow allosteric pocket located on the external receptor interface with the lipid bilayer, thus making it the first structurally characterized selective GPCR ligand that is situated entirely outside of the helical bundle.[81] The $P2Y_1R$ structure stabilizes the conformation of the ECLs with the presence of two disulfide bonds, one connecting the N-terminus to H7 and another connecting ECL2 to H3. Similar to the peptide-like receptors, the ECL2 of $P2Y_1R$ exhibits a hairpin structure. Interestingly, the conserved $D[E]R^{3.50}Y$ motif in class A GPCRs is replaced by an $HR^{3.50}Y$ motif in $P2Y_1R$, making this the first GPCR structure with a basic histidine residue at position 3.49. Unlike other class A GPCRs that possess a salt bridge in the $D[E]R^{3.50}Y$ motif, the $H148^{3.49}$ residue in $P2Y_1R$ repels $R149^{3.50}$, resulting in a more extended side chain conformation of this residue. Furthermore, $R149^{3.50}$ forms a hydrogen bond with the main chain of $A327^{7.56}$ at the intracellular end of H7, stabilizing the C-terminus in a unique conformation.

Structural comparisons of $P2Y_1R$ and $P2Y_{12}R$ reveal distinct characteristics. The extracellular end of H6 in $P2Y_1R$ has a position that is intermediate between the ligand-bound structures of $P2Y_{12}R$. Unlike $P2Y_{12}R$, $P2Y_1R$ possesses a highly conserved residue class A GPCR residue $P229^{5.50}$, whose presence results in a helical kink and displacement of the

DOI: 10.1021/acs.jmedchem.6b01453
J. Med. Chem. 2018, 61, 1−46

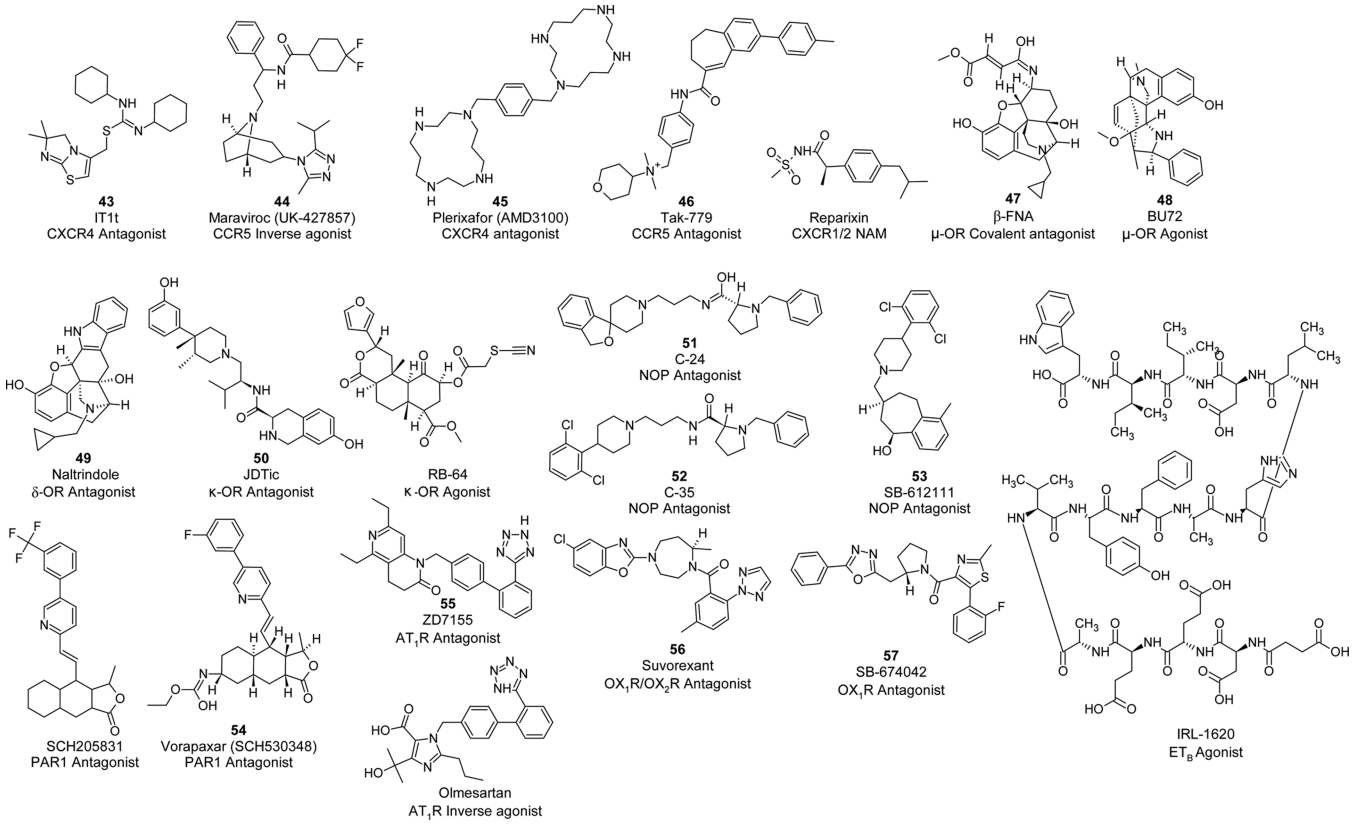

Figure 12. Chemical structures of the endogenous ligands and drug molecules of peptide-like GPCRs reported in this perspective.

extracellular tip of H5 above 4 Å. The H3 of P2Y$_1$R shifts away from the axis of the helical bundle by over 5 Å compared with that of P2Y$_{12}$R. The structural insights gained from the P2Y$_1$R structures could assist in the development of novel orthosteric and allosteric antithrombotic drugs with increased potency.

2.2.3. Peptide-like Receptors. Currently, more than 30 crystal structures of peptide GPCRs in both active and inactive states have been determined. Most of these solved structures were crystallized in the inactive states with nonpeptidic drug-like antagonists (Figure 12). However, a few peptide-like GPCRs, including CXCR4, δ-OR, and NTSR1, were crystallized in the presence of peptide/protein antagonists. CXCR4 structures were solved in complex with antagonists ranging from a few amino acids (cyclic peptide, CVX15)[89] in length to small proteins (viral macrophage inflammatory protein (vMIP)-II).[90] Human NOP has been crystallized in complex with peptide mimetic antagonist **51** (C-24).[91] Moreover, peptide GPCRs, including NTSR1, μ-OR, and ET$_B$, have been determined in active conformations with the peptide agonist NTS$_{8-13}$,[92] nonpeptidic drug-like agonist **48** (BU72),[73] and peptide agonist endothelin-1,[93] respectively.

2.2.3.1. Chemokine Receptors (CXCR4 and CCR5). Chemokines (chemotactic cytokines) are a family of chemoattractant molecules that attract leukocytes to areas of inflammation and lesions, and they play a key role in leukocyte activation. The chemokine family is divided into four classes based on the number and spacing of their conserved cysteines: (1) two adjacent cysteine residues (CC), (2) cysteines separated by an intervening residue (CXC), (3) cysteines separated by three intervening residues (CX3C), or (4) only one of the first two cysteine residues is present (C). For over 50 distinct chemokines, 19 human chemokine receptors are reported. A two-site model of chemokine binding was proposed to explain the binding and signaling roles of chemokine ligands.[94] The chemokine interacts with the receptor N-terminus and ECLs (chemokine recognition site 1 (CRS1)) via its globular domain, defining the affinity and specificity, and controls receptor signaling through its disordered N-terminus with the receptor TM helical core (CRS2). After the binding of their specific chemokine ligands, chemokine receptors trigger a flux of intracellular calcium, causing cell responses, such as chemotaxis, that traffics the cell to a desired location in the body. Until now, inactive structures of human chemokine receptor 4 (CXCR4) were solved in the presence of small molecule nonpeptidic inhibitor **43** (IT1t),[89] a 16-residue cyclic peptide inhibitor (CVX15),[89] and an 80-residue viral chemokine inhibitor (vMIP-II).[89,90] Similarly, the inactive structure of chemokine receptor 5 (CCR5) was determined in the presence of inverse agonist **44** (maraviroc, UK-427857, marketed as an HIV drug).[95] However, the CXCR4 and CCR5 active structures in the presence of an agonist remain to be determined.

Human CXCR4, which is activated exclusively by stromal-derived-factor-1 (SDF-1, also called CXCL12), was the first member of the chemokine family whose crystal structure was solved. Although there is a list of antagonist ligands available against CXCR4, including marketed antagonist **45** (plerixafor, AMD3100), peptide antagonist, anti-CXCR4 antibodies, modified CXCL12 derivatives, and so forth,[96] many aspects of ligand binding and signaling were poorly understood, especially the binding site to small molecules, prior to the publication of crystal structures.

In 2010, the X-ray crystal structure of CXCR4 was resolved in complex with 16-residue cyclic peptide antagonist CVX15 and with small molecule antagonist **43**, which is an isothiourea derivative developed by Novartis as a highly potent, orally

DOI: 10.1021/acs.jmedchem.6b01453
J. Med. Chem. 2018, 61, 1−46

bioavailable, and selective CXCR4 antagonist. The ligand binding pocket of CXCR4 is widely opened, negatively charged, and can be divided into major and minor subpockets. CVX15 fills most of the binding pocket and induces few conformational changes compared with the CXCR4-**43** structure. The major conformational differences include the movements at the N-terminus, including the extracellular tips of TM6 (1.5 Å inward), TM7 (1.5 Å tangential), and TM5 (0.5 Å outward). Compared with CVX15, **43** was found to bind much deeper into the pocket (Figure 13A, C). The isothiourea nitrogen atoms and the

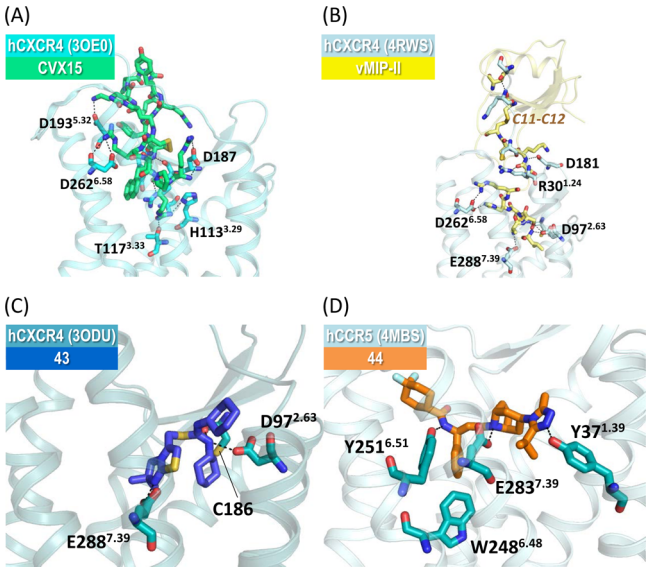

Figure 13. Ligand−receptor interactions observed in the crystal structures of chemokine receptors. Key residues are represented as sticks, and the hydrogen bonds are marked with black dashed lines. The displayed receptor−ligand complexes correspond to (A) human CXCR4-CVX15, (B) human CXCR4-vMIP-II, (C) human CXCR4-**43**, and (D) human CCR5-44. The binding of vMIP to the CXCR4 receptor is similar to the **43** binding, where the majority of the interactions take place in the minor subpocket, whereas key interactions of CVX15 peptide antagonist are at the major subpocket. The key hydrophobic interaction between W248$^{6.48}$ and **44** plays a potent role in maintaining the inactive state of the human CCR5-**44** complex. The orthosteric binding pocket of CCR5 is more open to the extracellular surface than that of CXCR4.

imidazothiazole of **43** formed salt bridge interactions with D97$^{2.63}$ and E288$^{7.39}$, respectively. The methylation of isothiourea induced a 100-fold reduction of binding and confirmed the importance of this salt bridge to D97$^{2.63}$. The hydrophobic interactions between the cyclohexane rings and the small subpockets of the receptor also contributed to the ligand binding. Interestingly, at the top of the orthosteric site, **43** binding is capped by the residues in ECL2, and the authors proposed that this feature may explain the high potency of **43** for CXCR4.

The recently solved structure of CXCR4 bound with a viral macrophage inflammatory protein (vMIP-II) shows that the receptor N-terminus differs from previously reported structures by adopting an orientation that is almost perpendicular to the membrane to form a β-sheet interaction between CRS1.5 (the intermediate region of CRS) and the chemokine residues C11 and C12. The binding of the viral chemokine antagonist is similar to that of **43** in which the majority of the vMIP-II (N-terminus) interactions are in the minor subpocket (Figure 13B). In comparison, most of the interactions of the CVX15 peptide are in the major subpocket. Thus, the limited overlap between the N-terminus vMIP-II and CVX15 may present possibilities for the design of modulators that could occupy both subpockets simultaneously.

The X-ray crystal structure of CCR5 was solved in complex with **44**, a marketed antiretroviral CCR5 inverse agonist developed by Pfizer. The endogenous ligands of CCR5 and their derivatives were shown to prevent HIV-1 infection. Compound **46** (TAK-779)[97] was the first discovered non-peptidic antagonist for CCR5 that was shown to be selective and potent against HIV-1 infection. Later, through Pfizer's high-throughput screening (HTS) program, another potent CCR5 antagonist, **44** (an approved drug for the treatment of HIV-1 infection), was identified.[98] Compounds **44** and **46** are considered as potent inverse agonists that act via allosteric mechanisms to antagonize the actions of endogenous chemokines. The inactive state of CCR5 can be defined by the hydrophobic interaction between W248$^{6.48}$ and **44** (Figure 13D), which prevents the activation-related conformational changes of the receptor, as further evidenced by the tight packing of the 7TM bundle helices at the intracellular side of CCR5, thereby preventing G protein binding.

A structural comparison revealed that CCR5 has a more open binding pocket than that of CXCR4, which is partially covered by its N-terminus and ECL2. Other significant differences were also observed between CCR5 and CXCR4. For example, in CCR5, the extracellular end of TM7 is shifted away from the central axis by 3 Å, resulting in a shift of the CCR5 N-terminus. The salt bridge in ECL2 is broken in CCR5, whereas in CXCR4, the β-hairpin tip of ECL2 is shifted approximately 6 Å toward the ligand binding pocket. In addition, the entrance to the CXCR4 binding pocket is partially covered by its N-terminus and ECL2, but the CCR5 ligand binding pocket is more open. Despite engaging the conserved binding determinants, the chemokines tend to bind to different regions of the ligand pocket due to chemokine receptor conformational plasticity. This aspect may allow the receptor to accommodate ligands of different classes, including both CC- and CXC-type chemokines, as well as allosteric inhibitors. Thus, the increasing number of chemokine receptor structures with different ligands may present opportunities for the rational design of ligands with improved inhibition profiles and mechanisms of action.

2.2.3.2. Opioid Receptors Including Nociceptin Receptor (δ-OR, κ-OR, μ-OR, and NOP). Opioids control pain, reward, and addictive behaviors by exerting their pharmacological actions through the activation of three opioid receptor subtypes, namely, δ-OR, κ-OR, and μ-OR. These classical opioid receptors share a high sequence identity of approximately 75%. The heptadecapeptide nociceptin NOP was identified as the fourth member of the opioid receptor family. All of the opioid receptors described above play potent roles in the CNS by regulating pain perception and mood.[99] Opioid agonists are widely utilized in the management of pain but also present severe undesired effects. These side effects could be reduced by designing ligands with customized subtype selectivity, intrinsic activity, and biased signaling profiles.[100] To accomplish these goals, high-resolution crystal structures of all four opioid receptors (μ, δ, κ, and NOP) in inactive conformations, and the active conformation of μ-OR, have been elucidated. Additionally, the first X-ray crystallographic-[101] and NMR-based[102] peptide-bound opioid structures were recently solved. Determination of these structures could accelerate the structure-guided design of new opioid drugs.

DOI: 10.1021/acs.jmedchem.6b01453
J. Med. Chem. 2018, 61, 1−46

To understand the structural basis for μ-OR activation and inhibition mechanisms, Kobilka's group solved both the antagonist-[103] and agonist-bound[73] structures of the receptor. The first crystal structure solved among opioid receptors was the T4L-modified μ-OR from the murine origin in complex with the irreversible antagonist **47** (β-funaltrexamine (β-FNA)).[103] This ligand is a morphine derivative with a fumaric amide side chain that forms a covalent bond with the amino group of K233$^{5.39}$ via Michael addition (Figure 14A). Furthermore, the recent active

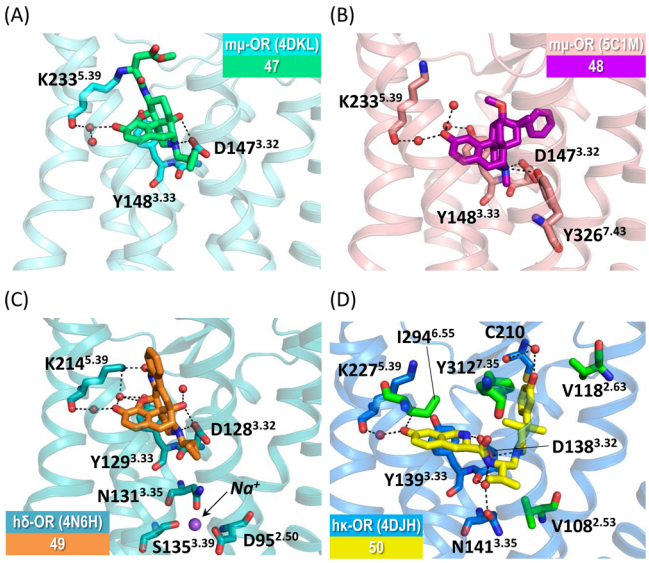

Figure 14. Ligand–receptor interactions observed in the crystal structures of classical opioid receptors. Key residues are represented as sticks, and the hydrogen bonds are marked with black dashed lines. Water oxygens mediating ligand–receptor interactions are depicted as small red spheres. The displayed receptor–ligand complexes correspond to (A) μ-OR-**47**, (B) μ-OR-**48**, (C) δ-OR-**49**, (D) κ-OR-**50**. In both active and inactive structures of μ-OR, an ionic interaction is observed between the receptor residue D147$^{3.32}$ and the ligand. In addition to the orthosteric binding pocket, δ-OR-**49** complex structure reveals the presence of an allosteric Na^+ ion (represented as purple sphere), thus proving the allosteric modulation of opioid receptors. In the antagonist **50**-bound state of κ-OR, V-shaped conformation of the ligand is observed due to the presence of a salt bridge between receptor residue D138$^{3.32}$ and the protonated amines of the ligand. The subtype selectivity of **50** can be defined by the unique interactions with four residues: V108$^{2.53}$, V118$^{2.63}$, I294$^{6.55}$, and Y312$^{7.35}$ (represented as green sticks).

crystal structure of murine μ-OR bound to morphinan agonist **48** and a G protein mimetic camelid antibody fragment was also determined (Figure 14B). To date, μ-OR structures represent the only example of peptide-like GPCRs crystallized in both active and inactive conformations. In the inactive state, the receptor was crystallized in a similar manner to CXCR4 as intimately associated pairs where the dimer interface is mainly formed via TM5 and -6. However, the TM5-TM6 interface seen in the inactive state is not compatible with that in the active state due to the steric clashes observed in this region. Moreover, there are no significant structural changes observed in the extracellular surface of both states with the exception of the N-terminus. In the active state, there is a significant amount of conformational changes in the cytoplasmic surface of the receptor, where TM6 undergoes a large outward shift and TM5 and -7 undergo smaller inward movements. Furthermore, TM6 undergoes a 10 Å outward displacement upon receptor activation. The E/DRY motif plays a potent role in maintaining the receptor in its inactive conformation (showing a polar interaction between R$^{3.50}$ and T$^{6.34}$) in a similar manner to that of rhodopsin.

Because both **47** and **48** share similar ligand binding poses and a morphinan scaffold, the overall structural differences observed in the binding pockets of both states are subtle. The major interaction of **48** with μ-OR is hydrophobic or aromatic with the exception of two conserved polar interactions and a water-mediated interaction between the phenolic hydroxyl of the agonist with H297$^{6.52}$. In both the active and inactive states, an ionic interaction was observed between the morphinan tertiary amine and D147$^{3.32}$ (Figure 14A, B). Interestingly, there is an unexpected interaction between **48** and the amino terminus of the receptor, which forms a lid-like structure over the binding pocket. In both of the receptor states, there is a water-filled cavity lined with polar and aromatic side chains, which extends off of the intracellular end of the orthosteric binding pocket. However, in the active state, this cavity appears to be larger and contiguous with the agonist binding site. Additionally, in the active structure, an extensive reorganization of the polar network and pronounced rearrangements in the conserved core triad were observed. Overall, the subtle ligand-specific differences in the polar network connections may contribute to the preferential activation of signaling effectors.

Following the release of the μ-OR structure in 2012, the inactive T4L-fused δ-OR structure from *Mus musculus* was solved in complex with subtype-selective ligand **49** (naltrindole).[104] The ligand–receptor key interactions observed in the δ-OR-**49** complex are similar to those in the μ-OR-**47** structure. As observed in the μ-OR-**47** structure, the ligand binds deeply in the orthosteric binding pocket, which may be due to the presence of a β-strand fold in the ECL2 region that is typical of all opioid receptor subtypes. A comparison of the μ-OR-**47** and δ-OR-**49** structures revealed that the lower portion of the binding pocket is highly conserved and forms a contact with the core morphinan moiety, resulting in changes to ligand efficacy. However, the upper portion is less conserved, serving as an important subtype selectivity determinant. This finding highlights the "message-address" concept of opioid pharmacology. Subsequently, a high-resolution structure of human BRIL-δ-OR in complex with the same antagonist **49** was determined at 1.8 Å.[79] Overall, the structure is similar to the previously resolved mouse δ-OR-**49** structure. However, a few distinctions were observed, including a fully resolved ICL3 adopting an inactive receptor conformation, water-mediated ligand–receptor interactions in the binding pocket, a different conformation of ECL3, and significant characterization of the 7TM core by the presence of an allosteric Na^+ binding site, water molecules, and an extensive network of hydrogen bond interactions. Interestingly, the structure reveals the presence of a Na^+ ion in the allosteric binding site (Figure 14C), confirming the previously described allosteric modulation of opioid receptors by Na^+ ions.[105] As seen in other class A GPCRs, the Na^+ binding site is centrally positioned within a polar interaction network in the 7TM bundle core, thus stabilizing the conformation of a reduced agonist affinity state. Site-directed mutagenesis and functional studies demonstrated that mutating the allosteric Na^+ site residue N131 to an A or V could increase constitutive β-arrestin-mediated signaling. Further mutations of D95A, N310A, and N314A shifted the pharmacological profile of the δ-OR typical antagonist into a β-arrestin-biased agonist.

Recently, another structure of human δ-OR bound to the bifunctional δ-OR antagonist and μ-OR agonist tetrapeptide H-Dmt-Tic-Phe-Phe-NH_2 (DIPP-NH_2) was solved by xFEL,

DOI: 10.1021/acs.jmedchem.6b01453
J. Med. Chem. 2018, 61, 1–46

revealing distinct ligand binding determinants.[101] Overall, the inactive structure of δ-OR-DIPP-NH2 is similar to the previously resolved hδ-OR-**49** structure. However, the DIPP-NH2 binding is distinct compared with the binding of other ligands to opioid structures. The peptide ligand occupies most of the ligand binding pocket and is oriented such that a Dmt residue penetrates deep toward the core of the receptor and interacts with M132$^{3.36}$, Y129$^{3.33}$, V217$^{5.43}$, V281$^{6.55}$, I277$^{6.51}$, and W284$^{6.58}$ residues. Phe4 is placed in the extracellular entrance of the binding pocket with the Phe4-NH_2 main chain interacting with ECL2, whereas the other peptide residues H-Dmt, Tic, and Phe3 bind tightly in the well-defined cavity. The peptide binding induces an expansion in the ligand binding pocket through the outward movement of TM2 and -6, which increases the distance between Y109$^{2.64}$ and W284$^{6.58}$ residues accompanied by an outward movement of approximately 2 Å of ECL2. This peptide-bound opioid structure presents an opportunity to examine the binding mode of a prototype peptide analogue and provides a structural platform for the rationalization of structure−activity relationship (SAR) studies of several other reported peptides with distinct pharmacological aspects.

The crystal structure of human T4L-modified κ-OR in complex with the selective antagonist **50** (JDTic, tetrahydroisoquinoline-3-carboxamide)[106] was solved at 2.9 Å resolution. This inactive structure was crystallized as a parallel dimer with contacts involving TM1 and -2 and helix 8. The overall structure of κ-OR-**50** shares key features with chemokine and aminergic GPCRs along with unique structural characteristics of opioid receptors. The orthosteric binding pocket of κ-OR is wider than that in the reported aminergic GPCRs but appears to be tighter and deeper than that of the related CXCR4 receptor. The extracellular facing domains are similar between opioid receptor subtypes μ-OR and δ-OR. Compound **50** fit tightly at the bottom of the binding pocket, with both protonated amines forming salt bridges with D138$^{3.32}$, which fixes the V-shaped conformation of the ligand (Figure 14D). Interestingly, unique interactions with four residues, V108$^{2.53}$, V118$^{2.63}$, I294$^{6.55}$, and Y312$^{7.35}$, that are not present in other opioid subtypes were observed, which explains the subtype selectivity of **50** (see the green-colored residues in Figure 14D). Additionally, structure-based docking was performed for morphinan-based κ-OR ligands and the salvinorin-derived ultrapotent ligand 22-thiocyanatosalvinorin A (RB-64)[107] to identify the possible binding modes of structurally diverse κ-OR ligands.

The nociceptin/orphanin FQ (N/OFQ) peptide receptor (NOP) was discovered as the fourth member of opioid receptors because its substrate, heptadecapeptide nociceptin, showed structural homologies to the classical opioid peptides. Despite these similarities, nociceptin does not show a distinct affinity for the opioid receptor subtypes μ, δ, and κ. For its 3D structure to be determined, NOP was stabilized by BRIL modification and crystallized in the presence of peptide-mimetic antagonist **51**.[91] A comparison with other structures revealed modularity in the 7TM helical core and variations in the extracellular regions with boundaries defined by proline-induced kinks. Compared with the κ- and μ-OR structures, the extracellular tip of TM5 is shifted by more than 4 Å, which creates a gap between TM4 and -5, resulting in the expansion of the ligand binding pocket. Upon comparison with CXCR4, the extracellular tips of TM6 and -7 are shifted inward toward the binding pocket. Substantial differences observed in the geometry of the ligand binding pockets between NOP and classical opioid receptors were mainly due to variations in a small number of residues. Recently, two inactive crystal structures of NOP were also elucidated in complex with antagonists **52** (C-35) and **53** (SB-612111)[108] showing similar binding modes with that of **51**. These findings contribute to the molecular understanding of ligand selectivity of NOP and provide a novel structural template for the design of NOP ligands.

2.2.3.3. Neurotensin Receptor (NTSR$_1$). Neurotensin (NTS) is a 13-residue neuromodulatory peptide, and its carboxy-terminal 6-residue fragment, NTS$_{8-13}$, was found to be the portion responsible for agonism. NTS exerts its biological role through activation with any of the neurotensin receptor subtypes: NTSR$_1$, NTSR$_2$, or NTSR$_3$. Because of its widespread expression in the brain and gut, NTS was linked to the treatment of several neurological disorders, such as hypothermia, antinociception, cancer, and obesity. To date, two separate groups have crystallized NTSR$_1$ in complex with the natural substrate peptide NTS$_{8-13}$.[92,109] Modeling and mutagenesis studies addressed some of the ligand binding aspects; however, the molecular details of ligand binding are still poorly understood.

In 2012, the X-ray crystal structure of NTSR$_1$ bound to the full agonist peptide NTS$_{8-13}$ was determined with six thermostabilizing mutations (NTSR$_1$-GW5).[92] The binding site of NTS$_{8-13}$ showed significant differences in the ligand position compared with the agonists bound in β_2AR or A_{2A}AR. The binding cavity is located near the receptor surface, and this peptide agonist does not deeply penetrate the receptor. NTS$_{8-13}$ adopts an extended conformation nearly perpendicular to the lipid bilayer, which is consistent with the solid-state NMR analysis of the structure of wild-type NTSR$_1$ bound with NTS$_{8-13}$.[110] On the basis of the partial outward tilt of the intracellular end of TM6 and the presence of a hydrogen bond between R167$^{3.50}$ and N257$^{5.58}$, the authors suggested that the structure represents an active-like conformation. However, despite the characteristics of an active state-like receptor, this mutated thermostabilized structure did not catalyze the nucleotide exchange at the G protein in response to NTS. This result suggests that the present structure does not fully reflect the active conformation but rather represents an active-like state.

Four other structures were reported in 2014 using a directed evolution technology approach for high functional expression and enhanced stability in short-chain detergents.[109] These structures differ from the previously reported one by the observed differences in the cytosolic regions and the presence of amphipathic helix 8. Additionally, a single α-helical turn of ECL3 with several ligand contacts was noted on the extracellular side of the receptor. Although this structure is bound to its agonist and is capable of processing nucleotide exchange, the TM5 and -6 conformations were reported to have been captured in an inactive state that is highly similar to the dark-state rhodopsin. In the following year, another two structures of NTSR$_1$, namely NTSR$_1$-LF and NTSR$_1$-ELF mutants, were solved,[111] which provided mechanistic insights into the agonist-bound active-like peptide GPCR. These structures may support the development of other peptide and nonpeptide ligands for disease management.

2.2.3.4. Protease-Activated Receptor 1 (PAR1). Thrombin is formed by the proteolytic cleavage of prothrombin (coagulation factor II) in the coagulation cascade. It acts as a serine protease converting soluble fibrinogen into insoluble strands of fibrin as well as catalyzing many other coagulation-related reactions. Therefore, thrombin regulates numerous cellular responses, including platelet aggregation, endothelial cell activation, hemostasis, and inflammation. PAR1 is a prototypical GPCR

DOI: 10.1021/acs.jmedchem.6b01453
J. Med. Chem. 2018, 61, 1−46

that is irreversibly activated by thrombin through the specific proteolytic cleavage of the amino terminal exodomain of the receptor. This tethered N-terminal peptide binds intramolecularly to the receptor and affects G protein activation. The identification of PAR inhibitors is challenging because compounds with low molecular weight must compete with the very high local concentration of the tethered peptide. Initially, PAR1 antagonists were designed as peptidomimetics based on the tethered peptide sequence. The first nonpeptide PAR1 antagonist with a pyrroloquinazoline scaffold was reported in 1999 by Schering-Plough.[112] In 2005, HTS provided (3R,3a*S*,4-*S*,4a*R*,8a*S*,9a*R*)-3-methyl-4-{(*E*)-2-[5-(3-trifluoromethylphenyl)pyridin-2-yl]vinyl}decahydronaphtho[2,3-*c*]furan-1-one (SCH205831)[113] as a novel PAR1 antagonist based on the natural product himbacine, and through further optimization, **54** (vorapaxar, SCH530348)[113] was discovered as a potent orally available antiplatelet agent. In 2014, this functionally irreversible inhibitor of PAR1 with a slow off rate, high affinity, and PAR1 selectivity was approved by the US Food and Drug Administration (FDA) as the first in a new class of PAR1 antagonists.[114]

One X-ray crystal structure of PAR1 is available to date in which PAR1 is complexed with the antagonist **54**.[78] This structure is unique compared with other class A GPCRs. The ligand binds at an unusual location, i.e., in close proximity to the extracellular surface of the receptor, whereas other class A GPCR ligands penetrate much deeper into the TM core. In addition, none of the three PAR1 extracellular openings were sufficiently large to accommodate the passage of the ligand, whereas other class A GPCRs have a solvent-exposed ligand entry to the binding pocket. Compound **54** seems to access the binding pocket through the lipid bilayer between TM6 and -7 in a similar mode proposed for the binding of retinal to rhodopsin and sphingosine-1-phosphate (S1P) to the $S1P_1$ receptor. Another interesting observation was the identification of an allosteric modulator, the Na^+ ion, which resides in a central water-mediated hydrogen bond network with highly conserved residues of class A GPCRs.

2.2.3.5. Angiotensin II Type-1 Receptor (AT_1R). One of the angiotensin receptor subtypes, AT_1R, serves as an interesting target for its role in cardiovascular pathophysiology. It has been reported that both G protein-dependent and -independent signaling are vital for normal cardiovascular homeostasis and cardioprotective benefits, respectively. However, chronic activation of the receptor could lead to detrimental outcomes, such as cardiac hypertrophy and heart failure. Hence, it is necessary to regulate the receptor signaling by the introduction of AT_1R inhibitors. Previously, several antihypertensive drugs were developed as AT_1R blockers (ARBs). However, the structural data on the activation and inhibition mechanisms remain elusive, thereby preventing the rational optimization of lead compounds.

The room-temperature crystal structure of the inactive human AT_1R in complex with a high-affinity inhibitor **55** (ZD7155)[115] was recently determined using the latest developed method of serial femtosecond crystallography with LCP as a growth and carrier matrix for delivering microcrystals into an xFEL beam. The antagonist-bound AT_1R structure shares structural similarities with other GPCR members, and it possesses many new and unique structural aspects of the receptor. The structural architecture of AT_1R is composed of the canonical 7TM helices with an extracellular N-terminus, three ICLs, three ECLs, an amphipathic helix 8, and an intracellular C-terminus. The overall fold is similar to that of the peptide receptors, including chemokine and opioid receptors. In most of the solved GPCR structures, helix 8 runs parallel to the membrane bilayer, whereas in AT_1R, the orientation of helix 8 is similar to that of CCR5 in which the amphipathic helix is angled away from the membrane. The binding mode of antagonist **55** in AT_1R partially overlaps with the known ligand binding sites of chemokine and opioid receptors. The ligand forms critical interactions with three unique AT_1R residues, $Y35^{1.39}$, $W84^{2.60}$, and $R167^{ECL2}$, which have not been previously implicated in the binding of small molecule ligands. $R167^{ECL2}$ and $Y35^{1.39}$ are involved in ionic and hydrogen interactions, and $W84^{2.60}$ is involved in $\pi-\pi$ interactions with the ligand. These nonconserved residues define the unique ligand binding pocket of AT_1R and explain the reason for the paucity of cross-reactivity observed between ligands binding to this receptor and other peptide receptors. Furthermore, on the basis of the AT_1R-**55** crystal structure, the authors performed mutagenesis and energy-based docking simulations to elucidate the structural basis for the receptor modulation by several other antihypertensive drugs.

2.2.3.6. Orexin Receptors (OX_1R and OX_2R). The orexin (also called hypocretin) receptor binds to the neuropeptides orexin A and orexin B, resulting in an increase in the intracellular calcium levels. There are two receptor subtypes, OX_1R and OX_2R, and orexin B shows 10-fold selectivity for OX_2R, whereas orexin A is equipotent for both subtypes. Because the inhibition of this signaling serves as an effective therapy for treating insomnia, obesity, pain, and addiction, dual orexin receptor antagonists (DORAs) were developed and tested over the past decade, resulting in FDA approval of the first in-class inhibitor **56** (suvorexant) for insomnia.[116] This drug binds to both human orexin receptor subtypes with subnanomolar affinity and antagonizes orexin signaling. High-resolution 3D structures of both OX_1R and OX_2R bound to this anti-insomnia drug **56** have been solved.[117,118] In 2016, another structure of hOX_1R was crystallized in complex with its selective antagonist **57** (SB-674042).[118]

The overall topology of hOX_2R is highly similar to other peptide-like receptors (NTSR1, μ-OR, and CXCR4). The β-hairpin structure has been observed in the ECL2 of OX_2R, which contains residues critical for orexin binding and activation. In the hOX_1R structures, an N-terminal helix is present on top of the orthosteric site, which appears to be important in the recruitment and binding of orexin peptides for receptor activation but not visible in the hOX_2R structure. However, sequence conservation suggests that this structural motif is present in both receptor subtypes. In both receptor subtypes, **56** binds deeply in the ligand binding pocket without making any direct contacts with the divergent extracellular regions and adopts a π-stacked horseshoe-like conformation (Figure 15A). Moreover, the binding conformation of **57** in hOX_1R is found to be similar to that of **56** despite their differences in chemotype (Figure 15B).

The ligand selectivity of these two subtypes was elucidated with the help of docking experiments using hOX_1R-selective compound **57** into the binding site of the hOX_2R structure.[118] The authors identified unfavored contacts with two threonine residues ($T135^{3.33}$ and $T111^{2.61}$), which upon mutation significantly increased the affinity of the hOX_1R-selective compound but did not affect the binding of other nonselective compounds. On the basis of the structure of hOX_2R-**56**, the authors performed molecular docking analysis for three additional orexin inhibitors that possess distinct chemical scaffolds. The predictions of similar π-stacked conformations suggested that this pharmacophore characterization would be a

DOI: 10.1021/acs.jmedchem.6b01453
J. Med. Chem. 2018, 61, 1−46

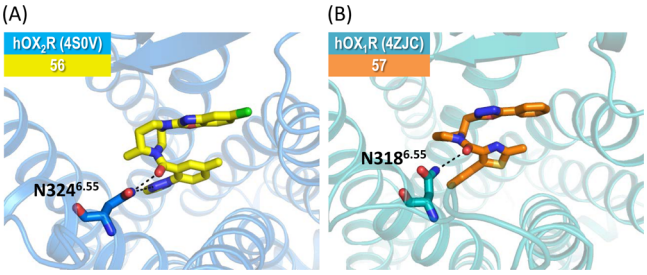

Figure 15. Ligand–receptor interactions observed in the crystal structures of orexin receptors. Key residues are represented as sticks, and the hydrogen bonds are marked with black dashed lines. The extracellular view of receptor–ligand complexes correspond to (A) OX_2R-**56** and (B) OX_1R-**57**.

generally favorable design aspect for other synthetic molecules targeting the receptor. These structural studies could provide clues for understanding how different small molecule drugs might be better designed to tune sleep and wake disorders in humans.

2.2.3.7. Endothelin ET_B Receptor. Endothelin (ET)-1, ET-2, and ET-3 participate in endothelin signal transduction via the receptor subtypes ET_A and ET_B. Both subtypes are involved in a number of physiological functions, such as cell proliferation, neural crest development, and regulation of vascular tone, Na^+ excretion, and salt homeostasis.[119−121] The ET_B receptor primarily induces NO-mediated vasorelaxation and also acts as a scavenger. A highly ET_B-selective peptide agonist, *N*-succinyl-(Glu,[9] Ala[11,15])-ET-1_{8-21} (IRL-1620), which is in clinical trials, aids the delivery of anticancer agents to the tumor by improving blood flow.[122] This agonist is also found to decrease the progression of Alzheimer's disease (AD) in animal studies, thereby signifying the importance of the ET_B receptor in AD and other neurovascular degenerative diseases.[123] The structures of ET_B receptor in both the ligand-free form and in complex with its natural agonist ET-1 were recently elucidated.[93]

Similar to other peptide receptors, the ECL2 of ET_B receptor forms long and antiparallel β-strands with a short hairpin structure. ET-1 adopts a bicyclic architecture with two intrachain disulfide bonds. As observed in the previous X-ray or NMR structures of ET-1 and ET-1-like peptide,[124−126] the N-terminus and α-helical regions of ET-1 are stable, whereas the C-terminus is highly disordered. In the complex structure of ET-1 and ET_B receptor, the C-terminus of ET-1 penetrates into the receptor core and is in close proximity to the N-terminus, thus attaining its stability. The orthosteric binding pocket of the ET_B receptor is much larger than that of other peptide-like receptors. The C-terminal W21 of the ET-1 peptide interacts with K182$^{3.33}$ and simultaneously with W336$^{6.48}$ (CWxP motif), thereby maintain-

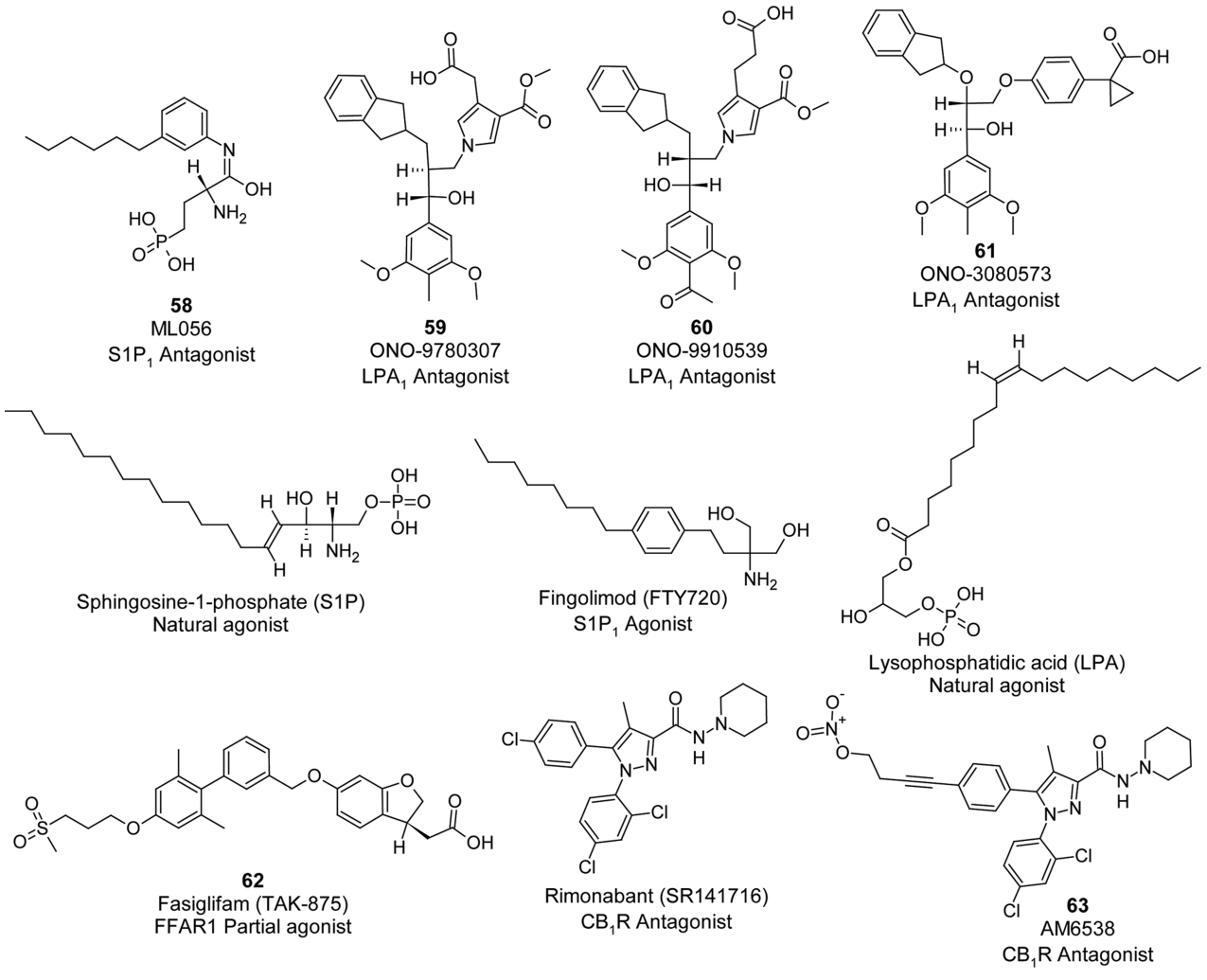

Figure 16. Chemical structures of the endogenous ligands and drug molecules of lipid-like GPCRs reported in this perspective.

DOI: 10.1021/acs.jmedchem.6b01453
J. Med. Chem. 2018, 61, 1−46

ing the agonistic potency of the ligand. Moreover, mutation analysis also emphasized the importance of the C-terminus and α-helical regions of ET-1 in the tight binding of ligand−receptor interactions.[93]

The structural comparison between ligand-free and -bound complex systems showed significant rearrangements in the extracellular orthosteric binding pocket. In the ligand-free structure, the TM helices are loosely packed, thus creating a broad entrance for the binding of peptide ligands, whereas in the ET-1 bound structure, the binding pocket contracts and adopts a compact, closed configuration associated with the movements of TM helices and enables a tighter interaction with the substrate. Furthermore, the N-terminus and ECL2 β-sheet of the receptor form a lid-like structure covering the ligand binding pocket. These structural aspects account for the quasi-irreversible binding nature of ET-1. The binding of ET-1 also induces large reorganization in the polar interaction network ($N119^{1.50}$, $D147^{2.50}$, $N378^{7.45}$, and $N382^{7.49}$) of the receptor bridging TM1, -2, and -7 and inward motion of the extracellular portions of TM6 and -7. These structural rearrangements are considered crucial in receptor activation.

2.2.4. Lipid-like Receptors. Some lipids interact directly with their targets, whereas others interact with extracellular or intracellular receptors. It has been suggested that minor modifications to lipid mediators abolish their effect, further indicating that lipid-like GPCRs may identify their ligands in a highly selective manner.[127] The mechanisms by which GPCRs recognize lipid-like ligands have received a considerable amount of attention.[128] In the last five years, more than five structures have been solved for four lipid-like receptors, including lysophospholipid receptors ($S1P_1$ and LPA_1),[129,130] FFAR1[131] (also known as GPR40), and CB_1R. These crystal structures have been solved in the presence of antagonists (Figure 16) and could provide new insights into the development of ligands with therapeutic potential.

2.2.4.1. Lysophospholipid Receptors ($S1P_1$ and LPA_1). Sphingosine 1-phosphate (S1P) and lysophosphatidic acid (LPA) are the most well-studied lysophopholipids, which exert their biological effects through receptor subtypes designated as $S1P_{1-5}$ and LPA_{1-6}, respectively.[132] Both $S1P_1$ and LPA_1 receptors belong to the endothelial differentiation gene (EDG) family of lipid receptors, which recognize similar ligands. These receptors share a sequence similarity of 41% in their TM domains; however, they show diversity in their overall structures.[133] $S1P_1$ has become a promising therapeutic target in cancer and chronic inflammatory diseases, and LPA_1 has been implicated in treating cancer, fibrosis, hydrocephalus, infertility, and pain. Remarkably, one nonselective $S1P_1$ agonist prodrug, 2-amino-2-[2-(4-octyl-phenyl)ethyl]propane-1,3-diol hydrochloride (FTY720, fingolimod), has been approved for the treatment of multiple sclerosis.[134] Moreover, compounds developed targeting LPA receptors have entered Phase II clinical trials for treating systemic sclerosis and pulmonary fibrosis.[130]

Two crystal structures of T4L-fused $S1P_1$ in complex with the sphingolipid mimic antagonist **58** (ML056)[129] were solved at resolutions of 3.35 and 2.8 Å, respectively, using different X-ray diffraction data processing methods. Three structures of the second member of EDG, LPA_1, was recently determined in complex with ONO compounds (**59** (ONO-9780307), **60** (ONO-9910539), and **61** (ONO-3080573)) in the inactive state.[130] Overall, a structural comparison of $S1P_1$ and LPA_1 revealed similar helical orientations, although a few structural divergences were observed, particularly in the orthosteric pocket. Similar to most class A GPCRs, LPA_1 ligands presumably enter from the extracellular surface, whereas in $S1P_1$, the orthosteric pocket is blocked from the outside by the N-terminal helix cap and ECL2. Therefore, the $S1P_1$ ligands may gain access to the orthosteric pocket through the gap between the TM1 and -7 helices. In the orthosteric binding site, the zwitterionic headgroup of **58**, which mimics the natural substrate S1P, forms a strong ionic interaction with the charged amino acid residues. The lipophilic tails of **58** are located in an aromatic pocket formed by the residues in TM3−7.

Moreover, the TM1 tip of LPA_1 is positioned 3 Å closer to TM7 compared to that of $S1P_1$, further supporting the differences observed in the ligand binding pathways. The short region between TM1 and the N-terminal helix cap is a helical segment in $S1P_1$ but is a loop (lacks secondary structure) in LPA_1, possibly providing easy accessibility to the ligand binding pocket. The shape of the LPA_1 extracellular ligand binding pocket is spherical, enabling the receptor to recognize a larger set of diverse chemical compounds than does $S1P_1$, whose binding pocket is rigid and linear. The difference in the binding pockets between the receptors is caused by three changes in the residue compositions: (1) at position 3.33, the residue is D in LPA_1 and an F in $S1P_1$; (2) at position 5.43, LPA_1 has a W, whereas $S1P_1$ has a C; and (3) at position 6.51, LPA_1 has a G, whereas $S1P_1$ has an L.

2.2.4.2. Free Fatty-Acid Receptor 1 (FFAR1). FFAR1 (previously known as human GPR40) binds free fatty acids and is primarily localized in pancreatic β-cells; it has been implicated in the treatment of type II diabetes due to its involvement in the regulation of insulin secretion, glucose homeostasis, and metabolic processes. Compound **62** (TAK-875, fasiglifam)[135] is an orally available, highly potent, and selective FFAR1 ago-allosteric modulator, which was discovered via HTS and optimized by Takeda Pharmaceuticals. This compound was further examined in clinical trials for the treatment of type II diabetes; however, the development was discontinued at the end of 2013 due to liver safety concerns.

After termination of the clinical trial, Takeda published the high-resolution X-ray crystal structure of FFAR1 bound to **62**.[131] This complex structure reveals a unique noncanonical site for the binding of **62** formed by TM3−5 and ECL2 and is closer to the exterior membrane surface than most other GPCR ligands. ECL2 serves as the roof of the ligand binding cavity with $E172^{ECL2}$ hydrogen bonded to $R258^{7.35}$. Additionally, $W174^{ECL2}$ is oriented in a perpendicular manner to the plane of the dihydroisobenzofuran ring of **62**, forming an edge-on interaction. Despite having low sequence identity, this receptor shows structural similarity with peptide-like GPCRs. Compound **62** has been suggested to enter the ligand binding pocket of the receptor through the lipid bilayer interface from the extracellular side between TM3 and -4. The carboxylate moiety of this modulator interacts with the arginine residues of the receptor, including $R183^{5.39}$ and $R258^{7.35}$. The structure further reveals that the stabilization of the carboxylate moiety is achieved via tyrosine residues $Y91^{3.37}$ and $Y240^{6.51}$, indicating the presence of a complex charge network. In addition to the binding site of **62** (site 1), the structure revealed two extra binding pockets (sites 2 and 3). Site 2 is adjacent to **62**, potentially allowing a ligand to pass between TM4 and -5. This site may also support the entry of additional ligands via the lipid bilayer. The third binding pocket, site 3, is located close to the orthosteric binding pocket between TM1 and -7, similar to the binding site of allosteric modulator **23** in M_2R. This structure

DOI: 10.1021/acs.jmedchem.6b01453
J. Med. Chem. 2018, 61, 1−46

reveals the lipid entry of the ligand and the structural conservation between lipid- and peptide-like receptors.

2.2.4.3. Cannabinoid Receptor (CB_1R). Cannabinoid receptors are primarily activated by three groups of ligands, such as endocannabinoids, plant cannabinoids, and synthetic cannabinoids. So far, only two subtypes of cannabinoid receptors, CB_1R and CB_2R, have been cloned, which share a sequence identity of 48% and differ in their sensitivity and signaling mechanisms. CB_1R is the most highly expressed GPCR in the human brain (CNS), and also in the lungs, liver, and kidneys, whereas CB_2R is expressed primarily in the immune system and hematopoietic cells. Molecules that target CB_1R have shown therapeutic promise for treating a variety of conditions, including pain, inflammation, neurodegenerative diseases, multiple sclerosis, obesity-related metabolic disorders, and liver fibrosis. 5-(4-Chlorophenyl)-1-(2,4-dichlorophenyl)-4-methyl-*N*-1-piperidinyl-1*H*-pyrazole-3-carboxamide (SR141716, rimonabant)[136] was the first identified CB_1R-selective antagonist approved by the European medical agency for treating obesity; however, this drug was not approved in the U.S. due to safety concerns.[136,137] For structural insights into the binding mechanism of human CB_1R to be obtained, the crystal structure of the receptor in complex with stabilizing antagonist **63** (AM6538)[138] was recently elucidated.

The structural features of CB_1R include a unique V-shaped N-terminal loop conformation (acting as a plug) that inserts into the ligand binding pocket. The ligand binding pocket seems to be quite enlarged and complicated with multiple subpockets and channels. Compound **63** is observed to be situated at a lower position in the pocket, right above the conserved $W356^{6.48}$. The ligand forms hydrophobic interactions with ECL2, N-terminus, as well as with all TM helices except helix IV. The structure of this ligand consists of a pyrazole ring core with three functional groups (forming three-arm structure): the 2,4-dichlorophenyl ring termed "arm 1", 4-aliphatic chain substituted phenyl ring termed "arm 2", and piperidin-1-ylcarbamoyl termed "arm 3". The 3D structure identified that the arm 1 part is important for high-affinity binding, arm 2 extends into the long channel, and the aromatic or aliphatic ring on arm 3 pushes on helices I and II, thereby modulating the pharmacological signaling state of the receptor. In addition to the structural data, modeling analysis also revealed that a bulky ring in arm 3 is essential for portraying CB_1R antagonism.[138] The authors suggest that this observation may pave way for the design of several pharmacologically effective compounds with novel therapeutics.

3. STRUCTURAL INS AND OUTS OF THE CLASS A GPCR SUPERFAMILY

3.1. Effect of Shuffling among TM Helices on Class A GPCR Signaling. From the available crystal structures of class A nonrhodopsin GPCRs, it is clear that the structure of the 7TM fold is highly conserved. However, structural diversity has been observed in the loop regions and helical bundle, which are more prominent on the extracellular side of the receptors. Several biochemical and biophysical studies emphasize that GPCR activation is associated with the remarkable large-scale structural rearrangement of TM helices, thereby leading to different receptor conformational states and differential effects on downstream signaling effectors.[139,140] The seven α-helices display different tilts and rotations, resulting in the ligand binding pocket differences, which vary dramatically in size and shape. The global reshuffling of TM helices is often designated as rigid body motions in the active state of the receptor.[141]

Comparisons of individual helices in the active and inactive structures of GPCRs reveal local deformations of the helices in the activated state. One of the most prominent deformations is the "Pro kink" observed around the highly conserved $P^{6.50}$ in TM6. The superimposition of the extracellular regions of TM6 in active and inactive structures of β_2AR shows a "swinging motion" and elastic bending of the intracellular region of TM6 in concert with a movement of TM5 in the activated state of the receptor. The magnitude of this motion varies among several class A GPCRs and shows different activated conformations.[142] Another pronounced structural rearrangement of TM helices has been observed in TM3 and -7 during receptor activation. The intracellular region of TM7 moves inward toward the middle axis of the 7TM bundle and undergoes a substantial rearrangement in the backbone of the conserved NPxxY motif. Thus, in the active state of the receptor, the TM-helical rearrangements involve the outward movement of TM5 and -6 and the inward movement of TM7, which are essential for G protein coupling and subsequent activation. In addition to the intracellular motions of TM helices, the extracellular portions of the TM-helical bundle also play a critical role in the receptor activation. A comparison of $P2Y_{12}R$ active and inactive structures suggests that the extracellular tips of TM6 and -7 shift approximately 5−10 Å toward the central axis of the 7TM helical bundle (Figure 11C).[8]

Recently, it has been proposed that, although class A GPCRs show diverse "activation pathways", these pathways converge near the G protein coupling region.[143] Despite the diversity in the reshuffling of the residue contacts upon receptor stimulation, four contacts involving seven residues (3 × 46 in TM3 with 6 × 37 in TM6; 7 × 53 in TM7 with 1 × 53 and 8 × 50 in TM1 and -8, respectively; and 7 × 54 in TM7 with 8 × 51 in TM8; the notation represents the GPCRdb numbering scheme) and two contacts involving four residues (3 × 46 in TM3 with 7 × 53 in TM7, and 5 × 55 in TM5 with 6 × 41 in TM6) are maintained exclusively in all inactive- and active-state structures, respectively. Overall, the rearrangement of contacts involving residue positions 3 × 46 in TM3, 6 × 37 in TM6, and 7 × 53 in TM7 is likely to be conserved and potent for activation in all class A GPCRs. This finding explains the ability of GPCRs to bind to a common repertoire of G proteins although stimulated by diverse ligands.

3.2. Relevance of Conserved Structural Features among Class A GPCRs. One of the hallmarks of class A GPCR structures is the conservation of several functionally important signature sequence motifs commonly known as molecular microswitches in the 7TM helical bundle. The solved crystal structures of class A GPCRs illuminate the structure and function of these conserved motifs. Prior to the discovery of GPCR X-ray structures, the functional dynamics of these microswitches were identified based on the rhodopsin structure as well as mutational and biophysical data. In general, these motifs play important roles in the regulation of GPCR activation and signaling, behaving as a switch between the active and inactive receptor conformations.

One of the most conserved motifs is the $D[E]R^{3.50}Y$ motif in TM3, which forms an "ionic lock" by making a salt bridge with $D/E^{6.30}$ in TM6. This ionic lock has been suggested to play a role in maintaining the inactive state of GPCRs by locking helices 3 and 6 together, thus impairing the active conformation of the receptor marked by the outward shift of TM6. Upon comparison with rhodopsin structures, class A nonrhodopsin GPCRs reveal a slightly increased distance between TM3 and -6, which is sufficient to break the ionic bond.[141] Recent studies suggest that

DOI: 10.1021/acs.jmedchem.6b01453
J. Med. Chem. 2018, 61, 1−46

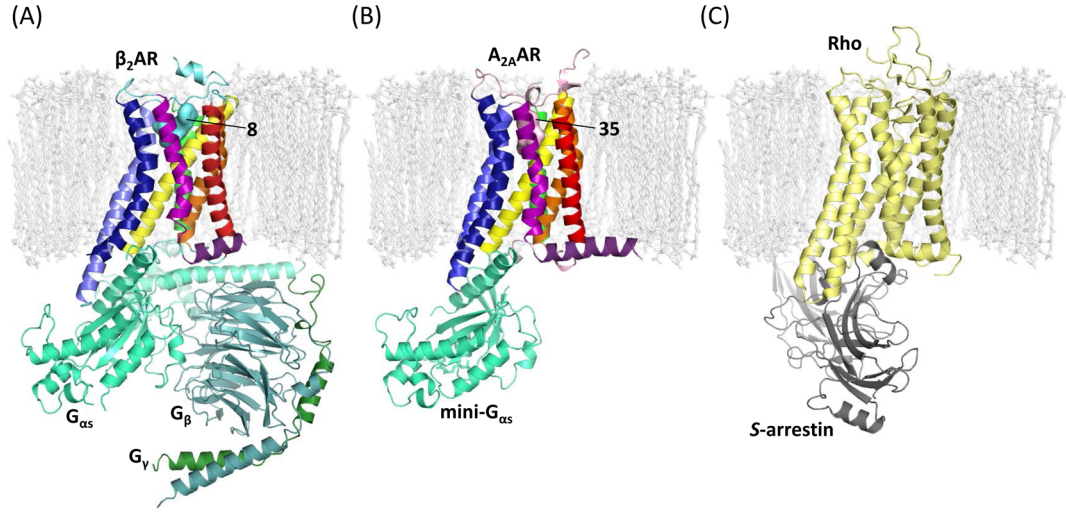

Figure 17. X-ray crystal structures of GPCR coupled to either G protein or arrestin. Direct structural visualization of GPCR signaling complexes is a major breakthrough in GPCR biology. Considering the transient nature of these signaling complexes, advanced technologies were required to capture such receptor−effector complexes to understand the molecular basis of GPCR signaling. Such structural advances in GPCR biology were accomplished with the release of GPCR structures coupled to either G protein or arrestin. The displayed GPCR signaling complexes correspond to (A) β_2AR and the heterotrimeric Gs protein, (B) A_{2A}AR and the mini-Gs, and (C) rhodopsin (Rho) and S-arrestin. The surrounding lipid bilayers are displayed as light-gray sticks.

this motif is not universally present in all GPCR classes; however, it can form during conformational dynamics as observed by microsecond MD simulations. In the rhodopsin and A_{2A}AR structures, the $R^{3.50}$ residue forms an "ionic lock" with $E^{6.30}$, which appears to be broken in the active state of the receptors.

The $C^{6.47}W^{6.48}xP^{6.50}$ motif in TM6 is considered as another common microswitch, which serves as a marker for the activation state of the receptor. This "transmission switch" (previously known as a "Toggle switch") harbors the highly conserved $W^{6.48}$ residue. Before the advent of GPCR crystal structures, it was hypothesized that the $W^{6.48}$ residue "toggles" or flips between two conformations in the receptor active and inactive states. However, a comparison of active and inactive receptor conformations revealed that there is a shift in the $W^{6.48}$ side chain toward TM5 and not a flip, which serves as a link between the ligand binding site and the movement of TM5 and -6 via the rearrangement of the TM3, -5, and -6 interfaces. In the rhodopsin and A_{2A}AR structures, a conformational shift in the $W^{6.48}$ side chain and a movement of TM6 has been observed upon agonist binding.

Another conserved $N^{7.49}P^{7.50}xxY^{7.53}$ motif positioned in the cytoplasmic end of TM7 plays a potent role in the activation of GPCRs, which is known to constrain TM7 with TM1 and -2 and TM7 with helix 8. In the ligand-free opsin structure, the $Y^{7.53}$ residue rotates to face the TM helical bundle, thus preventing the transition of the receptor into its inactive state by blocking TM6 from moving back toward TM3. Furthermore, the active structure of β_2AR in complex with the G_s protein showed the significance of the $Y^{7.53}$ residue ($N^{7.49}P^{7.50}xxY^{7.53}$ motif) in packing the interaction of $R^{3.50}$ (D[E]$R^{3.50}$Y motif) with the G protein binding partner, indicating the concerted action of both motifs.

In addition to the presence of conserved motifs in the TM bundle, some portions of the extracellular regions are also highly conserved. Except for the $S1P_1$ and $P2Y_{12}$ receptors, a highly conserved disulfide bridge connecting two cysteine residues in the extracellular tip of TM3 ($C^{3.25}$) and ECL2 was observed in most of the GPCRs. This disulfide bond is critical in stabilizing the conformation of extracellular regions and shaping the ligand binding site entrance. $S1P_1$ is one of the receptors that lacks the highly conserved $C^{3.25}$ residue, the corresponding disulfide bridge, and the secondary structure in ECL2. The $P2Y_{12}R$ structure has the conserved $C^{3.25}$ residue but lacks the disulfide bridge between ECL2 and TM3, thereby suggesting that the bridge may be labile in the native structure.[82]

3.3. Molecular Intricacies of GPCR Signaling Transduction. For the molecular mechanisms of GPCR signal transduction to be understood, it is necessary to solve the active structures of the receptor in complex with a G protein as well as the inactive structures. Recent breakthroughs in X-ray crystallography have led to a better understanding of the molecular basis of 7TM receptor signaling via the determination of complex structures of GPCRs coupling to either G protein or arrestin. Consequently, the complex structures of bovine rhodopsin bound to a G protein peptide (rhodopsin/GαCT),[144] β_2AR coupled to Gs-protein (β_2AR/Gs complex)[27] (Figure 17A), β_2AR coupled to β-arrestin 1,[29] human rhodopsin in complex with a preactivated mouse visual arrestin[145] (Figure 17C), and A_{2A}AR coupled to a mini-Gs protein (A_{2A}AR/mini-Gs)[75] (Figure 17B) have been determined in recent years.

The long awaited structure of agonist-bound active β_2AR coupled with the full heterotrimeric Gs protein was released in 2011, and it became the first active complex to elucidate the molecular basis of receptor activation. In general, any active structure will undergo large-scale motions; hence, it would be difficult to crystallize these transient active-state conformations. The structures were captured in a transient active conformation state of β_2AR with an intracellular binding partner, which was either a G protein mimicking nanobody, Nb80 (heavy chain of a camelid antibody),[26] or the native nucleotide-free G protein.[27] Additionally, the complexes were further stabilized by high-affinity low-dissociating agonist **8**. The activated ternary complex β_2AR/Gs revealed significant changes in the intracellular regions of the TM helices. An outward movement of TM5 and -6 followed by the inward movement of TM3 and -7 helices resulted in a cavity that could accommodate the intracellular G protein

DOI: 10.1021/acs.jmedchem.6b01453
J. Med. Chem. 2018, 61, 1−46

binding partner. The Gs protein is observed to bind at a cleft between TM5 and -6 induced by a large shift of TM6 and the helical extension of TM5. Specifically, R131$^{3.50}$ and F139$^{3.58}$ form critical contacts with the α-subunit of the Gs protein. Additionally, conformational changes were observed in the highly conserved motifs, including R$^{3.50}$ of the DRY-motif, Y$^{7.53}$ of the NPxxY-motif, and Y$^{5.58}$ at the bottom of TM5. The extracellular regions of the β_2AR/Gs complex exhibited less pronounced differences compared to those of the intracellular domains. Hydrogen bond interactions of **8** to S$^{5.42}$ and S$^{5.46}$ residues lead to an inward shift of TM5 around S$^{5.46}$, thus altering the conformation of a hydrophobic switch. Interestingly, electron microscopy studies have gleaned structural insights into the association of β_2AR with β-arrestin 1, which has been observed to interact using a biphasic mechanism, initiating contact with the C-terminal domain of β_2AR followed by weak interactions with the receptor core.[29] The architecture of the β_2AR/β-arrestin 1 complex reveals that the N-terminal of β-arrestin primarily engages with the receptor, leaving the C-terminal domain outside the interaction interface, which serves as a nucleation point for β-arrestin interaction proteins.

After a gap of five years, the highly anticipated structure of A_{2A}AR in complex with an engineered G protein was solved very recently. The complex was stabilized by engineering a minimal thermostabilized version of a Gαs protein, referred to as mini-Gs, containing several truncations and eight mutations to stabilize the receptor in the absence of other G protein binding partners, G$\beta\gamma$. Mini-Gs binds to A_{2A}AR via an extensive interface area of approximately 1048 Å^2, which is similar but not identical to that of the β_2AR/Gs complex interface. The transition of the receptor from an active intermediate state to an active G protein-coupled state is characterized by a 14 Å shift in the cytoplasmic end of TM6 away from the 7TM core, a slight shift in the positions of the cytoplasmic ends of TM5 and -7, and rotamer changes in the highly conserved amino acid side chains, including R$^{3.50}$, Y$^{5.58}$, and Y$^{7.53}$, with no substantial changes in the extracellular half of the receptor. A superimposition of the receptors in the A_{2A}AR/mini-Gs and β_2AR/Gs complexes reveals a similar architecture. However, the G proteins do not superimpose in an identical position, showing a slight difference in the orientation of the C-terminal α5-helix, which may be due to differences in the amino acid residues between receptors or from different stabilization and crystallization conditions. Although the orientations and atomic contacts differ, many of the contacts between the receptors and the α5-helix of the Gs proteins are highly conserved. The main differences seen in these two complexes are due to the disparity in the amino acid residues at the TM7-helix 8 boundary (where mini-Gs is observed to make a few contacts with the receptor boundary but Gs of β_2AR does not make any) and the cytoplasmic end of TM5, which is extended in β_2AR by an additional turn compared to A_{2A}AR. Furthermore, a comparison of the active-intermediate A_{2A}AR-**36** and active A_{2A}AR/mini-Gs complexes reveals major rearrangements in the cytoplasmic half of the receptor to accommodate G protein binding. The structural elucidation of these important oligomeric signaling complexes inspires a full spectrum of mechanistic studies into GPCR signaling that can eventually lead to their functional understanding and pharmacological targeting. Moreover, the highly conserved nature of GPCR activation in these two complexes (Figure 17A, B) suggests that the other class A nonrhodopsin GPCRs may also follow similar activation mechanisms. However, this notion can be confirmed only after the elucidation of other active signaling complexes.

3.4. Structural Insights into Allosteric Modulation by Sodium Ions. One of the most interesting findings among the crystallographic studies of class A GPCRs is the identification of a conserved allosteric Na^+ ion binding site.[146] Pioneering studies on opioid receptors using brain homogenates in the 1970s provided the first indication of the allosteric effects of Na^+ in class A GPCR signaling.[147] This seminal work suggested that the physiological concentrations of Na^+ negatively modulated the binding of agonists to opioid receptors without affecting the antagonist binding efficacy. Later, similar negative allosteric effects were observed for several class A GPCRs, including α-adrenergic, dopaminergic, neurotensin, serotonergic, and others.[146] Although the allosteric effects of Na^+ on GPCR agonist binding and activation have been known previously, their structural insights were only recently revived by the release of a few ultra-high-resolution crystallographic structures of class A GPCRs, which reveal important details about the "sodium allosteric site".

The high-resolution structure of A_{2A}AR provided the first direct experimental evidence of a Na^+/water cluster in the 7TM core region, which suggests the existence of a Na^+ allosteric site of GPCR.[77] Shortly thereafter, high-resolution inactive crystallographic structures of PAR1,[78] β_1AR,[80] and δ-OR[79] also revealed the presence of the Na^+ ion in the same position. The Na^+ ion binding to highly conserved residue D$^{2.50}$ appears to be a common characteristic among class A GPCRs.[146] This highly conserved D$^{2.50}$ site forms an allosteric pocket composed of a bound Na^+ ion and a cluster of structurally ordered water molecules forming hydrogen bonds with several highly conserved class A GPCR residues, including L$^{2.46}$, A$^{2.49}$, W$^{6.48}$, N$^{7.45}$, and N$^{7.49}$, in the inactive state of the receptor.[77] The activation of GPCRs requires the collapse of the D$^{2.50}$ allosteric pocket, leading to the structural rearrangement of TM helices, especially the inward shift of the NPxxY motif in TM7,[77] further resulting in a smaller binding pocket, which contains a maximum of three water molecules. This narrow binding pocket would not provide sufficient coordination for a Na^+ ion, thus supporting the notion that high-affinity agonist binding and the presence of Na^+ are mutually exclusive. Therefore, the availability of these high-resolution structures might explain the observed negative allosteric effects of Na^+ ions on agonist binding.

Along with these breakthroughs in GPCR structural biology, computational simulations were also conducted to investigate the binding of a Na^+ ion to D$^{2.50}$ and its allosteric effects on the class A GPCR dynamics. The mechanistic insights into the modulation of Na^+ for class A GPCR signaling were investigated using conventional molecular dynamics (cMD) for A_{2A}AR,[148] β_2AR,[149] D_2R,[150] and opioid receptors (μ-OR, δ-OR, and κ-OR[151,152]) and accelerated molecular dynamics (aMD) for muscarinic receptor M_3R.[153] Earlier cMD simulations performed at the microsecond time scale for D_2R captured the Na^+ binding to D$^{2.50}$ and identified three low-energy sites, including a D$^{3.32}$ ligand binding pocket, a cavity close to W$^{6.48}$, and a D$^{2.50}$ allosteric pocket along the binding pathway.[150] The 100 ns time scale MD simulations performed for A_{2A}AR in the presence or absence of a Na^+ ion implied that the binding of the ions and the high-affinity agonist binding are mutually exclusive by suggesting that the ion negatively modulates the activation-related conformational changes and prefers the inactive state of the receptor.[148] Previous microsecond time scale cMD simulations and free-energy calculations of β_2AR suggested that the protonation of the D79$^{2.50}$ residue shifts the conformation of the receptor toward more active-like states.[149]

DOI: 10.1021/acs.jmedchem.6b01453
J. Med. Chem. 2018, 61, 1−46

Several unbiased ms-scale MD simulations on the three opioid subtypes were performed to understand the differences observed in the Na^+ ion diffusion, and their results were interpreted along with the radio-ligand binding experiments.[152] The simulation results of all three ligand-free receptor systems showed that rapid ion permeation occurred, and they followed similar binding pathways. However, extra densities of the ions were observed near the nonconserved residues of κ-OR ($E^{6.58}$ and ECL2 D204) and δ-OR (D293 and D288 residues in ECL3) but not in μ-OR, which may account for its observed differentially increased antagonist binding affinity. This study further supported the notion that the binding of the Na^+ ion reduced the binding affinity of agonists in all three receptor subtypes. For the mechanistic implications of these ligand-free systems and the experimental evidence to be further supported, additional biased and unbiased MD simulations were conducted using the δ-OR high-resolution crystal structure as a model system.

Recently, extensive aMD simulations were conducted to study the effect of Na^+ ion binding on the dynamic activation of M_3R.[153] The ion was observed to bind to the deprotonated $D^{2.50}$ but not the protonated one. Following the binding of the Na^+ ion to the deprotonated $D^{2.50}$, M_3R tended to reduce the flexibility of the receptor, thereby shifting the conformation of the receptor toward the inactive state. Conversely, protonated $D^{2.50}$ M_3R undergoes activation by sampling a significantly larger conformational space.

3.5. Dimers or Higher-Order Oligomers. GPCRs were previously considered to exist only as monomers in the plasma membrane; however, emerging evidence in the past two decades has suggested that GPCRs can cross-react to form homodimers, heterodimers, and/or higher-order oligomers, which are primarily required for the modulation of receptor function.[154] In addition to receptor function, dimerization can also affect cellular trafficking, ligand pharmacology, mediation of cross-talk between GPCR pathways, and signaling processes. Both homo- and heterodimerization of GPCRs have been linked to specific functional outcomes; hence, targeting these oligomers as potential drug candidates could provide a novel source of drug specificity. However, the development of drugs against GPCR oligomers remains a demanding task because the extent, stability, and physiological consequence of dimerization are highly controversial even for the well-characterized class A GPCRs. In addition to the accumulation of experimental data from biochemical and biophysical studies, 3D structural information from X-ray diffraction techniques has garnered interest in the therapeutic targeting of GPCR oligomers. Structural intricacies into class A GPCR dimerization were provided by crystal structures of rhodopsin,[155] β_1AR and β_2ARs,[19,35] CXCR4,[89] and the opioid receptor subtypes κ-OR[106] and μ-OR.[103]

The first structural evidence supporting class A GPCR dimerization was based on the atomic force microscopy (AFM) map of rhodopsin, which showed arrays of dimers.[156] In the parallel receptor dimer, different TM helices are arranged in a head-to-head fashion. In κ-OR, the parallel receptor dimer structures are formed via TM1, TM2, and helix 8. In the CXCR4 structure, the parallel and symmetric dimer is mediated through TM5 and -6 covering ~850 Å of buried surface area. In addition to the TM5-TM6 interface contacts, the CXCR4 dimer structure also showed contacts at the intracellular ends of TM3 and -4. The dimer interface is virtually identical in all five different crystal packing forms of the chemokine receptor complexes with either a peptide or small molecule antagonist, suggesting its functional significance.[89] Two different interfaces were observed for μ-OR with one interface formed in a similar manner to κ-OR, involving TM1, TM2, and helix 8 burying 615 Å of the surface area. The second interface is formed through contacts with TM5 and -6 with a buried surface area of 1492 Å, which is analogous to that of the CXCR4 structure. However, this second TM5-TM6 interface may prevent either protomer from proper coupling to the G protein because the agonist-induced receptor-G protein interactions depend on these TM5 and -6 helical rearrangements.[103] The parallel dimer structure of β_2AR is formed by the ordered lipids composed of two cholesterols and two palmitic acid molecules in the C-terminal region. The crystal structure of the dimeric β_1AR is formed by two different interfaces with one interface formed through contacts with TM1 and -2, helix 8, and ECL1 and a second one involving TM4 and -5, ICL2, and ECL2, both of which were suggested to be physiologically relevant with cysteine cross-linking experiments.[35] It has been suggested that the inferred dimer interfaces may depend on the ligand-specific conformational state of the receptor.[157] The structural comparisons of the dimeric interfaces of β_1AR, CXCR4, and μ-OR suggested that the TM5 interface can partner in the interaction with TM4 or -6 depending on the conformational state of the receptor.[35] These solved dimer structures may serve as structural scaffolds to better understand the role of dimerization or oligomerization in the receptor signaling and in the potent development of bivalent ligands.

Although the solved structures described above provide atomistic details into the GPCR dimerization, unanswered issues remain, such as the rationale for receptor dimerization, the necessity of receptor dimers or oligomers in signaling processes, and the functional significance of oligomers in the physiological state. It is also necessary to understand the effect of different ligands and various conformational receptor states on the formation of different dimer interfaces. Thus, advanced structural and mechanistic insights into the oligomerization process and its effect on the signaling transduction are essential to provide additional information for the pharmacological exploitation of GPCR higher-order oligomers.

4. GPCR-TARGETING LIGANDS

4.1. Classification of GPCR Ligands. In classical medicinal chemistry approaches, drug discovery targeting GPCRs has evolved into either mimicking endogenous substrates resulting in the activation of GPCR signaling pathways (i.e., agonists) or designing structurally related compounds that occupy the same binding site like the natural agonist, i.e., orthosteric site, but do not cause receptor activation (i.e., antagonists). An inverse agonist is a molecule that binds to this orthosteric site; however, it elicits the opposite effect to that of a normal agonist demonstrating negative efficacy.

Recent advances in technology and our understanding of receptor structure and function have conferred several other possible opportunities targeting GPCRs.[100] For example, a novel type of GPCR ligand acts in a topologically distinct binding site, i.e., the allosteric site, from that of the endogenous ligand. These allosteric ligands can modulate the actions of the endogenous ligand to make it more potent (positive allosteric modulator (PAM)), less potent (negative allosteric modulator (NAM)), identical (silent allosteric modulator (SAM)), or may even have potency of its own (ago-allosteric). Some molecules act by targeting both orthosteric and allosteric sites (bitopic ligands) or even bridge a dimeric construct of GPCRs by binding simultaneously to the adjacent receptors (bivalent ligands). Another emerging approach for drug action is biased agonism in

DOI: 10.1021/acs.jmedchem.6b01453
J. Med. Chem. 2018, 61, 1−46

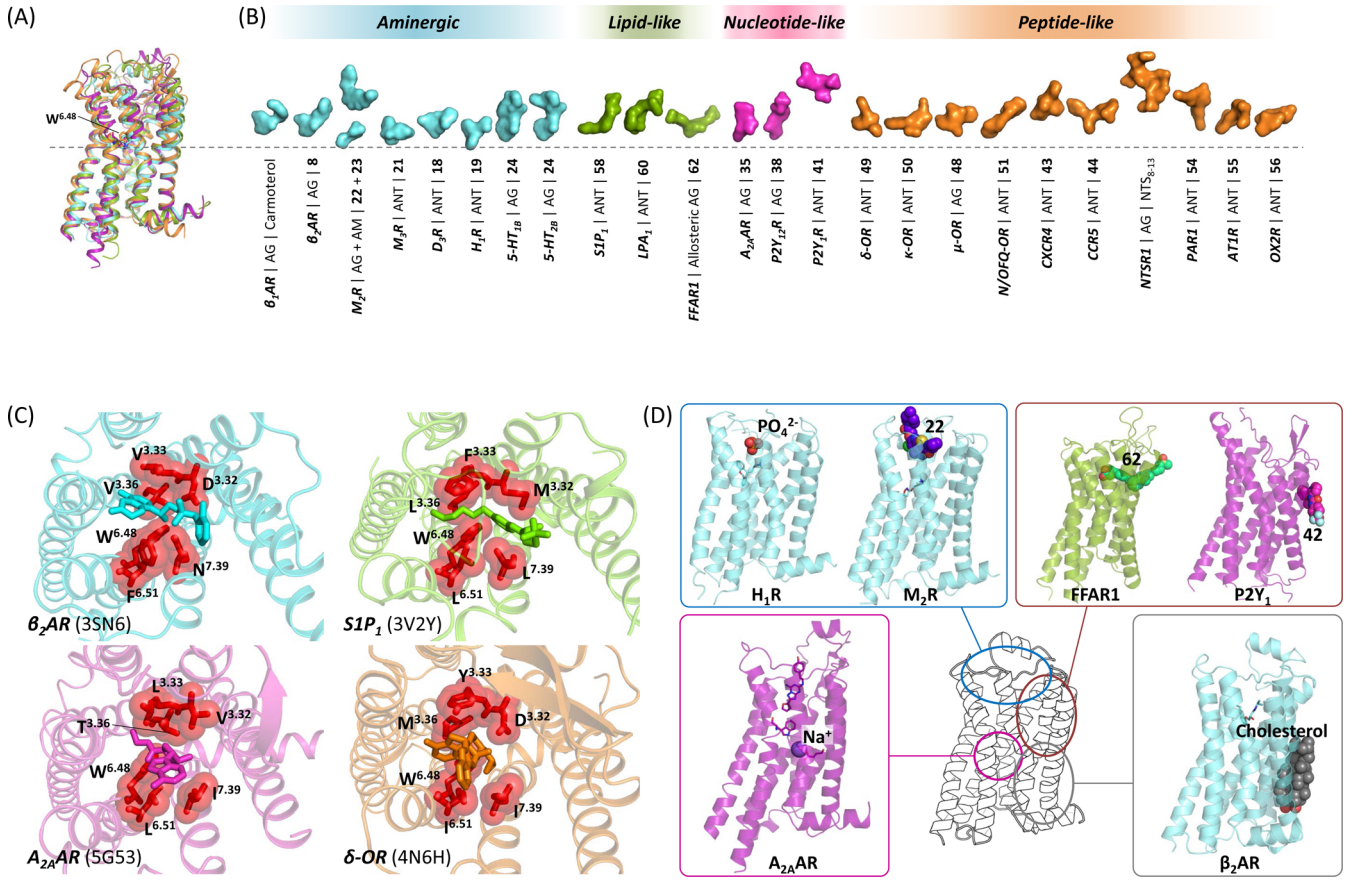

Figure 18. Orthosteric and allosteric binding sites of the class A nonrhodopsin GPCR family. (A) Aligned structures of the antagonist-bound β_2AR (cyan, PDB ID: 3NYA), A_{2A}AR (purple, 4EIY), $S1P_1$ (green, 3V2Y), and CCR5 (orange, 4MBS). In each structure, the $W^{6.48}$ residue of the CWxP motif is displayed as sticks. (B) Ligand binding depth in the orthosteric binding site of each class A nonrhodopsin receptor type. This figure is inspired and updated from the work by Venkatakrishnan et al.[158] (C) Positions of the consensus ligand binding contact across class A GPCRs. The secondary structures of β_2AR (PDB ID: 3SN6), $S1P_1$ (3V2Y), A_{2A}AR (5G53), and δ-OR (4N6H) are represented in cyan, green, purple, and orange, respectively, and the bound ligands are stick representations. Consensus ligand binding residues are depicted as red sticks with transparent spheres. The extracellular view is shown. (D) Location of the allosteric binding sites of the class A nonrhodopsin GPCR family identified by X-ray crystallography. Orthosteric and allosteric ligands are displayed as sticks and spheres, respectively. In the A_{2A}AR structure, the $W246^{6.48}$ and $D52^{2.50}$ residues are also represented as sticks for efficient visualization of the location of the sodium ion.

which a ligand can stabilize a unique receptor conformation resulting in the biased activation of one signaling pathway over another (biased ligands).[100]

4.2. Ligand Binding at the Orthosteric Site. All class A GPCRs share a common hepta-helical structure, and the ligands usually bind to the extracellular half of the 7TM helical bundle (Figure 18A, B). A remarkable feature of this finely tuned receptor family is its ability to bind with various endogenous ligands that display diverse shapes, sizes, and chemical properties and transmit signals corresponding to each ligand. Although the receptor family shares a common structural architecture, the sizes, shapes, and electrostatic properties of their orthosteric binding pockets are strikingly diverse among different receptors. Even in the same receptor family with a high overall structural similarity, ligand binding modes can vary depending on the receptor subtypes. Because detailed receptor−ligand interactions for each receptor family were described in section 2, here, we will focus on the common interaction pattern between class A nonrhodopsin GPCRs and the orthosteric ligands.

A systematic comparison of the receptor−ligand contacts revealed that there are some common structural features shared in all class A GPCRs. Although different ligands penetrate to different depths within the pocket (Figure 18B), most of the ligand-contacting residues are present on the inner side of the TM helices with the exception of peptidic ligands.[158] In particular, the topologically equivalent residues of TM3, -6, and -7 interact with diverse ligands in most of the receptors, whereas TM1 is not directly involved in contact with the ligand. The positions that form a consensus ligand contact across class A GPCRs include 3.32, 3.33, 3.36, 6.48, 6.51, and 7.39 (Figure 18C). In addition, among the consensus ligand-contacting residues, two pairs of residues (i.e., 3.36−6.48 and 6.51−7.39) are observed to form the consensus inter-TM contact network. A noncovalent contact seen between residues 6.48 and 6.51 in TM6 is also maintained in the structures. Additionally, water molecules are present in several structures mediating indirect contacts between the ligand and the receptor.[158]

These key positions in TM3, -6, and -7 are reported to form a "ligand binding cradle" in the helical bundle of nearly all class A GPCRs, whereas the residues in other TMs interact with specific ligands to different extents. Indeed, biochemical studies have shown that mutations in these consensus positions affect receptor conformational selectivity and ligand binding affinity. The variation in the amino acids occupying the topologically equivalent positions may contribute to ligand specificity in different receptors. This set of consensus ligand binding

DOI: 10.1021/acs.jmedchem.6b01453
J. Med. Chem. 2018, 61, 1−46

positions provides information regarding the ligand binding pockets of other GPCRs, the specificity of ligands among subfamilies of receptors, the molecular basis of cross-reactivity, and poly-pharmacology as well as aids in fragment-based drug design.

4.3. Biased Ligands. Over the past decade, the biased agonism concept has progressed due to technological and methodological advances.[159,160] The classical GPCR signaling paradigm has been redefined by the discovery of "biased signaling" (often used interchangeably with "functional selectivity"). Classically, GPCR was believed to function as a binary switch in which the receptor undergoes active and inactive conformational states upon ligand binding.[161] In the mid-1990s, it became clear that the GPCR signaling was more complex than the typical binary switch model. Distinct ligands referred to as "biased ligands" preferentially activate one downstream pathway over another, a phenomenon known as "biased agonism", which can produce distinct physiological outcomes.[162,163] Ligand bias can emerge from favored receptor coupling to β-arrestin over a G protein and vice versa. Most of the drug discovery efforts related to GPCR-biased signaling focus on identifying biased, orthosteric, and allosteric ligands that bind to the receptor extracellular regions with the aim of tuning the receptor conformation to couple to a specific signaling pathway.[164] More recently, several studies have focused on biasing GPCR signaling by targeting the intracellular regions of the receptors.[165,166]

Structural insights into the GPCR-biased signaling can be gleaned from the high-resolution structures of GPCRs bound to biased ligands.[167] These structures not only present intrinsic details about ligand−receptor interactions but also provide specifics of biased signaling at the receptor level. It has been suggested that biased ligands appear to be competitive with classical agonists and antagonists for several GPCRs by occupying the same ligand binding pocket. This type of biased ligand binding has been observed in the crystal structures of β_1AR bound to β-arrestin-biased ligands **16** or **17** (Figure 4D, E).[34] Comparisons of these biased ligand-bound β_1AR structures with agonist- or antagonist-bound ones reveal no large conformational changes on the cytoplasmic side of the receptor, and a few conspicuous differences could be noted in their orthosteric binding pockets. The arrestin-biased ligands show weaker interactions with TM5 than with full agonists, but additional ligand−receptor interactions with TM7 could affect the conformational states of this helix via a conserved activation pathway through TM2 or -7.[158]

Similarly, comparisons of β_1AR-biased ligand **17** with inactive β_2AR structure revealed that this ligand generated additional contacts with the receptor for inducing ligand bias.[168] The alteration of the local environment of the TM7-helix 8 interface is also confirmed by recent ^{19}F-NMR spectroscopy experiments and lanthanide-based resonance energy transfer spectroscopy studies.[168] These additional ligand−receptor contacts are speculated to be responsible for inducing ligand bias; however, this idea can be validated only in the case of β_2AR. Molecular understanding of how these conformational changes in the receptor are translated into cellular signaling events remains to be elucidated.

Another class A GPCR that elucidated the molecular basis for ligand bias is the serotonin receptor in complex with **24**. Biological assays revealed that **24** exhibits strong β-arrestin bias for the 5-HT$_{2B}$ receptor but shows only a weak bias for the other receptor subtype 5-HT$_{1B}$.[168] A comparison between these two subtypes reveals no global structural changes; however, few structural features are observed upon closer inspection. These local structural changes suggest that the 5-HT$_{2B}$-**24** complex represents an intermediate receptor structure that is more efficient for inducing β-arrestin-biased signaling than G protein signaling.[168] For understanding mechanistic details about the intriguing features observed in the biased crystal structures, it is necessary to interpret these structural data in conjunction with the functional data and complementary dynamic studies.

Currently, GPCRs are not simply considered as a binary switch model; instead, they have a wide range of active and inactive conformations. The biased ligands preferably stabilize selected conformational states, thus activating a favored biological response that returns therapeutic benefits and not harmful side effects. The observation of biased signaling has tremendously changed the perception of GPCR activation and effector coupling and has provided a new avenue for GPCR drug discovery.[169−171] However, the detection of small structural changes that are related to signaling bias is difficult; hence, the implementation of rational drug design for this type of molecule remains a daunting task.

4.4. Binding Modes of Allosteric Modulators. In addition to the recognition of orthosteric ligands, GPCR functions are also modulated by a variety of endogenous allosteric modulators, including lipids, ions, water, and sterols. These modulators bind to alternative receptor regions (allosteric) that are generally less conserved than the orthosteric binding site. Because of this inherently less conserved binding pocket, allosteric ligands can show a higher selectivity than that of the orthosteric ligands, making them highly beneficial as therapeutic candidates with fewer adverse effects. Recently, several X-ray crystal structures of GPCRs bound with allosteric modulators have become available, which deepen our understanding about the receptor allosteric modulation (Figure 18D). These structures reveal various allosteric binding sites present within the 7TM helical bundle (in CCR5, mGluR1, and mGluR5), the extracellular region of the receptor (in M$_2$R), or on the external lipidic interface of the TM domain (in P2Y$_1$R).[8]

In the CCR5 structure, allosteric inverse agonist **44** stabilizes the receptor in an inactive conformation and inhibits its function. In the case of P2Y$_1$R, antagonist **42** binds to the unique allosteric binding site that is located on the external receptor surface. This observation broadens the new scope of future GPCR ligand discovery outside of the canonical orthosteric ligand binding pocket. In the histamine H$_1$R structure, a phosphate ion binding site in the extracellular subpocket and in the D$_3$R structure and a druggable extracellular extension of the orthosteric subpocket were observed. New insights into the allosteric modulation by Na^+ ions arise from the structure of inactive A$_{2A}$AR, revealing a tight water-filled channel connecting the extracellular and intracellular sides of the receptor. In the β_2AR and A$_{2A}$AR structures, specific cholesterol binding sites were observed, which modulate the receptor thermostability and binding affinity for inverse agonists. Interestingly, a recent study on β_2AR showed that the single domain antibodies (nanobodies), which were used to mimic downstream signaling partners, also allosterically regulated the binding of orthosteric ligands.[172] Pharmacological, biophysical, and crystallographic analyses showed that the nanobody Nb60 exerted its negative allosteric effect on agonist binding by stabilizing the inactive β_2AR conformation, and Nb80 lowered the energy of the active receptor states, driving the receptor toward more active conformations.

DOI: 10.1021/acs.jmedchem.6b01453
J. Med. Chem. 2018, 61, 1−46

5. STRUCTURE-BASED DRUG DISCOVERY TARGETING CLASS A GPCRS

Over the past decade, there has been rapid growth in crystallographic structural information due to the development of improved crystallization protocols and crystallographic procedures. For GPCRs, more than a hundred X-ray crystal structures are available, and these structural data provide invaluable insights into GPCR function and pharmacology. In particular, numerous ligand-bound 3D receptor structures unveil details of GPCR−ligand interactions, triggering a shift from traditional HTS methods to less expensive and more efficient SBDD approaches for the identification of novel ligands at the receptor level. Major endeavors of these approaches are focused on the hit identification through virtual screening (VS) using solved crystal structures. In the case of target proteins for which no direct crystallographic data are available, the construction and screening of homology models can be performed.[173] Direct structural information on ligand−receptor interactions allows the rational design and optimization of molecules to drive increased affinity and selectivity for the receptor of interest. In the following section, we will briefly survey the recent methodological advances in protein structure-based computational modeling for GPCRs and ligand design approaches, and we present the application of a few thriving models from the literature for drug discovery.

5.1. Receptor Structure Prediction. *5.1.1. Methodological Steps of Homology Modeling.* Despite recent crystallization breakthroughs, only a small fraction (>30 different GPCR structures) of the ∼800 GPCRs in the human genome is available to date. Hence, alternative computational modeling becomes a powerful tool to fill this gap.[174] For protein modeling or structural prediction, there are two main strategies: (i) homology (or comparative) modeling, which builds structural models of a given protein target based on the experimentally solved structure of a homologous protein (template), and (ii) de novo modeling, whose algorithms do not rely on homologous templates and predict structures directly from the sequence.[174] To date, homology modeling remains the most practical, accurate, and widely used tool for GPCR structure predictions.

Traditionally, homology modeling approaches follow two main hypotheses: (i) each amino acid sequence determines a unique 3D structure of a protein and (ii) evolutionarily conserved proteins possess similar sequences, adopting similar stable tertiary structures. On the basis of these hypotheses, homology modeling aims to predict an unknown protein structure from a related homologous protein (template) whose 3D structure has already been experimentally solved by X-ray crystallography, cryo-EM, or NMR. For the accurate prediction of the target structure using this approach, template selection is extremely important, and the quality of the model is directly related to the similarity between the template and the target protein sequence.[175] For reliable homology-based prediction, it has been found that, in general, the template protein should possess at least 35−40% sequence identity, identified as the empirical cutoff, with the target protein. The exponential growth of PDB structures could derive a general rule, which is depicted in Figure 19. If the length and percentage of identical residues of the two sequences fall into the safe region, then the two sequences are practically guaranteed to adopt a similar structure. The methodological steps of homology modeling can be summarized as follows: (1) identification of the template structure, (2) pairwise or multiple sequence alignment (MSA) of the model sequence of interest and template sequence(s), (3) initial model construction, (4) model refinement, and (5) model validation. Table 2 summarizes the working principles of each process along with the list of available methods.

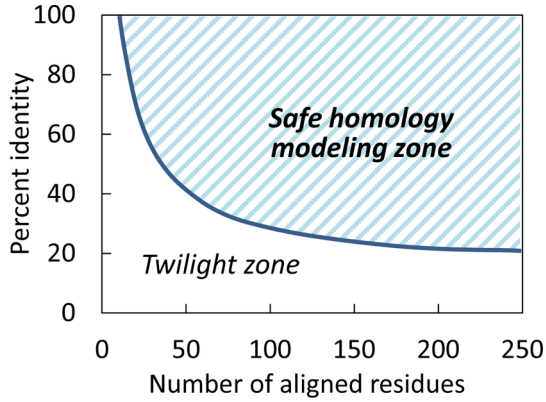

Figure 19. Criteria of the percent identity and number of aligned residues for reliable homology modeling.

5.1.2. Complexity in Homology Modeling. The application of a homology model in drug discovery requires high accuracy of the local side chain positions and orientations in the binding site.[175] As previously mentioned, for constructing a reasonable model with high quality, the selection of the appropriate templates with high sequence identity, as well as their alignment with the model sequence, is extremely important. Prior to the release of the first high-resolution crystal structure of bovine rhodopsin (Rho),[176] bacteriorhodopsin structures served as the structural templates for modeling GPCRs. Since 2007, the development of novel crystallization techniques has contributed to the resolution of more than 30 different druggable GPCR structures. This remarkable breakthrough in the past decade has introduced a wider template diversity for in silico modeling. Additionally, several important structural inferences about GPCR−ligand interaction patterns, activation and inhibition mechanisms, evidence for sequence-induced structural changes, and illustrated conformational loop diversity can be derived.[174] Despite the increase in the amount of structural information, it is still not possible to cover the entire GPCR space. Moreover, accurate homology modeling of the receptors, whose experimental structural information is not available, even for their isotypes, requires a great amount of effort and consideration in each step.

First, in the template selection step, it should be noted that if the sequence identity is less than 30%, BLAST cannot find a reliable homology template. It has been suggested that a target receptor must have at least 30−35% sequence identity to its template for accurate modeling.[177] In the case of GPCRs, although the sequence identity among homologous proteins is often below the recommended threshold (30−35%), the structural constraints imposed by the TM helical domains as well as the presence of highly conserved structural motifs makes this approach generally successful. However, because of these highly conserved TM motifs, the sequence alignment procedure requires more careful attention (as discussed in the following section).

Even if the correct template is chosen, errors in sequence alignment are the main cause of deviations in homology modeling. For class A GPCRs in particular, there are highly conserved structural motifs scattered throughout the TM helices. These residues should be precisely aligned because only one or

DOI: 10.1021/acs.jmedchem.6b01453
J. Med. Chem. 2018, 61, 1−46

Table 2. Procedure of Homology Modeling and Example of Available Methods

	steps	methods
1. template search	compare the sequence of unknown structure (model sequence) with known structures stored in PDB and identify the template structure with the most similar sequence	BLAST
2. pairwise or multiple sequence alignment	align the model sequence of interest and the selected template sequence(s)	ClustalW, ClustalX, TM-coffee, PRALINE, MP-T
3. crude model building	build a protein model for the target via a variety of methods: (i) rigid-body assembly, (ii) segment matching, (iii) spatial restraints, and (iv) artificial evolution	MODELER, SwissModel, HHPred, COMPOSER, PRISM
4. model refinement	refine the errors in the initial model through tuning alignment, modeling side chains and loops, energy minimization, molecular dynamics, Monte Carlo or genetic algorithm-based sampling, etc.	ModRefiner, 3Drefine, KoBaMIN, ViTO, SUMMA
5. model validation	examine the model quality or accuracy based on the information gathered in the previously known structural database	Ramachandran plot, PROCHECK, WHATIF, VERIFY3D, RFMQA

two mismatched residues may cause an error in the entire helical structure. Loop regions are the most flexible and variable and often determine the functional specificity of a protein structure. Because the loop regions also contribute to the active conformation or ligand binding site, the accuracy of loop modeling also plays a major role in the determination of the utility of the resulting homology models.[175]

One of the complexities involved in the homology modeling of GPCRs is their existence in different conformational states (inactive, active, or intermediate states). The X-ray crystal structures of GPCRs have been solved in different functional states bound with antagonists, inverse agonists, partial agonists, full agonists, or biased agonists. These structures provide insights into the varied shapes of the binding pockets and snapshots of multiple activation states. Among them, choosing a correct template is extremely crucial for accurate predictions of the homology model as well as for the orthosteric ligand binding. The state-of-the-art modeling technologies achieved close-to-experimental accuracy for small orthosteric ligands and models built by close homology; however, we are now facing a new set of challenges, such as reliable alignment between the target and distant homology targets, diverse binding pocket locations, prediction of long loops, and GPCR activation states. In addition, accurate modeling using a single template and model refinement has always been a challenge.[175] After the model is constructed, it should be further subjected to ligand-guided optimizations.

Carefully built 3D models could accurately capture the structural features of binding sites and are suitable for ligand discovery through VS and structure-based lead optimization.[174] In addition to its use in the SBVS approaches, GPCR homology models are invaluable for rationalizing known experimental observations, studying off-target effects using docking, guiding the design of small molecule and peptide ligands, rationalizing SAR data and substrate specificity, designing site-directed mutagenesis (SDM) experiments, aiding molecular replacement in X-ray structure refinement, and assisting MD studies to understand ligand binding mechanisms and protein dynamics.[174]

5.2. Ligand−Receptor Recognition, Binding Mode, and Affinity Prediction. *5.2.1. Molecular Docking as a Tool for the Identification of Protein−Ligand Interactions.* One of the most common applications for SBDD is molecular docking, which predicts the most likely binding conformations of small molecule ligands at the appropriate target binding site. After the development of the first algorithm in the 1980s, docking of small molecules into a protein of interest became a well-established and often used method in industry and academics for the rational design of drugs with better affinity, subtype selectivity, or efficacy. Through the binding modes and affinities predicted by a docking simulation, one can investigate key interactions between the ligands and target protein, prioritize compounds to be synthesized, and analyze the SAR for rational drug design.

Docking calculations consist of the following steps: (1) extensive conformation sampling of ligand conformations representing various potential binding modes at the receptor binding site, (2) calculation of the interaction energy of the predicted binding conformation, and (3) ranking of the ligand conformation by specific scoring function(s) with a recursive process until converging to a solution of minimum energy.[178] Tables 3 and 4 summarize the methodologies, characteristics, and example methods for conformational search algorithms and scoring functions.

For reliable docking results to be obtained, a predocking process is necessary with careful considerations. Because the presence of more than one structure for a given receptor is available, the input receptor structure must be carefully selected based on its structural resolution, suitable activation state, and conformational changes resulting from the interaction with ligands. The selected input structure has to undergo proper pretreatment procedures to prepare it for docking studies, which include the addition of hydrogen atoms, elimination of water molecules (except for those mediating key interactions between ligand and receptor), correct protonation and tautomerization of the binding site residues, and calculation of their partial charges.[178] Moreover, ligand structures should be converted into 3D structures with correct stereochemistry, ionization states, and partial charges. Using the prepared protein and ligand structures, docking calculations can be performed, which results in the prediction of ligand binding modes with ranking based on their predicted binding affinities.

5.2.2. Protein Flexibility in Docking Studies. Proteins are continuously fluctuating and undergo conformational changes during biological processes, including molecular recognition. This receptor flexibility is crucial but is frequently overlooked in molecular docking. Until recently, there has been a continuous effort to implement the protein flexibility concept in docking algorithms. The simplest applicable method is soft docking, which allows for a small degree of overlap between the ligand and the protein by softening of the interatomic vdW interactions during docking calculations.[179] This method is computationally efficient; however, it can only account for small conformational changes. Another docking program, GOLD, has an option to set side chain flexibility for several residues. In this method, side-chain conformations can be sampled using a rotamer library or by varying their dihedral angles starting from the initial coordinates of the input structure. One of the most popular modeling program packages, Schrödinger Maestro, includes the induced-fit docking module, which combines the docking and homology modeling methods. In this program, subsequent to the initial

DOI: 10.1021/acs.jmedchem.6b01453
J. Med. Chem. 2018, 61, 1−46

Table 3. Examples of Conformational Search Algorithms

	systematic search	random/stochastic search
methodology	promotes slight variations in the structural parameters, gradually changing the conformation of the ligands, and probes the energy landscape of the conformational space; after numerous search and evaluation cycles, converges to the minimum energy solution corresponding to the most likely binding mode	search conformational space by randomly modifying the structural parameters of the ligands; generates ensembles of molecular conformations and populates a wide range of the energy landscape.
virtues	effective for exploring conformational space	increases the probability of finding a global minimum through broader coverage of the energy landscape
limitations	possible to converge to a local minimum (this drawback can be overcome by performing simultaneous searches starting from distinct conformations)	computational cost as an important limitation
examples	FRED, Surflex-Dock, DOCK, GLIDE, FlexX, eHiTS, EUDOC, Hammerhead, Flog, SLIDE, ADAM	AutoDock, Gold, PRO_LEADS, EADock, ICM, LigandFit, CDocker, Molegro Virtual Docker, GlamDock, PLANTS, MolDock, MOE_Dock

Table 4. Examples of Scoring Functions for Docking Studies

	force field-based	empirical	knowledge-based
methodology	sum the contributions of bonded (bond stretching, angle bending, and dihedral variation) and nonbonded terms (electrostatic and van der Waals interactions) in a general master function with classical mechanics	series of protein−ligand complexes with known binding affinities used to train and generate a model; each term describing one type of physical event involved in ligand−receptor interactions (H-bonding, ionic, apolar interactions, desolvation, and entropic effects)	uses pairwise energy potentials extracted from known ligand−receptor complexes to obtain a general function; different type of interactions observed in the data set are classified and weighted according to their frequency of occurrence
virtues	applies an ab initio calculation to predict the energy accurately	simple and fast	suitable balance between accuracy and speed
limitations	inaccuracy in estimating entropic contributions and solvent effects	dependent on the accuracy of the receptor−ligand data set used to develop the model	dependent on the structural data set used in model building
examples	AutoDock, DOCK, ICM, SYBYL_G-score, SYBYL_D-score, Molegro Virtual Docker GoldScore, LigandFit, MedusaScore	Surflex-Dock, FlexX, AutoDock, GlideScore, ChemScore, X_Score, F_Score, Fresno, SCORE, LUDI, SFCscore, HYDE, LigScore, PLP	DrugScore, PMF_Score, MotifScore, RF_Score, PESD_SVM, SMoG, PoseScore

DOI: 10.1021/acs.jmedchem.6b01453
J. Med. Chem. 2018, 61, 1−46

docking of a ligand, the receptor structure is reconstructed according to the conformation of the bound ligand.

Following the docking of ligands, the ligand-induced protein flexibility or induced-fit effect can be managed by the relaxation of protein−ligand complex structures using Monte Carlo (MC) or molecular dynamics (MD) simulations. MD applies Newton's equation of motion, as described in classical mechanics, to specify the position and speed of each atom in the system under investigation. Although MD is computationally demanding for large systems, it is also receiving attention in this field. MD simulations of the protein−ligand complex structures optimize the active site residues surrounding the ligand, thereby stabilizing the complex structures. Additionally, it can also be utilized to estimate the stability of a ligand−receptor complex proposed by molecular docking.

Protein flexibility can also be considered in ensemble docking, where several structures belonging to the same target represent different possible conformational changes.[179] Upon binding, the ligand usually shifts the equilibrium toward the minimum energy structure, thereby stabilizing a subset of several possible conformations of the receptor. Therefore, docking to multiple structures provides an alternative opportunity for studying the conformational dynamics of a protein. Thus, from the structure ensemble, one can utilize multiple crystal structures of a particular molecular target. However, in the absence of suitable crystallographic structures (i.e., structures with inaccessible or poorly defined binding sites), simulated trajectories from MC, MD, or normal-mode analysis (NMA) are applied to generate a set of convenient docking structures.

5.2.3. Challenges in the Current Docking Method. Most of the docking programs are reported to successfully predict the binding conformations of ligands within the target binding site, which can be confirmed by a comparison of the docked conformation with the corresponding crystallographic data. For the binding mode prediction of ligands, which have different chemical scaffolds from the cocrystallized ligand, protein flexibility or induced-fit complexities could be adjusted by techniques, such as MD. Regarding the current scoring functions, significant challenges and acknowledged limitations exist. Because every scoring algorithm has its own virtues and limitations, the simultaneous use of different scoring functions has been increasingly employed in various consensus scoring protocols, which includes X-Cscore, MultiScore, SCS, GFscore, SeleX-CS, and CONSENSUS-DOCK.[178] Consensus scoring combines the advantages and simultaneously attenuates the shortcomings of each method; however, it is still limited in reproducing the absolute interaction energy between the ligand and target receptor with satisfactory agreement. In addition, other challenges to be addressed include prediction of desolvation energy and entropic effects.[178]

The treatment of water molecules in molecular docking and SBDD remains a complicated task. Few water molecules that strongly bind to the receptors have been captured across several GPCR crystallographic structures. Usually, structural water molecules are located in deep pockets of the receptor, mediating multiple hydrogen bonds between the ligand and the receptor binding site. The release of these tightly bound water molecules from the binding site is entropically favorable; however, the process causes a simultaneous loss of enthalpy.[178] If a specific moiety of the ligand forms an equivalent interaction with the receptor, then the water molecule can be released to the bulk side. A balance between these two different properties (entropy and enthalpy) can place or displace the structural water molecules depending on the bound ligands. Therefore, whether these structural water molecules could be removed or retained as part of the target protein should be carefully determined in the docking campaigns.

In cases for which the ligand of interest binds covalently, some differences may be found in the thermodynamics of ligand binding compared with those of noncovalent molecular interactions. However, the formation of covalent bonds is not satisfactorily explicated by the current docking algorithms, which are mainly based on molecular mechanics (MM).[178] In programs, such as Gold, Dock, AutoDock, or Glide, covalent docking algorithms have been implemented that employ definite approaches to artificially link the two atoms from the receptor and ligand, explore the possible energy landscape available to the covalently attached ligand, and evaluate the binding energetics of the interaction. Despite the recent resurgence of covalent binders as drugs, modeling methods that can address the limitation of covalent docking seem to be in a nascent stage.

In addition to these issues, various limitations still exist in ligand docking, including errors in predicting binding modes of high molecular weight molecules, difficulties in envisaging allosteric binding sites, and complications in identifying ligand binding at the protein−protein interaction interface.

5.3. Discovery of Novel Scaffolds. For finding novel ligands modulating a target protein of interest, the HTS approach, which relies on the screening of a large number of chemical compound libraries as the primary readout, can be performed. The screened candidate hits are further confirmed by an in-depth analysis of their affinities and efficacies and can be optimized using extensive SAR studies. However, the HTS approach is expensive and requires significant resources to be successful, which is also true for GPCRs. In addition, HTS sometimes delivers potential hits with high molecular weight and suboptimal physicochemical characteristics that give rise to a significant challenge during optimization.[180] Therefore, alternative approaches, such as VS or fragment-based drug design (FBDD), are continuously desired as a first step in the drug discovery pipeline.

5.3.1. Structure-Based Virtual Screening in the GPCR Ligand Search. One of the most widely used strategies in the discovery of new molecules is the computational or biological screening of large and chemically diverse compound libraries. This search can be facilitated utilizing VS as a fast and cost-effective method for the evaluation of immense compound libraries. Structure-based VS (SBVS) involves docking of large and diverse virtual chemical libraries into an X-ray crystal structure or homology model of the target protein. As observed in the crystal structure, the orthosteric ligand binding pocket is primarily defined as the binding site in docking. Theoretically, other nonorthosteric binding pockets, i.e., allosteric sites, can also be targeted as potential sites for the binding of allosteric ligands, but it should be combined with experimental validation constraining the location of the allosteric binding pocket and confirming the ligand mode of action.

Along with the binding mode predictions, SBVS also provides a ranking of docked molecules, which can be used as a sole criterion in the selection of promising molecules or can be combined with other evaluation methods. Generally, the selection criteria of molecules for biological testing are based on the docking score or the energy calculation, chemical diversity, predicted binding poses, and interactions with key residues.[177] Another facet that can be assessed through the visualization of the predicted structures is whether the solutions

DOI: 10.1021/acs.jmedchem.6b01453
J. Med. Chem. 2018, 61, 1−46

match predetermined requirements combined with ligand-based approaches, such as pharmacophore hypotheses, which will be discussed in the following section. Top-scoring virtual hits are selected subsequent to experimental validation through cell-based functional assays of effector coupling and second messenger generation. The selected hits can also be characterized using biophysical approaches, such as surface plasmon resonance (SPR) or radio-ligand binding assays, to confirm their direct binding to target receptors and to measure their binding affinities. The experimental validation of virtual hits aids in the prioritization of the real hits for subsequent optimization. Further crystallization and structure determination of the target receptor with the lead compound would greatly aid SAR studies and lead optimization.[180]

5.3.2. Ligand-Based Virtual Screening. Ligand-based VS (LBVS), which utilizes the information on compounds previously known to be active, is commonly applied in drug discovery, particularly when the structural information on the target protein is not available. Applying the resulting models as a molecular filter, a set of virtual hit molecules with high matching scores is selected from the screening libraries. One of the popular LBVS approaches is the use of structural features collected from several known active molecules to generate 3D pharmacophore models. A pharmacophore model is a 3D compilation of functional or structural features associated with biological activities. For a reliable model to be created, it is critical to predict the bioactive conformations of the molecules and properly align them. This goal can be achieved using a docking-based simulation; therefore, if the 3D structure of the target protein is available, then SBVS is usually combined with the LBVS approach for efficient and more accurate screening.

5.3.3. Fragment-Based Drug Design (FBDD) Approaches. FBDD is a strategy utilized in the identification of novel hits with small size (typically 100−250 Da) and high ligand-efficiency in an early stage of the drug discovery process.[173] Currently, this approach is well-established and has been used frequently in combination with SBDD approaches, especially for soluble protein targets such as proteases and kinases.[173] By screening small fragment libraries, which can bind to various subsites of a target, the FBDD approach effectively probes a diverse chemical space. Because large molecules with many functional groups may present more steric hindrance or electrostatic clashes than the fragment molecule in a binding site, FBDD could achieve higher hit rates compared to those from conventional HTS. In general, compounds optimized from fragments exhibit high binding efficiency per atom compared to those of compounds optimized from HTS. In silico methods can also play a role in screening with FBDD. A fragment library can be designed and screened using a secondary virtual approach, generally molecular docking. The prioritized fragments can be optimized using computational methods for growing, linking, or both. However, there are still a few limitations in computational FBDD approaches, including relatively low accuracy of predictions of fragment binding modes and rapid accumulation of errors. These computational methods are reported to be most useful when used in combination with experimental approaches.

5.4. Applications of Computational Approaches to GPCR Drug Discovery. Currently, the computational approaches described above are extensively used in drug discovery for discovering novel compounds based on 3D protein structures. The exponential growth in the structural information on GPCRs assures a large number of available templates, thereby guaranteeing an improvement in the quality of GPCR homology models for VS. In the following section, we provide an overview of the widely used structure-based approaches for identifying novel ligands, which target orthosteric and/or allosteric binding sites for some of the class A nonrhodopsin GPCRs.

5.4.1. Screening of Orthosteric Ligands. The first application of SBVS using a nonrhodopsin GPCR crystal structure was reported by Sabio et al.[181] The authors screened the proprietary (Lundbeck) and public (ZINC) databases for the inactive structure of β_2AR bound to the inverse agonist **1** (PDB ID: 2RH1). Compared with the low hit rate obtained with a set of random compounds (0.01%), their hit rates were successful for the proprietary database (36%) and satisfactory for ZINC compounds (12%). Using the same crystal structure, Kolb et al.[182] docked ∼1,000,000 commercially available compounds and selected 25 virtual hits, which were submitted for biological evaluation. Among the hits, six compounds were active with binding affinities of less than 4 uM, and the best compound showed a K_i of 9 nM. All six hit molecules had novel chemotypes for β_2AR, and five of them were confirmed to be inverse agonists with the same pharmacological efficacy as that of cocrystallized ligand **1**. In the case of β_1AR, Christopher et al.[18] conducted biophysical fragment screening, and their derived ligands were further crystallized with the receptor. The application of SPR as well as a subsequent hit to lead follow-up resulted in moderate affinity and high-ligand efficiency (LE) hit molecules with an arylpiperazine scaffold.

Following the release of the crystal structures of A_{2A}AR, many efforts have focused on the discovery of novel scaffolds that bind to A_{2A}AR. In 2010, Katritch et al.[183] screened the ICM ScreenPub database using a modified A_{2A}AR crystal structure. They slightly optimized the receptor conformation and included three crystallographic water molecules during the docking calculations. The resulting highly ranked molecules were clustered based on structural similarity and were then tested in vitro. Eventually, the authors identified the final hits with nine different chemotypes, which were relatively dissimilar to the cocrystallized compound. However, the retrieved hits showed high ligand efficiency (>0.3 kcal/mol per heavy atom), thus offering good starting points as a lead compound. Similarly, to obtain a novel scaffold for A_{2A}AR ligands, Carlsson et al.[184] performed VS of the lead-like subset of the ZINC database using an interesting manipulation in the docking simulation. They applied an increased dipole moment for residue D253$^{6.55}$ to favor a key hydrogen bond with the ligands, as suggested by site-directed mutagenesis studies.[185] This interaction was also confirmed for prototypic antagonist **28** with X-ray crystallography.[65] The top 500 compounds were manually revised, and the resulting diverse set of 20 compounds was biologically tested, obtaining a hit rate of 35%, which included two compounds with submicromolar affinity.

One of the most successful stories of SBDD is the identification of highly potent and novel chemotype (1,3,5-triazine derivative and a chromone scaffold) ligands for adenosine receptors by Langmead et al.[186] At the time of their work, structural data for A_{2A}AR were not available, and therefore, homology models were constructed with β_1AR structure as a template and refined using in-house site-directed mutagenesis (SDM) data. Using this experimentally enabled and enhanced model structure, a virtual library with 545 K compounds was screened, and initial hit molecules were selected by taking into account the shape and electrostatic properties of the binding site, ligand conformation, and desired regions for interactions. It led to a 9% hit rate followed by rational modification of the structures

DOI: 10.1021/acs.jmedchem.6b01453
J. Med. Chem. 2018, 61, 1−46

using X-ray crystallography and structure-based optimization. The optimized series finally lead to the identification of AZD4635 (HTL-1071) (structure not disclosed), which is currently in clinical trials for immunooncology.[187]

In addition to the above-mentioned pioneering studies of VS campaigns, there are several computational works available regarding the discovery of novel ligands for various types of GPCRs (which is summarized well in several review articles[100,173,174,177]). For example, Agelis et al.[188] designed a series of symmetrically bis-substituted imidazole analogues based on docking studies utilizing an extra hydrophobic binding cleft of the modeled AT_1R. Among the selected hits, four compounds showed a high binding affinity to AT_1R and a high antagonistic activity that was similar or even superior to that of Losartan. In the case of κ-OR, Negri et al.[189] performed VS to discover new binders to this receptor type, and the resulting compounds were additionally tested against the δ- and μ-opioid receptors, thereby discovering a selective κ-OR agonist. Interestingly, this agonist was identified using the VS protocol against the inactive structure, indicating that the ligand selectivity was not a part of the prediction but rather was evaluated later. The VS for receptor selectivity will be further discussed in the next section.

5.4.2. Discovery of Subtype- Or Conformation-Selective Ligands. The selectivity of compounds for receptors with different subtypes is an important issue to consider in current drug discovery; however, the routine modeling approaches have difficulty determining the selectivity. To discover subtype-selective ligands for adenosine receptors, Katritch et al.[190] developed ligand-guided homology models, discriminating interactions that promote subtype selectivity in a retrospective evaluation. In 2012, Kolb et al.[191] evaluated the limits of homology modeling and docking to identify new subtype-selective ligands with their A_1AR models. The ligands were screened using the model structure of A_1AR and subsequently tested against three (A_1, A_{2A}, A_3) of the four AR subtypes. They identified several A_1AR-binding ligands, although most of them lacked subtype selectivity, concluding that the screening against the structure of a single subtype is not sufficient to predict selectivity.

In practice, subtype selectivity can be achieved in cases where the structural information on the subtypes of interest is available. Kruse et al.[192] utilized the M_2R and M_3R structures to identify novel muscarinic ligands using structure-based docking simulation. Focusing on the structural differences between the crystal structures of these two subtypes, docking performed well in identifying several new substances with measurable affinity and modest selectivity for the M_2 and M_3 receptors. Exceptionally, a partial M_3R agonist showed high selectivity over that of M_2R; however, the binding mode could not clearly explain the selectivity, leading the authors to the conclusion that subtype-selective compounds are still challenging to predict. In 2014, Rodriguez et al.[193] applied similar approaches using the available crystal structures of $5\text{-}HT_{1B}$ and $5\text{-}HT_{2B}$ receptors to discover ligands that were selective for $5\text{-}HT_{1B}$ rather than for the $5\text{-}HT_{2B}$ receptor subtype. They showed a high performance in VS and identified a compound with more than 300-fold selectivity to the target ($5\text{-}HT_{1B}$) over the antitarget ($5\text{-}HT_{2B}$). In the example of CXC chemokine receptors, Schmidt et al.[194] recently predicted and verified new ligands for CXCR3 and CXCR4. Compared to these studies, their approaches focused on identifying ligands that bind to both GPCRs instead of selective ligands for a specific subtype. The authors found ligands selective for either of the receptors and ligands bound to CXCR3 and CXCR4. Among the selected virtual hits, 11 compounds were tested, and more than half of them showed the predicted activity profiles.

Achieving selectivity toward closely related GPCRs is difficult, especially in the VS process. Therefore, screening toward different activation states of the same GPCR represents an important challenge. In this case, no differences in the primary sequence of the receptors can be exploited; thus, we need to carefully consider the subtle differences in receptor conformation during the activation process. Recently, because of the release of agonist-bound and biased-agonist-bound GPCR structures, the prediction of particular ligand efficacies using molecular docking has started to gain attention. In 2013, Weiss et al.[195] used the first active-state structure of β_2AR to model the D_2R structure in the active conformation. They reported a prospective, large library virtual screen of 2.7 million lead-like and 400 K fragment-like molecules from the ZINC database, yielding several full agonists and partial agonists. Unfortunately, the resulting hits had low affinity; the agonism was weak, and the scaffolds were similar to the known dopamine receptor ligand. Although the β_2AR structure possesses a high sequence identity and it was the correct template for the inactive conformation, the active structure of β_2AR might not be a suitable template for the active D_2R. The authors suggested that structural information obtained from the active β_2AR was not transferable to the active D_2R structure; however, this fact might be a singular case and must be further examined with many other GPCR cases.

5.4.3. Screening of Allosteric Modulators and Bitopic Ligands. Within the class A GPCRs, the orthosteric binding sites are highly conserved due to the evolutionary pressure for binding of the endogenous ligands.[196] In contrast, allosteric sites are less conserved and have much greater structural diversity than the orthosteric sites, such that high selectivity for a receptor subtype could be achieved by targeting these allosteric sites.[197] The effect of allosteric ligands on receptor activation could be in a positive (PAM), negative (NAM), or neutral manner (SAM). Allosteric ligands modulate the receptor affinity via conformational coupling between the orthosteric and allosteric binding sites, or they modulate the efficacy by altering the functional response of the receptor to orthosteric ligand binding.[196] Because the allosteric modulators generally have a chemical structure unrelated to that of competitive agonist or antagonist drugs, this approach offers a novel class of small molecule drug candidates. To date, two NAMs for class A GPCRs have been approved for clinical use: Mozobil (**45**, plerixafor) and Selzentry (**44**, maraviroc).[198] Compound **45** is a NAM of the chemokine receptor CXCR4 and is used to promote the release of stem cells into the bloodstream after autologous stem cell transplantation. Compound **44** is a high-affinity NAM of the CCR5 receptor and was discovered by Pfizer via the HTS and medicinal chemistry approaches; it was approved in 2007 for the treatment of HIV in combination with antiretroviral agents. In recent years, some GPCR allosteric modulators, such as Reparixin,[199] a NAM for CXCR1/2, have entered clinical stages.

In the case of the dopamine receptor, the X-ray crystal structure of D_3R, complexed with antagonist **18**, indicated that a second potential allosteric site extended toward ECL2 is formed by TM1, -2, and -7. A large-scale VS study was performed by Lane et al.,[200] which reported interesting results for the orthosteric and allosteric ligands of D_3R. On the basis of the crystal structure of D_3R, they prepared two optimized D_3R models: one representing an apo state and another bound to dopamine. First, for considering the protein flexibility, conformers of D_3R models were generated by introducing minor

DOI: 10.1021/acs.jmedchem.6b01453
J. Med. Chem. 2018, 61, 1−46

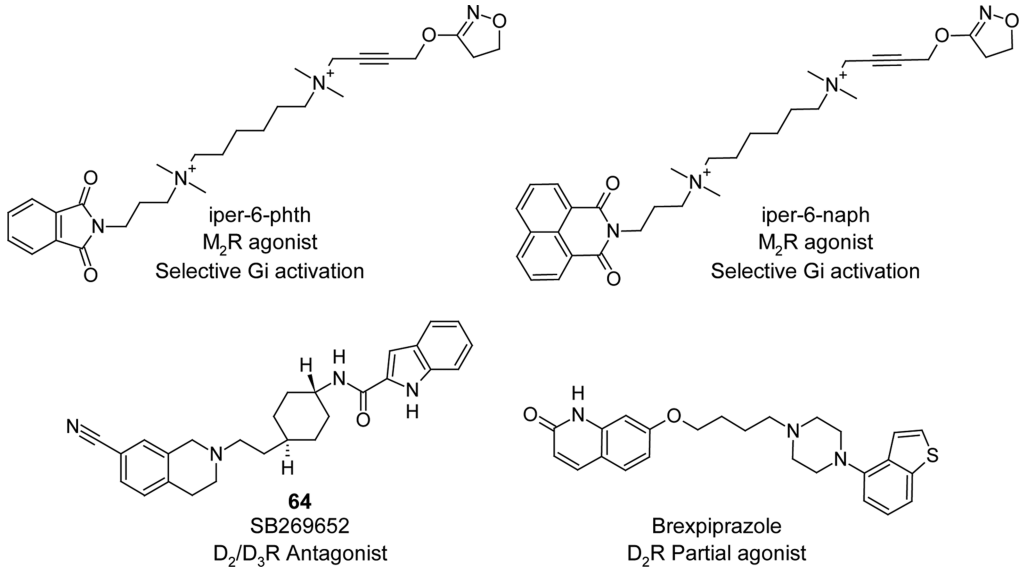

Figure 20. Chemical structures of the bitopic ligands and drug-like molecule of M_2R, D_2/D_3R, and D_2R reported in this perspective.

variations (~0.1 Å) in the protein backbone using energy-based side chain sampling with known antagonist sets. The established conformers of the binding pocket were assessed by the VS performance, which can distinguish the D_3R ligand from decoys. Second, 4.1 million compounds from the Molsoft Screen Pub database (Molsoft, LLC, San Diego, CA) were virtually screened by docking calculations. The top 300 compounds in each model were selected and clustered by chemical similarity (with 0.3 Tanomoto distance). The top 25 candidates selected by the dopamine-bound model did not have a positively charged amine forming a conserved salt bridge to $D110^{3.32}$, which is contrary to the D_3R apo model, but has interactions with TM1, -2, -3, and -7 as well as ECL1 and -2. These hits also reach dopamine and $D110^{3.32}$ at the end of the orthosteric pocket. Finally, the authors also experimentally validated their predicted novel allosteric ligands, which showed distinct functional profiles on dopamine-signaling efficiency to provide a starting platform for further optimization of selectivity.

A new class of ligands, which are termed bitopic or dualsteric ligands, have been reported to bind to both orthosteric and allosteric sites simultaneously. Because these ligands consist of two pharmacophores connected by a linker adapted to fit the orthosteric and allosteric sites, the molecular fragments that can bind to these sites need to be carefully selected, and the linker must be optimized with respect to its attachment point, length, composition, and flexibility.[201] Although rational design of these type of ligands is still challenging, some bitopic ligands show significant promise (Figure 20). For instance, compared to conventional M_2R agonists, the iperoxo-derived bitopic agonists iper-6-phth and iper-6-naph[202] lead to a selective Gi activation, simultaneously binding to both the orthosteric and allosteric binding sites, which are located near the extracellular vestibule of M_2R. Compound **64** (SB269652), which was originally discovered as an antagonist of D_2/D_3R, was proposed as a bitopic ligand by Silvano et al.[203] Later, evidence provided by Lane et al.[204] confirmed the role of **64** as a bitopic ligand of D_2R. This ligand shares the same charge−charge interaction between the basic amino nitrogen and the carboxyl of D114 within the orthosteric pocket and forms strong hydrogen bonding with $E95^{2.65}$ in the allosteric pocket among TM1, -2, and -7. The high molecular weight extended ligands that resemble SB compound were also developed as bitopic ligands, recently launching a novel atypical antipsychotic drug Brexpiprazole (Rexulti).[205] The strength of these bitopic ligands is the combination of high affinity derived from orthosteric binding and high selectivity, which is achieved via allosteric site binding. The discovery of bitopic ligands will introduce a new era of GPCR ligand design.

6. DYNAMICS SIMULATION AS A POTENT TOOL TO UNDERSTAND THE STRUCTURAL AND MECHANISTIC INTRICACIES OF CLASS A GPCRS

As briefly mentioned in the previous section, any crystal structure represents a snapshot of the system (receptor or protein) that has been captured in a particular state. However, the full spectrum of receptor activation is undoubtedly more complex than the simple active or inactive states. Although several experimental techniques, such as NMR, fluorescence-based microscopy, and electron resonance spectroscopic techniques, have been able to provide a more complete picture of the conformational dynamics of GPCRs, their inherent resolution limitations require the implementation of other complementary approaches. Computational simulations, which capture the receptor motion at an atomic scale, have emerged as an important tool to complement and substantiate experimental findings.[206] An increasing amount of computing power and improvements in the simulation techniques have enabled the computational studies to probe the functionally relevant dynamics during biological processes. Simulation studies are also able to determine detailed molecular mechanisms and driving forces of these processes.[207] In the following section, we provide an overview of the computational approaches to study dynamical facets of GPCRs and their suitability and limitations.

6.1. Multiscale Simulation Techniques. The dynamics of GPCRs can be considered as a hierarchical process that occurs through a broad spectrum of time scales.[206] At the ligand binding site, fast dynamics occur, such as the femtosecond isomerization of retinal in rhodopsin. Ligand binding often results in pico-to-nanosecond time scale rearrangements at the active site. The activation of the receptor after ligand binding, i.e., the conformational changes from the inactive to the active state, occurs at a millisecond-to-second time scale. With a much longer time scale, the spatiotemporal organization of GPCRs occurs

DOI: 10.1021/acs.jmedchem.6b01453
J. Med. Chem. 2018, 61, 1−46

over micrometers in seconds or longer. For these different levels of biological processes to be investigated, highly sophisticated simulation techniques are required with varying length and time scales, including quantum chemical descriptors, classical models with an atomistic or coarse-grained representation, and a phenomenological system-level model.[206]

6.1.1. Quantum Mechanical (QM) Model. At the QM level, a molecule is represented in subatomic detail with its molecular orbitals (MOs) from the electron potentials of each atom. However, for describing the QM behavior of molecules, the Schrodinger equation must be solved, which is computationally demanding. To date, it is practical to restrict the number of atoms to include in the QM calculations, and only a small-sized molecule can be represented at the QM level. Therefore, QM methods are often combined with molecular mechanics (MM) methods, resulting in QM/MM multiscale models that efficiently represent a part of the system with quantum descriptors and represent the remaining at an atomistic resolution.[206]

6.1.2. Atomistic Model. In this model, every atom is explicitly represented as a point particle corresponding to its connectivity with other surrounding particles. On the basis of the atomistic representation, the specific position and velocity of each particle is solved at every particular time interval. This process requires a description of a potential function to compute the energetics along with the parameters defining the atomistic properties, such as mass, charge, and connectivity (bond length and angles). Potentials can be defined at various levels of physical accuracy, but the most commonly used one for the atomistic simulation in protein chemistry is based on classic Newtonian molecular mechanics, which reproduce structural and conformational changes but usually cannot reproduce chemical reactions.[206] This potential is usually referred to as a force field composed of bonded terms (harmonic potential for bonds and angles) and nonbonded terms (vdW and Coulombic interactions). Several force fields, including CHARMM, GROMOS, OPLS, and AMBER, are commonly used to study GPCR dynamics. All-atomistic simulations of GPCRs are typically composed of a membrane protein and a bound ligand surrounded by a lipid bilayer in the water bath. Membrane bilayers are composed of hundreds of lipids varying in dimensions in the range of several nanometers, and the GPCRs are embedded within them.[208]

6.1.3. Coarse-Grained Model. In this model, a set of atoms is considered as a single bead and each molecule as a set of beads to reduce the degrees of freedom of the system. This approach is gaining popularity and is suitable for certain applications due to its ability to study the dynamics of larger systems at a longer time scale. One of the most popular models in coarse-graining is the MARTINI force field.[206] This model has been extensively used to simulate dynamic processes of the lipid membrane. In this model, the head groups of lipid molecules are represented as beads and the tails as bonds. The MARTINI model has also been extended to proteins with amino acid residues represented by 1−5 beads based on their size, flexibility, and physicochemical properties. The parameters describing the bonded and nonbonded terms are included in the model.

6.1.4. Continuum Electrostatic Model. For the computational cost to be reduced, the membrane environment and the solvent particles can be considered implicitly by representing average electrostatic properties. Commonly used methods for continuum representation are the Poisson−Boltzmann (PB) and Generalized Born (GB) methods, which approximate the average influence of the environment on a solute. Proteins and ligands are usually represented at an atomistic scale with an additional surface area (SA) term in the hybrid MM/PBSA model.[206]

6.2. Molecular Dynamics (MD) Simulation of Membrane Proteins. MD simulation is a commonly used computational technique that aims to predict the time-dependent motion of biomolecules. For a system of interest, the initial positions and velocities are primarily defined. Using a predefined interaction potential for deriving the forces among all the particles, the time evolution of the molecular systems could be followed by solving classical equations of motion for all particles in the system. In the following section, we will describe the MD simulation steps focusing on GPCR-membrane simulation.

6.2.1. System Setup. Compared with cytosolic globular proteins, GPCRs are integrated in lipid bilayers; hence, building a realistic protein-embedded membrane system is challenging but remains a crucial aspect for simulations. For system setup, it is important to appropriately insert a protein into a lipid bilayer. There are two popular methods commonly used in modern simulations: (1) In the replacement method, pseudo atoms of the lipid head groups are distributed around a protein and then replaced by lipid molecules. (2) In the insertion method, a hole is first created in a pre-equilibrated lipid bilayer. Subsequently, the membrane protein is inserted into the hole, and overlapping lipids are removed.[209] To help users easily build a sophisticated protein−membrane system, web services are available, for example, the CHARMM-GUI Web site (http://www.charmm-gui.org), which provide a graphical user interface (GUI) for setting up the simulation systems through a generalized and automated building process, including system size determination as well as the generation of a lipid bilayer, pore water, bulk water, and ions.

6.2.2. Simulation Steps. In addition to preparing the receptor−ligand complex structure that is properly embedded in the lipid membrane, topology and force field files are required to start the simulation process. The topology file includes all the information about the input structure and connectivity among the atoms. The force field file contains a set of parameters describing the type of interaction that exists between each of the atoms or a group of atoms connected in the structure. On the basis of the topology and force field, simulation jobs are conducted via the following steps: (1) The initial system should be minimized to find a stable point or a minimum on the potential energy surface to initialize dynamics. (2) During the minimization step, we can consider the temperature as 0 K; therefore, the system must be gradually heated to the target temperature, generally 300 K, to initialize dynamics. (3) The dynamics run is performed by solving Newton's equations of motion: $F_i = m_i \cdot a_i$, where F_i is the force, m_i is the mass, and a_i is the acceleration of atom i. During the early dynamics run, the system should be equilibrated to reach steady-state for reliable dynamics simulation. (4) Then, the production dynamics stage is reached for determining thermodynamic averages or for sampling new configurations.[209]

6.2.3. Current Challenges in MD Simulation. Structural changes in proteins can occur in nanoseconds, microseconds, milliseconds, or even longer. Because simulations require short time steps (generally 1−2 fs) for numerical stability, millions to trillions of sequential time steps should be performed for nanosecond to millisecond events. In addition, if a high energy barrier exists between two low-energy states during the simulation, then it is unlikely that the simulation will cross this barrier and describe the second low-energy state unless the run is prolonged. Advances in computing power have enabled

DOI: 10.1021/acs.jmedchem.6b01453
J. Med. Chem. 2018, 61, 1−46

microsecond or, rarely, even longer simulations, but simulation time scales remain a challenge. For a method that enables longer time scale simulations to be determined, continuous efforts have focused on involving algorithmic improvements as well as a steady increase in computing power, which is provided by parallel or cloud computing, GPUs, tailored computer architectures, or cloud computing approaches.[208]

Accuracy in force fields is also a challenging issue in MD simulations because the molecular mechanics force fields are inherently approximations. They have improved substantially over the past decade, but several limitations remain. In addition, because an MD simulation cannot describe the electron transfer, a few covalent bonds form and break more frequently, such as disulfide bonds between cysteines or the protonation/deprotonation of acidic or basic amino acid residues, all of which can pose a problem.

In practice, one needs to know the underlying limitations in MD simulations, how to treat the simulation process to obtain reliable results, and what to trust in a simulation. Promisingly, the progress in the advancements of computing power or force field development will significantly contribute to the process of drug discovery and optimization with both accuracy and efficiency in the near future.

6.3. Investigation of the Dynamic Events Characterizing GPCR Function. As previously mentioned, the MD technique could be implemented in the molecular docking pipeline to include protein flexibility. In addition, recent advances in computational power and MD methodologies render this approach a complementary tool to experimental techniques. In the following section, we briefly introduce other aspects of multiscale simulation studies, analyzing receptor−ligand interactions and dynamic events involved in GPCR function.

6.3.1. Prediction of Binding Free Energy. During the SBDD process, potential ligands can be screened by analyzing the relative strengths of the receptor−ligand interactions, which are generally predicted by "docking scores". However, to date, this score is only based on the enthalpic contribution of ligand binding without considering the entropic or solvent effect of the environment. For the prediction of a more realistic binding free energy of the given ligands, the surrounding environment, such as the receptor, membrane, and solvated water molecules, should be considered. Solvation-free energies can be calculated by MM/PBSA approaches using a continuum membrane model, but their main limitation is the absence of the receptor and ligand dynamics.[206] Currently, MD simulations are considered the best method to explore a more diverse set of protein conformers, especially for those at a relatively high energy and those not detectable with the current experimental tools. Many studies have reported that the MD-based binding free energy calculations of small ligands using rigorous methods, such as free energy perturbation (FEP) and thermodynamic integration (TI) provide more accurate binding affinities, which are in good agreement with the experimental values.[206] However, practical applications to drive drug discovery remain limited because of the inaccuracy of force fields, insufficient sampling, time-consuming setup, and significant computational demands. In the case of GPCRs in particular, these limitations would be more challenging than those of the soluble enzymes due to the presence of the lipid bilayer, buried water molecules, finely tuned helical flexibility, and so forth.

6.3.2. State Transition and Formation of the Signaling Complex. The dynamics of GPCRs is a crucial aspect to their activation. Over the past decade, the structural determination and analysis of several GPCRs bound with various ligands provide important information about GPCR dynamics. Large conformational diversity in the inactive, active, as well as intermediate states has been observed, which is in line with the previous hypothesis and more recent NMR studies. Most of the studies on GPCR dynamics have focused on a comparison of these diverse states differentiated by bound ligands. A major focus of the current structural work on GPCRs pertains to the investigation of fully active states complexed with signaling partner proteins, G protein, or β-arrestin. However, to date, limited information regarding the dynamical features of GPCRs is available, for example, the conformational states that GPCRs can adopt, how dynamic each conformational state is, or how different conformational states are stabilized by the binding of ligands and associated signaling proteins. This uncertainty poses an obstacle to SBDD for GPCR targets, even if their corresponding crystal structures are available.

Computational studies have succeeded in analyzing activation-related dynamics, starting from the inactive state of the receptor to its active state.[24,53] Atomistic molecular simulations for hundreds of nanoseconds captured these transitions, but the number of studies has been restricted due to limited computational resources. These studies, taken together with site-directed mutation analysis, discovered that the inactive state conformations are stabilized by specific interhelical and intrahelical salt bridge interactions and hydrophobic interactions. In the active states, the highly conserved residues among the class A GPCRs were involved in a complex network of interhelical and intrahelical hydrogen bond interactions.

Upon the state transition of GPCRs, the coupling with their signaling partner proteins is facilitated, forming a ternary complex of the receptor, bound ligand, and corresponding signaling protein. The solved crystal structure of β_2AR bound with an agonist and heterotrimeric G protein[27] not only provides insight into understanding of the signaling complex of GPCRs but also paves the way for simulations of the fully activated state. Investigating the pathway of the association of the signaling complex or exploring the specificity of the G proteins or β-arrestin coupling promises to reveal further insights into GPCR biology.

6.3.3. Allosterism. Biologically active macromolecules in our body transmit the effect of substrate binding at one site to another functional site that is not close in most cases; this phenomenon is generally called "allostery".[210] Recently, experimental observations demonstrate that allostery can be facilitated by a dynamic and intrinsically disordered protein, resulting in a new paradigm for understanding allosteric mechanisms. Computational methods also offer the possibility of exploring allosteric events at the atomic scale, which is inaccessible experimentally. Many of these studies focus on detecting a transient allosteric site, a receptor conformational ensemble, and the statistical nature of the interactions responsible for the transmission of information.[210] There are many implementations of several theoretical properties, such as mutual information or network analysis, for studies on allosteric pathways.

6.3.4. Detection of the Binding Paths of GPCR Ligands. In addition to the conformational dynamics of a GPCR in a certain state, which was discussed in the previous sections, an understanding of the process of receptor−ligand association and dissociation is important to expand our knowledge of GPCR research. In a pioneering study by Dror et al.,[211] the pathways of

DOI: 10.1021/acs.jmedchem.6b01453
J. Med. Chem. 2018, 61, 1−46

ligand entry into β_2AR, its subsequent binding at the binding site, and the exit from the receptor were analyzed. They proposed two main entry points of the ligand with vestibule 1 being the most important entry site. This process can be studied using microsecond time scale unbiased atomistic MD simulations with a specialized hardware system; however, these time scales remain out of reach for most current computational studies, especially those performed to analyze multiple ligand-specific pathways. These works pave the way for studying ligand binding or unbinding mechanisms in other GPCRs, but further studies are required to examine the generality of these methods.

7. CONCLUSIONS AND FUTURE PERSPECTIVES

Structural evolution over the past decade has shown striking advances in GPCR structural biology. These recent breakthroughs have significantly contributed to our understanding of GPCR function, ligand binding, and its pharmacological action as well as in the design of new drugs. This perspective covered the latest advances in GPCR structural biology with a focus on the receptor−ligand interactions of each receptor family in class A nonrhodopsin GPCRs as well as the structural features for their activation, biased signaling, or allosteric mechanisms. The current state-of-the-art techniques of computational structure-based drug design (SBDD) approaches in the GPCR research field have also been summarized. Several collaborative works with the elucidation of GPCR structures illustrate how structural biology, molecular pharmacology, medicinal chemistry, and computational methods help to provide a comprehensive picture of the structural and functional characteristics of GPCRs and to discover new candidate molecules more efficiently.

Although success stories in GPCR ligand discovery using structural information have been continuously increasing, there are still limitations to SBDD approaches. Only a few of the molecules discovered by SBDD have led to clinical state drug candidates so far. In several virtual screening campaigns using high-resolution crystal structures, the achieved hit rates were impressively higher than 30−40%. However, the majority of GPCRs have not been crystallized yet, and the structural information for a significant amount of receptor classes requires homology modeling approaches. In these cases, the hit rates were expectedly lower due to the indirect crystallographic information used to refine the models of distant targets. Nevertheless, it is evident that further developments in the experimental methods and an expanded coverage of GPCR structures will continuously aid VS approaches and also lead to improved models with higher accuracy.

Given the highly dynamic nature of GPCRs, a more detailed understanding of the ligand binding sites with respect to the receptor flexibility and different activation states is required to support a more refined drug design. Conformational changes of proteins initiated or stabilized by different ligand binding (agonist, antagonist, inverse agonist, biased agonist, allosteric modulators, etc.) form an essential part of our understanding of protein function and downstream signaling. Although vast amounts of GPCR ligand binding data are increasingly becoming available, we have just started to understand the ligand interactions that trigger different receptor functional states. Only limited information is available on the dynamics of the interconversion among all of these states. Therefore, measuring or simulating the dynamic changes in receptor structure becomes a critical issue in the design and optimization of ligands with improved binding affinities, functional efficiency, selectivity, and other pharmacological properties. MD simulations facilitate exploration of various GPCR conformations that are not observed in static models. They provide new opportunities for studying protein dynamics and functional models of GPCRs as well as to rationally optimize lead compounds. The application of MD simulations is still limited in most drug discovery programs; however, continued efforts to improve advanced MD methodologies and computing power as well as the growing body of structural information will definitely produce many success stories in which computer simulations could empower a significant impact in the drug discovery process. We also believe that the combination of structural elucidation, in silico structural modeling, and dynamics methods can provide a clue for discriminating molecular interactions of ligands with different pharmacological activities, i.e., agonism or antagonism, as well as potentially biased agonism.

Another intriguing aspect is to explore communications with other functional sites, such as an allosteric binding site, G protein or β-arrestin binding sites, and oligomerization interfaces. To date, vast amounts of GPCR drug discovery studies are targeting the orthosteric sites in the TM region or extracellular domain. However, allosteric ligand binding at the intracellular side or at a lipid-exposed site is currently receiving more attention. In particular, the complex formation of GPCRs with signaling proteins, such as G proteins or arrestins, is considered a highly demanding area to understand GPCR function. The link between the ligand binding site and a certain signaling pathway is also one of the most provocative questions that will be studied in the near future both experimentally and computationally. All of these works require not only advances in GPCR structural biology but also information on relevant downstream signaling complexes as well as the development of computational techniques to study the complex signaling machinery. Despite the challenges, the rewards for scientific endeavors to understand the GPCR signaling mechanism and to achieve rational drug discovery will make these attempts worthwhile.

AUTHOR INFORMATION

Corresponding Author

*Tel: 82-2-3277-4503; fax: 82-2-3277-2851; e-mail: sunchoi@ewha.ac.kr.

ORCID

Sun Choi: 0000-0002-7669-7954

Author Contributions

†Y.L. and S.B. contributed equally to this work.

Notes

The authors declare no competing financial interest.

Biographies

Yoonji Lee majored in Pharmacy (B.S.) and completed her M.S. and Ph.D. in Molecular Modeling and Computer-Aided Drug Design at the College of Pharmacy and Graduate School of Pharmaceutical Sciences, Ewha Womans University, Seoul, Korea. After completing her Ph.D. in 2013, she has been working as a postdoctoral fellow and then research professor/research fellow in the same group. Her research interests are focused on biomolecular simulation to elucidate the conformational changes and dynamics required for protein function, protein structure modeling to predict the unknown 3D structures of proteins or complexes, as well as computational medicinal chemistry to guide the design of new molecules using structure- or ligand-based approaches.

Shaherin Basith obtained her M.Sc. degree in Bioinformatics from University of Madras, India. She then pursued her graduate studies at Ajou University, Seoul, Korea, where she obtained her Ph.D. in Medical

DOI: 10.1021/acs.jmedchem.6b01453
J. Med. Chem. 2018, 61, 1−46

Sciences in 2013. Her main area of research during graduate studies was to predict the protein−protein interaction sites in signaling complexes using existing in silico tools or software. She also concentrated on identifying the structure−function relationship of proteins using molecular modeling and phylogenetic analysis. All these predicted protein complexes are involved in Toll-like receptor downstream signaling. Currently, she is working as a postdoctoral fellow at the College of Pharmacy, Ewha Womans University, Seoul, Korea.

Sun Choi is a professor of College of Pharmacy and Graduate School of Pharmaceutical Sciences at Ewha Womans University, Seoul, Korea. She received her Ph.D. in Medicinal Chemistry from the State University of New York at Buffalo, USA in 1999. Then, she joined Prof. Richard B. Silverman's group at Northwestern University, USA as a postdoctoral fellow. From 2001 to 2005, she worked as a molecular modeler and computational chemist at the molecular design group in Tripos, Inc., USA. Her primary research interests focus on the state-of-the-art technologies of molecular modeling and computer-aided drug design (CADD), computational medicinal chemistry, cheminformatics, and biomolecular simulations targeting therapeutically important enzymes, GPCRs, and ion channels. She is also involved in interdisciplinary collaborations with several research groups worldwide for drug discovery in various diseases.

■ ACKNOWLEDGMENTS

This work was supported by the Midcareer Researcher Program (NRF-2017R1A2B4010084 to S. C.) funded by the Ministry of Science, ICT & Future Planning (MSIP) and Research Fellow Program (NRF-2016R1A6A3A11932436 to Y. L.) funded by the Ministry of Education through the National Research Foundation (NRF) of Korea.

■ ABBREVIATIONS USED

A_{2A}AR, A_{2A} adenosine receptor; AFM, atomic force microscopy; aMD, accelerated molecular dynamics; ARB, AT_1R blocker; AT_1R, angiotensin II type-1 receptor; BBB, blood-brain barrier; BRIL, cytochrome b562 RIL; β_2AR, β_2-adrenergic receptor; β-FNA, β-funaltrexamine; cAMP, cyclic adenosine monophosphate; CaSR, calcium-sensing receptor; CB_1R, cannabinoid receptor type 1; cMD, conventional molecular dynamics; CNS, central nervous system; COPD, chronic obstructive pulmonary disease; CRS, chemokine recognition site; D_3R, dopamine D_3 receptor; DAG, diacylglycerol; DORA, dual orexin receptor antagonist; δ-OR, δ-opioid receptor; δ-OR, δ-opioid receptor; EC, extracellular; ECL, extracellular loop; EDG, endothelial differentiation gene; ETB, endothelin receptor type-B; FBDD, fragment-based drug design; FDA, Food and Drug Administration; FEP, free-energy perturbation; FFAR1, free fatty acid receptor 1; GB, Generalized Born; GPCR, G protein-coupled receptor; GRK, GPCR kinase; GUI, graphical user interface; H_1R, histamine H_1 receptor; HTS, high-throughput screening; IC, intracellular; ICL, intracellular loop; IP3, inositol 1,4,5-triphosphate; κ-OR, κ-opioid receptor; LBVS, ligand-based VS; LCP, lipidic cubic phase; LE, ligand efficiency; LPA_1, lysophosphatidic acid receptor 1; M_1R, M_2R, M_3R, and M_4R, muscarinic acetylcholine M_1, M_2, M_3, and M_4 receptors; mAChR, muscarinic acetylcholine receptor; MAPK, mitogen-activated protein kinase; MD, molecular dynamics; MM, molecular mechanics; MO, molecular orbital; MSA, multiple sequence alignment; μ-OR, μ-opioid receptor; N/OFQ, nociceptin/orphanin FQ; nAChR, nicotinic acetylcholine receptor; NAM, negative allosteric modulator; NMA, normal-mode analysis; NOP, nociceptin/orphanin FQ peptide receptor; NTS, neurotensin; $NTSR_1$, neurotensin receptor 1; OX_1R and OX_2R, orexin type-1 and type-2 receptors; $P2Y_1$R, $P2Y_1$ purinergic receptor; PAM, positive allosteric modulator; PAR1, protease-activated receptor 1; PB, Poisson−Boltzmann; PI3K, phosphoinositide 3-kinase; PKC, protein kinase C; PKD_1, protein kinase D_1; PLC, phospholipase C; QM, quantum mechanical; QNB, 3-quinuclidinyl-benzilate; Rho, rhodopsin; $S1P_1$, sphingosine 1-phosphate receptor 1; SA, surface area; SAM, silent allosteric modulator; SAR, structure−activity relationship; SBDD, structure-based drug design; SBVS, structure-based VS; SDF-1, stromal-derived factor-1; SDM, site-directed mutagenesis; SPR, surface plasmon resonance; StaRs, stabilized receptors; T4L, T4 lysozyme; TCA, tricyclic antidepressant; TI, thermodynamic integration; vMIP-II, viral macrophage inflammatory protein; VS, virtual screening; XAC, xanthine amine congener; xFEL, X-ray-free electron laser; 5-HT, 5-hydroxytryptamine; 7TM, seven transmembrane

■ REFERENCES

(1) Conn, P. M.; Ulloa-Aguirre, A.; Ito, J.; Janovick, J. A. G protein-coupled receptor trafficking in health and disease: lessons learned to prepare for therapeutic mutant rescue in vivo. *Pharmacol. Rev.* **2007**, *59*, 225−250.

(2) Thomsen, W.; Frazer, J.; Unett, D. Functional assays for screening GPCR targets. *Curr. Opin. Biotechnol.* **2005**, *16*, 655−665.

(3) Schoneberg, T.; Hofreiter, M.; Schulz, A.; Rompler, H. Learning from the past: evolution of GPCR functions. *Trends Pharmacol. Sci.* **2007**, *28*, 117−121.

(4) Foord, S. M.; Bonner, T. I.; Neubig, R. R.; Rosser, E. M.; Pin, J. P.; Davenport, A. P.; Spedding, M.; Harmar, A. J. International union of pharmacology. XLVI. G protein-coupled receptor list. *Pharmacol. Rev.* **2005**, *57*, 279−288.

(5) Ghosh, E.; Kumari, P.; Jaiman, D.; Shukla, A. K. Methodological advances: the unsung heroes of the GPCR structural revolution. *Nat. Rev. Mol. Cell Biol.* **2015**, *16*, 69−81.

(6) Deupi, X. Relevance of rhodopsin studies for GPCR activation. *Biochim. Biophys. Acta, Bioenerg.* **2014**, *1837*, 674−682.

(7) Hanlon, C. D.; Andrew, D. J. Outside-in signaling–a brief review of GPCR signaling with a focus on the Drosophila GPCR family. *J. Cell Sci.* **2015**, *128*, 3533−3542.

(8) Zhang, D.; Zhao, Q.; Wu, B. Structural studies of G protein-coupled receptors. *Mol. Cells* **2015**, *38*, 836−842.

(9) Gether, U. Uncovering molecular mechanisms involved in activation of G protein-coupled receptors. *Endocr. Rev.* **2000**, *21*, 90−113.

(10) Salon, J. A.; Lodowski, D. T.; Palczewski, K. The significance of G protein-coupled receptor crystallography for drug discovery. *Pharmacol. Rev.* **2011**, *63*, 901−937.

(11) Ballesteros, J. A.; Weinstein, H. Integrated methods for the construction of three-dimensional models and computational probing of structure-function relations in G protein-coupled receptors. *Methods Neurosci.* **1995**, *25*, 366−428.

(12) Katritch, V.; Cherezov, V.; Stevens, R. C. Diversity and modularity of G protein-coupled receptor structures. *Trends Pharmacol. Sci.* **2012**, *33*, 17−27.

(13) Cherezov, V.; Rosenbaum, D. M.; Hanson, M. A.; Rasmussen, S. G.; Thian, F. S.; Kobilka, T. S.; Choi, H. J.; Kuhn, P.; Weis, W. I.; Kobilka, B. K.; Stevens, R. C. High-resolution crystal structure of an engineered human beta2-adrenergic G protein-coupled receptor. *Science* **2007**, *318*, 1258−1265.

(14) Xiang, J.; Chun, E.; Liu, C.; Jing, L.; Al-Sahouri, Z.; Zhu, L.; Liu, W. Successful strategies to determine high-resolution structures of GPCRs. *Trends Pharmacol. Sci.* **2016**, *37*, 1055−1069.

(15) Robertson, N.; Jazayeri, A.; Errey, J.; Baig, A.; Hurrell, E.; Zhukov, A.; Langmead, C. J.; Weir, M.; Marshall, F. H. The properties of thermostabilised G protein-coupled receptors (StaRs) and their use in drug discovery. *Neuropharmacology* **2011**, *60*, 36−44.

DOI: 10.1021/acs.jmedchem.6b01453
J. Med. Chem. 2018, 61, 1−46

(16) Cvicek, V.; Goddard, W. A.; Abrol, R. Structure-based sequence alignment of the transmembrane domains of all human GPCRs: phylogenetic, structural and functional implications. *PLoS Comput. Biol.* **2016**, *12*, 1−31.
(17) Strosberg, A. D. Structure, function, and regulation of adrenergic receptors. *Protein Sci.* **1993**, *2*, 1198−1209.
(18) Christopher, J. A.; Brown, J.; Dore, A. S.; Errey, J. C.; Koglin, M.; Marshall, F. H.; Myszka, D. G.; Rich, R. L.; Tate, C. G.; Tehan, B.; Warne, T.; Congreve, M. Biophysical fragment screening of the beta1-adrenergic receptor: identification of high affinity arylpiperazine leads using structure-based drug design. *J. Med. Chem.* **2013**, *56*, 3446−3455.
(19) Rasmussen, S. G.; Choi, H. J.; Rosenbaum, D. M.; Kobilka, T. S.; Thian, F. S.; Edwards, P. C.; Burghammer, M.; Ratnala, V. R.; Sanishvili, R.; Fischetti, R. F.; Schertler, G. F.; Weis, W. I.; Kobilka, B. K. Crystal structure of the human beta2 adrenergic G-protein-coupled receptor. *Nature* **2007**, *450*, 383−387.
(20) Hanson, M. A.; Cherezov, V.; Griffith, M. T.; Roth, C. B.; Jaakola, V. P.; Chien, E. Y. T.; Velasquez, J.; Kuhn, P.; Stevens, R. C. A specific cholesterol binding site is established by the 2.8 angstrom structure of the human beta2-adrenergic receptor. *Structure* **2008**, *16*, 897−905.
(21) Wacker, D.; Fenalti, G.; Brown, M. A.; Katritch, V.; Abagyan, R.; Cherezov, V.; Stevens, R. C. Conserved binding mode of human beta2 adrenergic receptor inverse agonists and antagonist revealed by X-ray crystallography. *J. Am. Chem. Soc.* **2010**, *132*, 11443−11445.
(22) Zou, Y.; Weis, W. I.; Kobilka, B. K. N-terminal T4 lysozyme fusion facilitates crystallization of a G protein coupled receptor. *PLoS One* **2012**, *7*, e46039.
(23) Huang, C. Y.; Olieric, V.; Ma, P.; Howe, N.; Vogeley, L.; Liu, X. Y.; Warshamanage, R.; Weinert, T.; Panepucci, E.; Kobilka, B.; Diederichs, K.; Wang, M. T.; Caffrey, M. In meso in situ serial X-ray crystallography of soluble and membrane proteins at cryogenic temperatures. *Acta Crystallogr., Sect. D: Struct. Biol.* **2016**, *72*, 93−112.
(24) Rosenbaum, D. M.; Zhang, C.; Lyons, J. A.; Holl, R.; Aragao, D.; Arlow, D. H.; Rasmussen, S. G.; Choi, H. J.; Devree, B. T.; Sunahara, R. K.; Chae, P. S.; Gellman, S. H.; Dror, R. O.; Shaw, D. E.; Weis, W. I.; Caffrey, M.; Gmeiner, P.; Kobilka, B. K. Structure and function of an irreversible agonist-beta2 adrenoceptor complex. *Nature* **2011**, *469*, 236−240.
(25) Weichert, D.; Kruse, A. C.; Manglik, A.; Hiller, C.; Zhang, C.; Hubner, H.; Kobilka, B. K.; Gmeiner, P. Covalent agonists for studying G protein-coupled receptor activation. *Proc. Natl. Acad. Sci. U. S. A.* **2014**, *111*, 10744−10748.
(26) Rasmussen, S. G. F.; Choi, H. J.; Fung, J. J.; Pardon, E.; Casarosa, P.; Chae, P. S.; DeVree, B. T.; Rosenbaum, D. M.; Thian, F. S.; Kobilka, T. S.; Schnapp, A.; Konetzki, I.; Sunahara, R. K.; Gellman, S. H.; Pautsch, A.; Steyaert, J.; Weis, W. I.; Kobilka, B. K. Structure of a nanobody-stabilized active state of the beta2 adrenoceptor. *Nature* **2011**, *469*, 175−180.
(27) Rasmussen, S. G. F.; DeVree, B. T.; Zou, Y. Z.; Kruse, A. C.; Chung, K. Y.; Kobilka, T. S.; Thian, F. S.; Chae, P. S.; Pardon, E.; Calinski, D.; Mathiesen, J. M.; Shah, S. T. A.; Lyons, J. A.; Caffrey, M.; Gellman, S. H.; Steyaert, J.; Skiniotis, G.; Weis, W. I.; Sunahara, R. K.; Kobilka, B. K. Crystal structure of the beta2 adrenergic receptor-Gs protein complex. *Nature* **2011**, *477*, 549−555.
(28) Ring, A. M.; Manglik, A.; Kruse, A. C.; Enos, M. D.; Weis, W. I.; Garcia, K. C.; Kobilka, B. K. Adrenaline-activated structure of beta2-adrenoceptor stabilized by an engineered nanobody. *Nature* **2013**, *502*, 575−579.
(29) Shukla, A. K.; Westfield, G. H.; Xiao, K.; Reis, R. I.; Huang, L. Y.; Tripathi-Shukla, P.; Qian, J.; Li, S.; Blanc, A.; Oleskie, A. N.; Dosey, A. M.; Su, M.; Liang, C. R.; Gu, L. L.; Shan, J. M.; Chen, X.; Hanna, R.; Choi, M.; Yao, X. J.; Klink, B. U.; Kahsai, A. W.; Sidhu, S. S.; Koide, S.; Penczek, P. A.; Kossiakoff, A. A.; Woods, V. L., Jr.; Kobilka, B. K.; Skiniotis, G.; Lefkowitz, R. J. Visualization of arrestin recruitment by a G-protein-coupled receptor. *Nature* **2014**, *512*, 218−222.
(30) Warne, T.; Serrano-Vega, M. J.; Baker, J. G.; Moukhametzianov, R.; Edwards, P. C.; Henderson, R.; Leslie, A. G.; Tate, C. G.; Schertler, G. F. Structure of a beta1-adrenergic G-protein-coupled receptor. *Nature* **2008**, *454*, 486−491.
(31) Moukhametzianov, R.; Warne, T.; Edwards, P. C.; Serrano-Vega, M. J.; Leslie, A. G.; Tate, C. G.; Schertler, G. F. Two distinct conformations of helix 6 observed in antagonist-bound structures of a beta1-adrenergic receptor. *Proc. Natl. Acad. Sci. U. S. A.* **2011**, *108*, 8228−8232.
(32) Sato, T.; Baker, J.; Warne, T.; Brown, G. A.; Leslie, A. G.; Congreve, M.; Tate, C. G. Pharmacological analysis and structure determination of 7-methylcyanopindolol-bound beta1-adrenergic receptor. *Mol. Pharmacol.* **2015**, *88*, 1024−1034.
(33) Warne, T.; Moukhametzianov, R.; Baker, J. G.; Nehme, R.; Edwards, P. C.; Leslie, A. G. W.; Schertler, G. F. X.; Tate, C. G. The structural basis for agonist and partial agonist action on a beta1-adrenergic receptor. *Nature* **2011**, *469*, 241−244.
(34) Warne, T.; Edwards, P. C.; Leslie, A. G.; Tate, C. G. Crystal structures of a stabilized beta1-adrenoceptor bound to the biased agonists bucindolol and carvedilol. *Structure* **2012**, *20*, 841−849.
(35) Huang, J.; Chen, S.; Zhang, J. J.; Huang, X. Y. Crystal structure of oligomeric beta1-adrenergic G protein-coupled receptors in ligand-free basal state. *Nat. Struct. Mol. Biol.* **2013**, *20*, 419−425.
(36) Huang, J.; Chen, S.; Zhang, J. J.; Huang, X. Y. Ligand occupancy in crystal structure of beta1-adrenergic G protein-coupled receptor. *Nat. Struct. Mol. Biol.* **2015**, *22*, 942.
(37) Leslie, A. G.; Warne, T.; Tate, C. G. Ligand occupancy in crystal structure of beta1-adrenergic G protein-coupled receptor. *Nat. Struct. Mol. Biol.* **2015**, *22*, 941−942.
(38) Beaulieu, J. M.; Gainetdinov, R. R. The physiology, signaling, and pharmacology of dopamine receptors. *Pharmacol. Rev.* **2011**, *63*, 182−217.
(39) Missale, C.; Nash, S. R.; Robinson, S. W.; Jaber, M.; Caron, M. G. Dopamine receptors: from structure to function. *Physiol. Rev.* **1998**, *78*, 189−225.
(40) Holmes, A.; Lachowicz, J. E.; Sibley, D. R. Phenotypic analysis of dopamine receptor knockout mice; recent insights into the functional specificity of dopamine receptor subtypes. *Neuropharmacology* **2004**, *47*, 1117−1134.
(41) Stemp, G.; Ashmeade, T.; Branch, C. L.; Hadley, M. S.; Hunter, A. J.; Johnson, C. N.; Nash, D. J.; Thewlis, K. M.; Vong, A. K.; Austin, N. E.; Jeffrey, P.; Avenell, K. Y.; Boyfield, I.; Hagan, J. J.; Middlemiss, D. N.; Reavill, C.; Riley, G. J.; Routledge, C.; Wood, M. Design and synthesis of trans-N-[4-[2-(6-cyano-1,2,3, 4-tetrahydroisoquinolin-2-yl)ethyl]-cyclohexyl]-4-quinolinecarboxamide (SB-277011): a potent and selective dopamine D3 receptor antagonist with high oral bioavailability and CNS penetration in the rat. *J. Med. Chem.* **2000**, *43*, 1878−1885.
(42) Newman, A. H.; Grundt, P.; Cyriac, G.; Deschamps, J. R.; Taylor, M.; Kumar, R.; Ho, D.; Luedtke, R. R. N-(4-(4-(2,3-dichloro- or 2-methoxyphenyl)piperazin-1-yl)butyl)heterobiarylcarboxamides with functionalized linking chains as high affinity and enantioselective D3 receptor antagonists. *J. Med. Chem.* **2009**, *52*, 2559−2570.
(43) Chien, E. Y.; Liu, W.; Zhao, Q.; Katritch, V.; Han, G. W.; Hanson, M. A.; Shi, L.; Newman, A. H.; Javitch, J. A.; Cherezov, V.; Stevens, R. C. Structure of the human dopamine D3 receptor in complex with a D2/D3 selective antagonist. *Science* **2010**, *330*, 1091−1095.
(44) Heidbreder, C. A.; Newman, A. H. Current perspectives on selective dopamine D3 receptor antagonists as pharmacotherapeutics for addictions and related disorders. *Ann. N. Y. Acad. Sci.* **2010**, *1187*, 4−34.
(45) Boeckler, F.; Gmeiner, P. The structural evolution of dopamine D3 receptor ligands: structure-activity relationships and selected neuropharmacological aspects. *Pharmacol. Ther.* **2006**, *112*, 281−333.
(46) Parsons, M. E.; Ganellin, C. R. Histamine and its receptors. *Br. J. Pharmacol.* **2006**, *147*, S127−S135.
(47) Hill, S. J.; Ganellin, C. R.; Timmerman, H.; Schwartz, J. C.; Shankley, N. P.; Young, J. M.; Schunack, W.; Levi, R.; Haas, H. L. International union of pharmacology. XIII. Classification of histamine receptors. *Pharmacol. Rev.* **1997**, *49*, 253−278.
(48) Shimamura, T.; Shiroishi, M.; Weyand, S.; Tsujimoto, H.; Winter, G.; Katritch, V.; Abagyan, R.; Cherezov, V.; Liu, W.; Han, G. W.; Kobayashi, T.; Stevens, R. C.; Iwata, S. Structure of the human histamine H1 receptor complex with doxepin. *Nature* **2011**, *475*, 65−70.

DOI: 10.1021/acs.jmedchem.6b01453
J. Med. Chem. 2018, 61, 1−46

(49) Cusack, B.; Nelson, A.; Richelson, E. Binding of antidepressants to human brain receptors: focus on newer generation compounds. *Psychopharmacology* **1994**, *114*, 559−565.
(50) Simons, F. E. Advances in H1-antihistamines. *N. Engl. J. Med.* **2004**, *351*, 2203−2217.
(51) Kruse, A. C.; Kobilka, B. K.; Gautam, D.; Sexton, P. M.; Christopoulos, A.; Wess, J. Muscarinic acetylcholine receptors: novel opportunities for drug development. *Nat. Rev. Drug Discovery* **2014**, *13*, 549−560.
(52) Haga, K.; Kruse, A. C.; Asada, H.; Yurugi-Kobayashi, T.; Shiroishi, M.; Zhang, C.; Weis, W. I.; Okada, T.; Kobilka, B. K.; Haga, T.; Kobayashi, T. Structure of the human M2 muscarinic acetylcholine receptor bound to an antagonist. *Nature* **2012**, *482*, 547−551.
(53) Kruse, A. C.; Hu, J. X.; Pan, A. C.; Arlow, D. H.; Rosenbaum, D. M.; Rosemond, E.; Green, H. F.; Liu, T.; Chae, P. S.; Dror, R. O.; Shaw, D. E.; Weis, W. I.; Wess, J.; Kobilka, B. K. Structure and dynamics of the M3 muscarinic acetylcholine receptor. *Nature* **2012**, *482*, 552−556.
(54) Thal, D. M.; Sun, B.; Feng, D.; Nawaratne, V.; Leach, K.; Felder, C. C.; Bures, M. G.; Evans, D. A.; Weis, W. I.; Bachhawat, P.; Kobilka, T. S.; Sexton, P. M.; Kobilka, B. K.; Christopoulos, A. Crystal structures of the M1 and M4 muscarinic acetylcholine receptors. *Nature* **2016**, *531*, 335−340.
(55) Tautermann, C. S.; Kiechle, T.; Seeliger, D.; Diehl, S.; Wex, E.; Banholzer, R.; Gantner, F.; Pieper, M. P.; Casarosa, P. Molecular basis for the long duration of action and kinetic selectivity of tiotropium for the muscarinic M3 receptor. *J. Med. Chem.* **2013**, *56*, 8746−8756.
(56) Gregory, K. J.; Sexton, P. M.; Christopoulos, A. Allosteric modulation of muscarinic acetylcholine receptors. *Curr. Neuropharmacol.* **2007**, *5*, 157−167.
(57) Kruse, A. C.; Ring, A. M.; Manglik, A.; Hu, J.; Hu, K.; Eitel, K.; Hubner, H.; Pardon, E.; Valant, C.; Sexton, P. M.; Christopoulos, A.; Felder, C. C.; Gmeiner, P.; Steyaert, J.; Weis, W. I.; Garcia, K. C.; Wess, J.; Kobilka, B. K. Activation and allosteric modulation of a muscarinic acetylcholine receptor. *Nature* **2013**, *504*, 101−106.
(58) Nichols, D. E.; Nichols, C. D. Serotonin receptors. *Chem. Rev.* **2008**, *108*, 1614−1641.
(59) Wang, C.; Jiang, Y.; Ma, J. M.; Wu, H. X.; Wacker, D.; Katritch, V.; Han, G. W.; Liu, W.; Huang, X. P.; Vardy, E.; McCorvy, J. D.; Gao, X.; Zhou, X. E.; Melcher, K.; Zhang, C. H.; Bai, F.; Yang, H. Y.; Yang, L. L.; Jiang, H. L.; Roth, B. L.; Cherezov, V.; Stevens, R. C.; Xu, H. E. Structural basis for molecular recognition at serotonin receptors. *Science* **2013**, *340*, 610−614.
(60) Wacker, D.; Wang, C.; Katritch, V.; Han, G. W.; Huang, X. P.; Vardy, E.; McCorvy, J. D.; Jiang, Y.; Chu, M. H.; Siu, F. Y.; Liu, W.; Xu, H. E.; Cherezov, V.; Roth, B. L.; Stevens, R. C. Structural features for functional selectivity at serotonin receptors. *Science* **2013**, *340*, 615−619.
(61) Liu, W.; Wacker, D.; Gati, C.; Han, G. W.; James, D.; Wang, D.; Nelson, G.; Weierstall, U.; Katritch, V.; Barty, A.; Zatsepin, N. A.; Li, D.; Messerschmidt, M.; Boutet, S.; Williams, G. J.; Koglin, J. E.; Seibert, M. M.; Wang, C.; Shah, S. T.; Basu, S.; Fromme, R.; Kupitz, C.; Rendek, K. N.; Grotjohann, I.; Fromme, P.; Kirian, R. A.; Beyerlein, K. R.; White, T. A.; Chapman, H. N.; Caffrey, M.; Spence, J. C.; Stevens, R. C.; Cherezov, V. Serial femtosecond crystallography of G protein-coupled receptors. *Science* **2013**, *342*, 1521−1524.
(62) Kaebisch, C.; Schipper, D.; Babczyk, P.; Tobiasch, E. The role of purinergic receptors in stem cell differentiation. *Comput. Struct. Biotechnol. J.* **2015**, *13*, 75−84.
(63) Dunwiddie, T. V.; Masino, S. A. The role and regulation of adenosine in the central nervous system. *Annu. Rev. Neurosci.* **2001**, *24*, 31−55.
(64) Dore, A. S.; Robertson, N.; Errey, J. C.; Ng, I.; Hollenstein, K.; Tehan, B.; Hurrell, E.; Bennett, K.; Congreve, M.; Magnani, F.; Tate, C. G.; Weir, M.; Marshall, F. H. Structure of the adenosine A2A receptor in complex with ZM241385 and the xanthines XAC and caffeine. *Structure* **2011**, *19*, 1283−1293.
(65) Jaakola, V. P.; Griffith, M. T.; Hanson, M. A.; Cherezov, V.; Chien, E. Y.; Lane, J. R.; Ijzerman, A. P.; Stevens, R. C. The 2.6 angstrom crystal structure of a human A2A adenosine receptor bound to an antagonist. *Science* **2008**, *322*, 1211−1217.
(66) Hino, T.; Arakawa, T.; Iwanari, H.; Yurugi-Kobayashi, T.; Ikeda-Suno, C.; Nakada-Nakura, Y.; Kusano-Arai, O.; Weyand, S.; Shimamura, T.; Nomura, N.; Cameron, A. D.; Kobayashi, T.; Hamakubo, T.; Iwata, S.; Murata, T. G-protein-coupled receptor inactivation by an allosteric inverse-agonist antibody. *Nature* **2012**, *482*, 237−240.
(67) Batyuk, A.; Galli, L.; Ishchenko, A.; Han, G. W.; Gati, C.; Popov, P. A.; Lee, M. Y.; Stauch, B.; White, T. A.; Barty, A.; Aquila, A.; Hunter, M. S.; Liang, M.; Boutet, S.; Pu, M.; Liu, Z. J.; Nelson, G.; James, D.; Li, C.; Zhao, Y.; Spence, J. C.; Liu, W.; Fromme, P.; Katritch, V.; Weierstall, U.; Stevens, R. C.; Cherezov, V. Native phasing of x-ray free-electron laser data for a G protein-coupled receptor. *Sci. Adv.* **2016**, *2*, e1600292.
(68) Segala, E.; Guo, D.; Cheng, R. K.; Bortolato, A.; Deflorian, F.; Dore, A. S.; Errey, J. C.; Heitman, L. H.; AP, I. J.; Marshall, F. H.; Cooke, R. M. Controlling the dissociation of ligands from the adenosine A2A receptor through modulation of salt bridge strength. *J. Med. Chem.* **2016**, *59*, 6470−6479.
(69) Congreve, M.; Andrews, S. P.; Dore, A. S.; Hollenstein, K.; Hurrell, E.; Langmead, C. J.; Mason, J. S.; Ng, I. W.; Tehan, B.; Zhukov, A.; Weir, M.; Marshall, F. H. Discovery of 1,2,4-triazine derivatives as adenosine A2A antagonists using structure based drug design. *J. Med. Chem.* **2012**, *55*, 1898−1903.
(70) Lebon, G.; Warne, T.; Edwards, P. C.; Bennett, K.; Langmead, C. J.; Leslie, A. G.; Tate, C. G. Agonist-bound adenosine A2A receptor structures reveal common features of GPCR activation. *Nature* **2011**, *474*, 521−525.
(71) Xu, F.; Wu, H.; Katritch, V.; Han, G. W.; Jacobson, K. A.; Gao, Z. G.; Cherezov, V.; Stevens, R. C. Structure of an agonist-bound human A2A adenosine receptor. *Science* **2011**, *332*, 322−327.
(72) Lebon, G.; Edwards, P. C.; Leslie, A. G.; Tate, C. G. Molecular determinants of CGS21680 binding to the human adenosine A2A receptor. *Mol. Pharmacol.* **2015**, *87*, 907−915.
(73) Huang, W.; Manglik, A.; Venkatakrishnan, A. J.; Laeremans, T.; Feinberg, E. N.; Sanborn, A. L.; Kato, H. E.; Livingston, K. E.; Thorsen, T. S.; Kling, R. C.; Granier, S.; Gmeiner, P.; Husbands, S. M.; Traynor, J. R.; Weis, W. I.; Steyaert, J.; Dror, R. O.; Kobilka, B. K. Structural insights into micro-opioid receptor activation. *Nature* **2015**, *524*, 315−321.
(74) Lebon, G.; Warne, T.; Tate, C. G. Agonist-bound structures of G protein-coupled receptors. *Curr. Opin. Struct. Biol.* **2012**, *22*, 482−490.
(75) Carpenter, B.; Nehme, R.; Warne, T.; Leslie, A. G.; Tate, C. G. Structure of the adenosine A2A receptor bound to an engineered G protein. *Nature* **2016**, *536*, 104−107.
(76) Tate, C. G.; Schertler, G. F. Engineering G protein-coupled receptors to facilitate their structure determination. *Curr. Opin. Struct. Biol.* **2009**, *19*, 386−395.
(77) Liu, W.; Chun, E.; Thompson, A. A.; Chubukov, P.; Xu, F.; Katritch, V.; Han, G. W.; Roth, C. B.; Heitman, L. H.; AP, I. J.; Cherezov, V.; Stevens, R. C. Structural basis for allosteric regulation of GPCRs by sodium ions. *Science* **2012**, *337*, 232−236.
(78) Zhang, C.; Srinivasan, Y.; Arlow, D. H.; Fung, J. J.; Palmer, D.; Zheng, Y.; Green, H. F.; Pandey, A.; Dror, R. O.; Shaw, D. E.; Weis, W. I.; Coughlin, S. R.; Kobilka, B. K. High-resolution crystal structure of human protease-activated receptor 1. *Nature* **2012**, *492*, 387−392.
(79) Fenalti, G.; Giguere, P. M.; Katritch, V.; Huang, X. P.; Thompson, A. A.; Cherezov, V.; Roth, B. L.; Stevens, R. C. Molecular control of delta-opioid receptor signalling. *Nature* **2014**, *506*, 191−196.
(80) Miller-Gallacher, J. L.; Nehme, R.; Warne, T.; Edwards, P. C.; Schertler, G. F.; Leslie, A. G.; Tate, C. G. The 2.1 A resolution structure of cyanopindolol-bound beta1-adrenoceptor identifies an intramembrane Na+ ion that stabilises the ligand-free receptor. *PLoS One* **2014**, *9*, e92727.
(81) Zhang, D.; Gao, Z. G.; Zhang, K.; Kiselev, E.; Crane, S.; Wang, J.; Paoletta, S.; Yi, C.; Ma, L.; Zhang, W.; Han, G. W.; Liu, H.; Cherezov, V.; Katritch, V.; Jiang, H.; Stevens, R. C.; Jacobson, K. A.; Zhao, Q.; Wu, B. Two disparate ligand-binding sites in the human P2Y1 receptor. *Nature* **2015**, *520*, 317−321.
(82) Zhang, K.; Zhang, J.; Gao, Z. G.; Zhang, D.; Zhu, L.; Han, G. W.; Moss, S. M.; Paoletta, S.; Kiselev, E.; Lu, W.; Fenalti, G.; Zhang, W.;

DOI: 10.1021/acs.jmedchem.6b01453
J. Med. Chem. 2018, 61, 1−46

Muller, C. E.; Yang, H.; Jiang, H.; Cherezov, V.; Katritch, V.; Jacobson, K. A.; Stevens, R. C.; Wu, B.; Zhao, Q. Structure of the human P2Y12 receptor in complex with an antithrombotic drug. *Nature* **2014**, *509*, 115−118.
(83) Zhang, J.; Zhang, K.; Gao, Z. G.; Paoletta, S.; Zhang, D.; Han, G. W.; Li, T.; Ma, L.; Zhang, W.; Muller, C. E.; Yang, H.; Jiang, H.; Cherezov, V.; Katritch, V.; Jacobson, K. A.; Stevens, R. C.; Wu, B.; Zhao, Q. Agonist-bound structure of the human P2Y12 receptor. *Nature* **2014**, *509*, 119−122.
(84) Jin, J.; Kunapuli, S. P. Coactivation of two different G protein-coupled receptors is essential for ADP-induced platelet aggregation. *Proc. Natl. Acad. Sci. U. S. A.* **1998**, *95*, 8070−8074.
(85) Jacobson, K. A.; Deflorian, F.; Mishra, S.; Costanzi, S. Pharmacochemistry of the platelet purinergic receptors. *Purinergic Signalling* **2011**, *7*, 305−324.
(86) Schmidt, P.; Ritscher, L.; Dong, E. N.; Hermsdorf, T.; Coster, M.; Wittkopf, D.; Meiler, J.; Schoneberg, T. Identification of determinants required for agonistic and inverse agonistic ligand properties at the ADP receptor P2Y12. *Mol. Pharmacol.* **2013**, *83*, 256−266.
(87) Bach, P.; Antonsson, T.; Bylund, R.; Bjorkman, J. A.; Osterlund, K.; Giordanetto, F.; van Giezen, J. J.; Andersen, S. M.; Zachrisson, H.; Zetterberg, F. Lead optimization of ethyl 6-aminonicotinate acyl sulfonamides as antagonists of the P2Y12 receptor. separation of the antithrombotic effect and bleeding for candidate drug AZD1283. *J. Med. Chem.* **2013**, *56*, 7015−7024.
(88) Kalantzi, K. I.; Tsoumani, M. E.; Goudevenos, I. A.; Tselepis, A. D. Pharmacodynamic properties of antiplatelet agents: current knowledge and future perspectives. *Expert Rev. Clin. Pharmacol.* **2012**, *5*, 319−336.
(89) Wu, B.; Chien, E. Y.; Mol, C. D.; Fenalti, G.; Liu, W.; Katritch, V.; Abagyan, R.; Brooun, A.; Wells, P.; Bi, F. C.; Hamel, D. J.; Kuhn, P.; Handel, T. M.; Cherezov, V.; Stevens, R. C. Structures of the CXCR4 chemokine GPCR with small-molecule and cyclic peptide antagonists. *Science* **2010**, *330*, 1066−1071.
(90) Qin, L.; Kufareva, I.; Holden, L. G.; Wang, C.; Zheng, Y.; Zhao, C.; Fenalti, G.; Wu, H.; Han, G. W.; Cherezov, V.; Abagyan, R.; Stevens, R. C.; Handel, T. M. Structural biology. Crystal structure of the chemokine receptor CXCR4 in complex with a viral chemokine. *Science* **2015**, *347*, 1117−1122.
(91) Thompson, A. A.; Liu, W.; Chun, E.; Katritch, V.; Wu, H.; Vardy, E.; Huang, X. P.; Trapella, C.; Guerrini, R.; Calo, G.; Roth, B. L.; Cherezov, V.; Stevens, R. C. Structure of the nociceptin/orphanin FQ receptor in complex with a peptide mimetic. *Nature* **2012**, *485*, 395−399.
(92) White, J. F.; Noinaj, N.; Shibata, Y.; Love, J.; Kloss, B.; Xu, F.; Gvozdenovic-Jeremic, J.; Shah, P.; Shiloach, J.; Tate, C. G.; Grisshammer, R. Structure of the agonist-bound neurotensin receptor. *Nature* **2012**, *490*, 508−513.
(93) Shihoya, W.; Nishizawa, T.; Okuta, A.; Tani, K.; Dohmae, N.; Fujiyoshi, Y.; Nureki, O.; Doi, T. Activation mechanism of endothelin ETB receptor by endothelin-1. *Nature* **2016**, *537*, 363−368.
(94) Rajagopalan, L.; Rajarathnam, K. Structural basis of chemokine receptor function–a model for binding affinity and ligand selectivity. *Biosci. Rep.* **2006**, *26*, 325−339.
(95) Tan, Q.; Zhu, Y.; Li, J.; Chen, Z.; Han, G. W.; Kufareva, I.; Li, T.; Ma, L.; Fenalti, G.; Zhang, W.; Xie, X.; Yang, H.; Jiang, H.; Cherezov, V.; Liu, H.; Stevens, R. C.; Zhao, Q.; Wu, B. Structure of the CCR5 chemokine receptor-HIV entry inhibitor maraviroc complex. *Science* **2013**, *341*, 1387−1390.
(96) Debnath, B.; Xu, S.; Grande, F.; Garofalo, A.; Neamati, N. Small molecule inhibitors of CXCR4. *Theranostics* **2013**, *3*, 47−75.
(97) Shiraishi, M.; Aramaki, Y.; Seto, M.; Imoto, H.; Nishikawa, Y.; Kanzaki, N.; Okamoto, M.; Sawada, H.; Nishimura, O.; Baba, M.; Fujino, M. Discovery of novel, potent, and selective small-molecule CCR5 antagonists as anti-HIV-1 agents: synthesis and biological evaluation of anilide derivatives with a quaternary ammonium moiety. *J. Med. Chem.* **2000**, *43*, 2049−2063.
(98) Dorr, P.; Westby, M.; Dobbs, S.; Griffin, P.; Irvine, B.; Macartney, M.; Mori, J.; Rickett, G.; Smith-Burchnell, C.; Napier, C.; Webster, R.; Armour, D.; Price, D.; Stammen, B.; Wood, A.; Perros, M. Maraviroc (UK-427,857), a potent, orally bioavailable, and selective small-molecule inhibitor of chemokine receptor CCR5 with broad-spectrum anti-human immunodeficiency virus type 1 activity. *Antimicrob. Agents Chemother.* **2005**, *49*, 4721−4732.
(99) Pasternak, G. W. Opioids and their receptors: are we there yet? *Neuropharmacology* **2014**, *76 Pt B*, 198−203.
(100) Shonberg, J.; Kling, R. C.; Gmeiner, P.; Lober, S. GPCR crystal structures: medicinal chemistry in the pocket. *Bioorg. Med. Chem.* **2015**, *23*, 3880−3906.
(101) Fenalti, G.; Zatsepin, N. A.; Betti, C.; Giguere, P.; Han, G. W.; Ishchenko, A.; Liu, W.; Guillemyn, K.; Zhang, H.; James, D.; Wang, D.; Weierstall, U.; Spence, J. C. H.; Boutet, S.; Messerschmidt, M.; Williams, G. J.; Gati, C.; Yefanov, O. M.; White, T. A.; Oberthuer, D.; Metz, M.; Yoon, C. H.; Barty, A.; Chapman, H. N.; Basu, S.; Coe, J.; Conrad, C. E.; Fromme, R.; Fromme, P.; Tourwe, D.; Schiller, P. W.; Roth, B. L.; Ballet, S.; Katritch, V.; Stevens, R. C.; Cherezov, V. Structural basis for bifunctional peptide recognition at human delta-opioid receptor. *Nat. Struct. Mol. Biol.* **2015**, *22*, 265−268.
(102) O'Connor, C.; White, K. L.; Doncescu, N.; Didenko, T.; Roth, B. L.; Czaplicki, G.; Stevens, R. C.; Wuthrich, K.; Milon, A. NMR structure and dynamics of the agonist dynorphin peptide bound to the human kappa opioid receptor. *Proc. Natl. Acad. Sci. U. S. A.* **2015**, *112*, 11852−11857.
(103) Manglik, A.; Kruse, A. C.; Kobilka, T. S.; Thian, F. S.; Mathiesen, J. M.; Sunahara, R. K.; Pardo, L.; Weis, W. I.; Kobilka, B. K.; Granier, S. Crystal structure of the micro-opioid receptor bound to a morphinan antagonist. *Nature* **2012**, *485*, 321−326.
(104) Granier, S.; Manglik, A.; Kruse, A. C.; Kobilka, T. S.; Thian, F. S.; Weis, W. I.; Kobilka, B. K. Structure of the delta-opioid receptor bound to naltrindole. *Nature* **2012**, *485*, 400−404.
(105) Costa, T.; Lang, J.; Gless, C.; Herz, A. Spontaneous association between opioid receptors and GTP-binding regulatory proteins in native membranes: specific regulation by antagonists and sodium ions. *Mol. Pharmacol.* **1990**, *37*, 383−394.
(106) Wu, H.; Wacker, D.; Mileni, M.; Katritch, V.; Han, G. W.; Vardy, E.; Liu, W.; Thompson, A. A.; Huang, X. P.; Carroll, F. I.; Mascarella, S. W.; Westkaemper, R. B.; Mosier, P. D.; Roth, B. L.; Cherezov, V.; Stevens, R. C. Structure of the human kappa-opioid receptor in complex with JDTic. *Nature* **2012**, *485*, 327−332.
(107) Yan, F.; Bikbulatov, R. V.; Mocanu, V.; Dicheva, N.; Parker, C. E.; Wetsel, W. C.; Mosier, P. D.; Westkaemper, R. B.; Allen, J. A.; Zjawiony, J. K.; Roth, B. L. Structure-based design, synthesis, and biochemical and pharmacological characterization of novel salvinorin A analogues as active state probes of the kappa-opioid receptor. *Biochemistry* **2009**, *48*, 6898−6908.
(108) Miller, R. L.; Thompson, A. A.; Trapella, C.; Guerrini, R.; Malfacini, D.; Patel, N.; Han, G. W.; Cherezov, V.; Calo, G.; Katritch, V.; Stevens, R. C. The importance of ligand-receptor conformational pairs in stabilization: spotlight on the N/OFQ G protein-coupled receptor. *Structure* **2015**, *23*, 2291−2299.
(109) Egloff, P.; Hillenbrand, M.; Klenk, C.; Batyuk, A.; Heine, P.; Balada, S.; Schlinkmann, K. M.; Scott, D. J.; Schutz, M.; Pluckthun, A. Structure of signaling-competent neurotensin receptor 1 obtained by directed evolution in Escherichia coli. *Proc. Natl. Acad. Sci. U. S. A.* **2014**, *111*, E655−E662.
(110) Luca, S.; White, J. F.; Sohal, A. K.; Filippov, D. V.; van Boom, J. H.; Grisshammer, R.; Baldus, M. The conformation of neurotensin bound to its G protein-coupled receptor. *Proc. Natl. Acad. Sci. U. S. A.* **2003**, *100*, 10706−10711.
(111) Krumm, B. E.; White, J. F.; Shah, P.; Grisshammer, R. Structural prerequisites for G-protein activation by the neurotensin receptor. *Nat. Commun.* **2015**, *6*, 7895.
(112) Ahn, H. S.; Arik, L.; Boykow, G.; Burnett, D. A.; Caplen, M. A.; Czarniecki, M.; Domalski, M. S.; Foster, C.; Manna, M.; Stamford, A. W.; Wu, Y. Structure-activity relationships of pyrroloquinazolines as thrombin receptor antagonists. *Bioorg. Med. Chem. Lett.* **1999**, *9*, 2073−2078.
(113) Chackalamannil, S.; Xia, Y.; Greenlee, W. J.; Clasby, M.; Doller, D.; Tsai, H.; Asberom, T.; Czarniecki, M.; Ahn, H. S.; Boykow, G.;

DOI: 10.1021/acs.jmedchem.6b01453
J. Med. Chem. 2018, 61, 1−46

Foster, C.; Agans-Fantuzzi, J.; Bryant, M.; Lau, J.; Chintala, M. Discovery of potent orally active thrombin receptor (protease activated receptor 1) antagonists as novel antithrombotic agents. *J. Med. Chem.* **2005**, *48*, 5884−5887.
(114) FDA approves Zontivity to reduce the risk of heart attacks and stroke. https://www.drugs.com/newdrugs/fda-approves-zontivity-reduce-risk-heart-attacks-stroke-4039.html (accessed Mar 21, 2017).
(115) Zhang, H.; Unal, H.; Gati, C.; Han, G. W.; Liu, W.; Zatsepin, N. A.; James, D.; Wang, D.; Nelson, G.; Weierstall, U.; Sawaya, M. R.; Xu, Q.; Messerschmidt, M.; Williams, G. J.; Boutet, S.; Yefanov, O. M.; White, T. A.; Wang, C.; Ishchenko, A.; Tirupula, K. C.; Desnoyer, R.; Coe, J.; Conrad, C. E.; Fromme, P.; Stevens, R. C.; Katritch, V.; Karnik, S. S.; Cherezov, V. Structure of the angiotensin receptor revealed by serial femtosecond crystallography. *Cell* **2015**, *161*, 833−844.
(116) Michelson, D.; Snyder, E.; Paradis, E.; Chengan-Liu, M.; Snavely, D. B.; Hutzelmann, J.; Walsh, J. K.; Krystal, A. D.; Benca, R. M.; Cohn, M.; Lines, C.; Roth, T.; Herring, W. J. Safety and efficacy of suvorexant during 1-year treatment of insomnia with subsequent abrupt treatment discontinuation: a phase 3 randomised, double-blind, placebo-controlled trial. *Lancet Neurol.* **2014**, *13*, 461−471.
(117) Yin, J.; Mobarec, J. C.; Kolb, P.; Rosenbaum, D. M. Crystal structure of the human OX2 orexin receptor bound to the insomnia drug suvorexant. *Nature* **2015**, *519*, 247−250.
(118) Yin, J.; Babaoglu, K.; Brautigam, C. A.; Clark, L.; Shao, Z.; Scheuermann, T. H.; Harrell, C. M.; Gotter, A. L.; Roecker, A. J.; Winrow, C. J.; Renger, J. J.; Coleman, P. J.; Rosenbaum, D. M. Structure and ligand-binding mechanism of the human OX1 and OX2 orexin receptors. *Nat. Struct. Mol. Biol.* **2016**, *23*, 293−299.
(119) Kedzierski, R. M.; Yanagisawa, M. Endothelin system: the double-edged sword in health and disease. *Annu. Rev. Pharmacol. Toxicol.* **2001**, *41*, 851−876.
(120) Kohan, D. E.; Rossi, N. F.; Inscho, E. W.; Pollock, D. M. Regulation of blood pressure and salt homeostasis by endothelin. *Physiol. Rev.* **2011**, *91*, 1−77.
(121) Davenport, A. P. International union of pharmacology. XXIX. Update on endothelin receptor nomenclature. *Pharmacol. Rev.* **2002**, *54*, 219−226.
(122) Maguire, J. J.; Davenport, A. P. Endothelin@25 - new agonists, antagonists, inhibitors and emerging research frontiers: IUPHAR review 12. *Br. J. Pharmacol.* **2014**, *171*, 5555−5572.
(123) Briyal, S.; Nguyen, C.; Leonard, M.; Gulati, A. Stimulation of endothelin B receptors by IRL-1620 decreases the progression of Alzheimer's disease. *Neuroscience* **2015**, *301*, 1−11.
(124) Janes, R. W.; Peapus, D. H.; Wallace, B. A. The crystal structure of human endothelin. *Nat. Struct. Mol. Biol.* **1994**, *1*, 311−319.
(125) Takashima, H.; Mimura, N.; Ohkubo, T.; Yoshida, T.; Tamaoki, H.; Kobayashi, Y. Distributed computing and NMR constraint-based high-resolution structure determination: applied for bioactive Peptide endothelin-1 to determine C-terminal folding. *J. Am. Chem. Soc.* **2004**, *126*, 4504−4505.
(126) Andersen, N. H.; Chen, C. P.; Marschner, T. M.; Krystek, S. R., Jr.; Bassolino, D. A. Conformational isomerism of endothelin in acidic aqueous media: a quantitative NOESY analysis. *Biochemistry* **1992**, *31*, 1280−1295.
(127) Houthuijzen, J. M.; Daenen, L. G.; Roodhart, J. M.; Oosterom, I.; van Jaarsveld, M. T.; Govaert, K. M.; Smith, M. E.; Sadatmand, S. J.; Rosing, H.; Kruse, F.; Helms, B. J.; van Rooijen, N.; Beijnen, J. H.; Haribabu, B.; van de Lest, C. H.; Voest, E. E. Lysophospholipids secreted by splenic macrophages induce chemotherapy resistance via interference with the DNA damage response. *Nat. Commun.* **2014**, *5*, 1−10.
(128) van Jaarsveld, M. T.; Houthuijzen, J. M.; Voest, E. E. Molecular mechanisms of target recognition by lipid GPCRs: relevance for cancer. *Oncogene* **2016**, *35*, 4021−4035.
(129) Hanson, M. A.; Roth, C. B.; Jo, E.; Griffith, M. T.; Scott, F. L.; Reinhart, G.; Desale, H.; Clemons, B.; Cahalan, S. M.; Schuerer, S. C.; Sanna, M. G.; Han, G. W.; Kuhn, P.; Rosen, H.; Stevens, R. C. Crystal structure of a lipid G protein-coupled receptor. *Science* **2012**, *335*, 851−855.
(130) Chrencik, J. E.; Roth, C. B.; Terakado, M.; Kurata, H.; Omi, R.; Kihara, Y.; Warshaviak, D.; Nakade, S.; Asmar-Rovira, G.; Mileni, M.; Mizuno, H.; Griffith, M. T.; Rodgers, C.; Han, G. W.; Velasquez, J.; Chun, J.; Stevens, R. C.; Hanson, M. A. Crystal structure of antagonist bound human lysophosphatidic acid receptor 1. *Cell* **2015**, *161*, 1633−1643.
(131) Srivastava, A.; Yano, J.; Hirozane, Y.; Kefala, G.; Gruswitz, F.; Snell, G.; Lane, W.; Ivetac, A.; Aertgeerts, K.; Nguyen, J.; Jennings, A.; Okada, K. High-resolution structure of the human GPR40 receptor bound to allosteric agonist TAK-875. *Nature* **2014**, *513*, 124−127.
(132) Rivera, R.; Chun, J. Biological effects of lysophospholipids. *Rev. Physiol., Biochem. Pharmacol.* **2006**, *160*, 25−46.
(133) Chun, J.; Goetzl, E. J.; Hla, T.; Igarashi, Y.; Lynch, K. R.; Moolenaar, W.; Pyne, S.; Tigyi, G. International union of pharmacology. XXXIV. Lysophospholipid receptor nomenclature. *Pharmacol. Rev.* **2002**, *54*, 265−269.
(134) Brinkmann, V.; Billich, A.; Baumruker, T.; Heining, P.; Schmouder, R.; Francis, G.; Aradhye, S.; Burtin, P. Fingolimod (FTY720): discovery and development of an oral drug to treat multiple sclerosis. *Nat. Rev. Drug Discovery* **2010**, *9*, 883−897.
(135) Negoro, N.; Sasaki, S.; Mikami, S.; Ito, M.; Suzuki, M.; Tsujihata, Y.; Ito, R.; Harada, A.; Takeuchi, K.; Suzuki, N.; Miyazaki, J.; Santou, T.; Odani, T.; Kanzaki, N.; Funami, M.; Tanaka, T.; Kogame, A.; Matsunaga, S.; Yasuma, T.; Momose, Y. Discovery of TAK-875: a potent, selective, and orally bioavailable GPR40 agonist. *ACS Med. Chem. Lett.* **2010**, *1*, 290−294.
(136) Rinaldi-Carmona, M.; Barth, F.; Heaulme, M.; Shire, D.; Calandra, B.; Congy, C.; Martinez, S.; Maruani, J.; Neliat, G.; Caput, D.; Ferrara, P.; Soubrié, P.; Brelière, J. C.; Le Fur, G. SR141716A, a potent and selective antagonist of the brain cannabinoid receptor. *FEBS Lett.* **1994**, *350*, 240−244.
(137) Janero, D. R.; Makriyannis, A. Cannabinoid receptor antagonists: pharmacological opportunities, clinical experience, and translational prognosis. *Expert Opin. Emerging Drugs* **2009**, *14*, 43−65.
(138) Hua, T.; Vemuri, K.; Pu, M.; Qu, L.; Han, G. W.; Wu, Y.; Zhao, S.; Shui, W.; Li, S.; Korde, A.; Laprairie, R. B.; Stahl, E. L.; Ho, J. H.; Zvonok, N.; Zhou, H.; Kufareva, I.; Wu, B.; Zhao, Q.; Hanson, M. A.; Bohn, L. M.; Makriyannis, A.; Stevens, R. C.; Liu, Z. J. Crystal structure of the human cannabinoid receptor CB1. *Cell* **2016**, *167*, 750−762.
(139) Nygaard, R.; Frimurer, T. M.; Holst, B.; Rosenkilde, M. M.; Schwartz, T. W. Ligand binding and micro-switches in 7TM receptor structures. *Trends Pharmacol. Sci.* **2009**, *30*, 249−259.
(140) Kobilka, B. K. G protein coupled receptor structure and activation. *Biochim. Biophys. Acta, Biomembr.* **2007**, *1768*, 794−807.
(141) Choe, H. W.; Park, J. H.; Kim, Y. J.; Ernst, O. P. Transmembrane signaling by GPCRs: insight from rhodopsin and opsin structures. *Neuropharmacology* **2011**, *60*, 52−57.
(142) Katritch, V.; Cherezov, V.; Stevens, R. C. Structure-function of the G protein-coupled receptor superfamily. *Annu. Rev. Pharmacol. Toxicol.* **2013**, *53*, 531−556.
(143) Venkatakrishnan, A. J.; Deupi, X.; Lebon, G.; Heydenreich, F. M.; Flock, T.; Miljus, T.; Balaji, S.; Bouvier, M.; Veprintsev, D. B.; Tate, C. G.; Schertler, G. F.; Babu, M. M. Diverse activation pathways in class A GPCRs converge near the G-protein-coupling region. *Nature* **2016**, *536*, 484−487.
(144) Scheerer, P.; Park, J. H.; Hildebrand, P. W.; Kim, Y. J.; Krauss, N.; Choe, H. W.; Hofmann, K. P.; Ernst, O. P. Crystal structure of opsin in its G-protein-interacting conformation. *Nature* **2008**, *455*, 497−502.
(145) Kang, Y.; Zhou, X. E.; Gao, X.; He, Y.; Liu, W.; Ishchenko, A.; Barty, A.; White, T. A.; Yefanov, O.; Han, G. W.; Xu, Q.; de Waal, P. W.; Ke, J.; Tan, M. H.; Zhang, C.; Moeller, A.; West, G. M.; Pascal, B. D.; Van Eps, N.; Caro, L. N.; Vishnivetskiy, S. A.; Lee, R. J.; Suino-Powell, K. M.; Gu, X.; Pal, K.; Ma, J.; Zhi, X.; Boutet, S.; Williams, G. J.; Messerschmidt, M.; Gati, C.; Zatsepin, N. A.; Wang, D.; James, D.; Basu, S.; Roy-Chowdhury, S.; Conrad, C. E.; Coe, J.; Liu, H.; Lisova, S.; Kupitz, C.; Grotjohann, I.; Fromme, R.; Jiang, Y.; Tan, M.; Yang, H.; Li, J.; Wang, M.; Zheng, Z.; Li, D.; Howe, N.; Zhao, Y.; Standfuss, J.; Diederichs, K.; Dong, Y.; Potter, C. S.; Carragher, B.; Caffrey, M.; Jiang, H.; Chapman, H. N.; Spence, J. C.; Fromme, P.; Weierstall, U.; Ernst, O.

DOI: 10.1021/acs.jmedchem.6b01453
J. Med. Chem. 2018, 61, 1−46

P.; Katritch, V.; Gurevich, V. V.; Griffin, P. R.; Hubbell, W. L.; Stevens, R. C.; Cherezov, V.; Melcher, K.; Xu, H. E. Crystal structure of rhodopsin bound to arrestin by femtosecond X-ray laser. *Nature* **2015**, *523*, 561−567.
(146) Katritch, V.; Fenalti, G.; Abola, E. E.; Roth, B. L.; Cherezov, V.; Stevens, R. C. Allosteric sodium in class A GPCR signaling. *Trends Biochem. Sci.* **2014**, *39*, 233−244.
(147) Pert, C. B.; Pasternak, G.; Snyder, S. H. Opiate agonists and antagonists discriminated by receptor binding in brain. *Science* **1973**, *182*, 1359−1361.
(148) Gutierrez-de-Teran, H.; Massink, A.; Rodriguez, D.; Liu, W.; Han, G. W.; Joseph, J. S.; Katritch, I.; Heitman, L. H.; Xia, L.; Ijzerman, A. P.; Cherezov, V.; Katritch, V.; Stevens, R. C. The role of a sodium ion binding site in the allosteric modulation of the A2A adenosine G protein-coupled receptor. *Structure* **2013**, *21*, 2175−2185.
(149) Ranganathan, A.; Dror, R. O.; Carlsson, J. Insights into the role of Asp79(2.50) in beta2 adrenergic receptor activation from molecular dynamics simulations. *Biochemistry* **2014**, *53*, 7283−7296.
(150) Selent, J.; Sanz, F.; Pastor, M.; De Fabritiis, G. Induced effects of sodium ions on dopaminergic G-protein coupled receptors. *PLoS Comput. Biol.* **2010**, *6*, 1−6.
(151) Yuan, S.; Vogel, H.; Filipek, S. The role of water and sodium ions in the activation of the mu-opioid receptor. *Angew. Chem., Int. Ed.* **2013**, *52*, 10112−10115.
(152) Shang, Y.; LeRouzic, V.; Schneider, S.; Bisignano, P.; Pasternak, G. W.; Filizola, M. Mechanistic insights into the allosteric modulation of opioid receptors by sodium ions. *Biochemistry* **2014**, *53*, 5140−5149.
(153) Miao, Y.; Caliman, A. D.; McCammon, J. A. Allosteric effects of sodium ion binding on activation of the m3 muscarinic G-protein-coupled receptor. *Biophys. J.* **2015**, *108*, 1796−1806.
(154) Devi, L. A. Heterodimerization of G-protein-coupled receptors: pharmacology, signaling and trafficking. *Trends Pharmacol. Sci.* **2001**, *22*, 532−537.
(155) Salom, D.; Lodowski, D. T.; Stenkamp, R. E.; Le Trong, I.; Golczak, M.; Jastrzebska, B.; Harris, T.; Ballesteros, J. A.; Palczewski, K. Crystal structure of a photoactivated deprotonated intermediate of rhodopsin. *Proc. Natl. Acad. Sci. U. S. A.* **2006**, *103*, 16123−16128.
(156) Liang, Y.; Fotiadis, D.; Filipek, S.; Saperstein, D. A.; Palczewski, K.; Engel, A. Organization of the G protein-coupled receptors rhodopsin and opsin in native membranes. *J. Biol. Chem.* **2003**, *278*, 21655−21662.
(157) Ferre, S.; Casado, V.; Devi, L. A.; Filizola, M.; Jockers, R.; Lohse, M. J.; Milligan, G.; Pin, J. P.; Guitart, X. G protein-coupled receptor oligomerization revisited: functional and pharmacological perspectives. *Pharmacol. Rev.* **2014**, *66*, 413−434.
(158) Venkatakrishnan, A. J.; Deupi, X.; Lebon, G.; Tate, C. G.; Schertler, G. F.; Babu, M. M. Molecular signatures of G-protein-coupled receptors. *Nature* **2013**, *494*, 185−194.
(159) Rahmeh, R.; Damian, M.; Cottet, M.; Orcel, H.; Mendre, C.; Durroux, T.; Sharma, K. S.; Durand, G.; Pucci, B.; Trinquet, E.; Zwier, J. M.; Deupi, X.; Bron, P.; Baneres, J. L.; Mouillac, B.; Granier, S. Structural insights into biased G protein-coupled receptor signaling revealed by fluorescence spectroscopy. *Proc. Natl. Acad. Sci. U. S. A.* **2012**, *109*, 6733−6738.
(160) Corbisier, J.; Gales, C.; Huszagh, A.; Parmentier, M.; Springael, J. Y. Biased signaling at chemokine receptors. *J. Biol. Chem.* **2015**, *290*, 9542−9554.
(161) Lefkowitz, R. J. Historical review: a brief history and personal retrospective of seven-transmembrane receptors. *Trends Pharmacol. Sci.* **2004**, *25*, 413−422.
(162) Wisler, J. W.; Xiao, K.; Thomsen, A. R.; Lefkowitz, R. J. Recent developments in biased agonism. *Curr. Opin. Cell Biol.* **2014**, *27*, 18−24.
(163) Violin, J. D.; Crombie, A. L.; Soergel, D. G.; Lark, M. W. Biased ligands at G-protein-coupled receptors: promise and progress. *Trends Pharmacol. Sci.* **2014**, *35*, 308−316.
(164) Kenakin, T.; Christopoulos, A. Signalling bias in new drug discovery: detection, quantification and therapeutic impact. *Nat. Rev. Drug Discovery* **2013**, *12*, 205−216.
(165) Quoyer, J.; Janz, J. M.; Luo, J.; Ren, Y.; Armando, S.; Lukashova, V.; Benovic, J. L.; Carlson, K. E.; Hunt, S. W., 3rd; Bouvier, M. Pepducin targeting the C-X-C chemokine receptor type 4 acts as a biased agonist favoring activation of the inhibitory G protein. *Proc. Natl. Acad. Sci. U. S. A.* **2013**, *110*, E5088−E5097.
(166) Staus, D. P.; Wingler, L. M.; Strachan, R. T.; Rasmussen, S. G.; Pardon, E.; Ahn, S.; Steyaert, J.; Kobilka, B. K.; Lefkowitz, R. J. Regulation of beta2-adrenergic receptor function by conformationally selective single-domain intrabodies. *Mol. Pharmacol.* **2014**, *85*, 472−481.
(167) Shukla, A. K. Biasing GPCR signaling from inside. *Sci. Signaling* **2014**, *7*, pe3.
(168) Shukla, A. K.; Singh, G.; Ghosh, E. Emerging structural insights into biased GPCR signaling. *Trends Biochem. Sci.* **2014**, *39*, 594−602.
(169) Shukla, A. K.; Xiao, K.; Lefkowitz, R. J. Emerging paradigms of beta-arrestin-dependent seven transmembrane receptor signaling. *Trends Biochem. Sci.* **2011**, *36*, 457−469.
(170) Correll, C. C.; McKittrick, B. A. Biased ligand modulation of seven transmembrane receptors (7TMRs): functional implications for drug discovery. *J. Med. Chem.* **2014**, *57*, 6887−6896.
(171) Khoury, E.; Clement, S.; Laporte, S. A. Allosteric and biased G protein-coupled receptor signaling regulation: potentials for new therapeutics. *Front. Endocrinol.* **2014**, *5*, 68.
(172) Staus, D. P.; Strachan, R. T.; Manglik, A.; Pani, B.; Kahsai, A. W.; Kim, T. H.; Wingler, L. M.; Ahn, S.; Chatterjee, A.; Masoudi, A.; Kruse, A. C.; Pardon, E.; Steyaert, J.; Weis, W. I.; Prosser, R. S.; Kobilka, B. K.; Costa, T.; Lefkowitz, R. J. Allosteric nanobodies reveal the dynamic range and diverse mechanisms of G-protein-coupled receptor activation. *Nature* **2016**, *535*, 448−452.
(173) Andrews, S. P.; Brown, G. A.; Christopher, J. A. Structure-based and fragment-based GPCR drug discovery. *ChemMedChem* **2014**, *9*, 256−275.
(174) Cavasotto, C. N.; Palomba, D. Expanding the horizons of G protein-coupled receptor structure-based ligand discovery and optimization using homology models. *Chem. Commun.* **2015**, *51*, 13576−13594.
(175) Vyas, V. K.; Ukawala, R. D.; Ghate, M.; Chintha, C. Homology modeling a fast tool for drug discovery: current perspectives. *Indian J. Pharm. Sci.* **2012**, *74*, 1−17.
(176) Palczewski, K.; Kumasaka, T.; Hori, T.; Behnke, C. A.; Motoshima, H.; Fox, B. A.; Le Trong, I.; Teller, D. C.; Okada, T.; Stenkamp, R. E.; Yamamoto, M.; Miyano, M. Crystal structure of rhodopsin: a G protein-coupled receptor. *Science* **2000**, *289*, 739−745.
(177) Ngo, T.; Kufareva, I.; Coleman, J. L. J.; Graham, R. M.; Abagyan, R.; Smith, N. J. Identifying ligands at orphan GPCRs: current status using structure-based approaches. *Br. J. Pharmacol.* **2016**, *173*, 2934−2951.
(178) Ferreira, L. G.; dos Santos, R. N.; Oliva, G.; Andricopulo, A. D. Molecular docking and structure-based drug design strategies. *Molecules* **2015**, *20*, 13384−13421.
(179) Huang, S. Y.; Zou, X. Advances and challenges in protein-ligand docking. *Int. J. Mol. Sci.* **2010**, *11*, 3016−3034.
(180) Kumari, P.; Ghosh, E.; Shukla, A. K. Emerging approaches to GPCR ligand screening for drug discovery. *Trends Mol. Med.* **2015**, *21*, 687−701.
(181) Sabio, M.; Jones, K.; Topiol, S. Use of the X-ray structure of the beta2-adrenergic receptor for drug discovery. Part 2: Identification of active compounds. *Bioorg. Med. Chem. Lett.* **2008**, *18*, 5391−5395.
(182) Kolb, P.; Rosenbaum, D. M.; Irwin, J. J.; Fung, J. J.; Kobilka, B. K.; Shoichet, B. K. Structure-based discovery of beta2-adrenergic receptor ligands. *Proc. Natl. Acad. Sci. U. S. A.* **2009**, *106*, 6843−6848.
(183) Katritch, V.; Jaakola, V. P.; Lane, J. R.; Lin, J.; Ijzerman, A. P.; Yeager, M.; Kufareva, I.; Stevens, R. C.; Abagyan, R. Structure-based discovery of novel chemotypes for adenosine A2A receptor antagonists. *J. Med. Chem.* **2010**, *53*, 1799−809.
(184) Carlsson, J.; Yoo, L.; Gao, Z. G.; Irwin, J. J.; Shoichet, B. K.; Jacobson, K. A. Structure-based discovery of A2A adenosine receptor ligands. *J. Med. Chem.* **2010**, *53*, 3748−3755.
(185) Kim, J.; Wess, J.; van Rhee, A. M.; Schoneberg, T.; Jacobson, K. A. Site-directed mutagenesis identifies residues involved in ligand

DOI: 10.1021/acs.jmedchem.6b01453
J. Med. Chem. 2018, 61, 1−46

recognition in the human A2a adenosine receptor. *J. Biol. Chem.* **1995**, *270*, 13987−13997.
(186) Langmead, C. J.; Andrews, S. P.; Congreve, M.; Errey, J. C.; Hurrell, E.; Marshall, F. H.; Mason, J. S.; Richardson, C. M.; Robertson, N.; Zhukov, A.; Weir, M. Identification of novel adenosine A2A receptor antagonists by virtual screening. *J. Med. Chem.* **2012**, *55*, 1904−1909.
(187) Jazayeri, A.; Andrews, S. P.; Marshall, F. H. Structurally enabled discovery of adenosine A2A receptor antagonists. *Chem. Rev.* **2017**, *117*, 21−37.
(188) Agelis, G.; Resvani, A.; Koukoulitsa, C.; Tumova, T.; Slaninova, J.; Kalavrizioti, D.; Spyridaki, K.; Afantitis, A.; Melagraki, G.; Siafaka, A.; Gkini, E.; Megariotis, G.; Grdadolnik, S. G.; Papadopoulos, M. G.; Vlahakos, D.; Maragoudakis, M.; Liapakis, G.; Mavromoustakos, T.; Matsoukas, J. Rational design, efficient syntheses and biological evaluation of N,N'-symmetrically bis-substituted butylimidazole analogs as a new class of potent Angiotensin II receptor blockers. *Eur. J. Med. Chem.* **2013**, *62*, 352−370.
(189) Negri, A.; Rives, M. L.; Caspers, M. J.; Prisinzano, T. E.; Javitch, J. A.; Filizola, M. Discovery of a novel selective kappa-opioid receptor agonist using crystal structure-based virtual screening. *J. Chem. Inf. Model.* **2013**, *53*, 521−526.
(190) Katritch, V.; Kufareva, I.; Abagyan, R. Structure based prediction of subtype-selectivity for adenosine receptor antagonists. *Neuropharmacology* **2011**, *60*, 108−115.
(191) Kolb, P.; Phan, K.; Gao, Z. G.; Marko, A. C.; Sali, A.; Jacobson, K. A. Limits of ligand selectivity from docking to models: in silico screening for A1 adenosine receptor antagonists. *PLoS One* **2012**, *7*, e49910.
(192) Kruse, A. C.; Weiss, D. R.; Rossi, M.; Hu, J.; Hu, K.; Eitel, K.; Gmeiner, P.; Wess, J.; Kobilka, B. K.; Shoichet, B. K. Muscarinic receptors as model targets and antitargets for structure-based ligand discovery. *Mol. Pharmacol.* **2013**, *84*, 528−540.
(193) Rodriguez, D.; Brea, J.; Loza, M. I.; Carlsson, J. Structure-based discovery of selective serotonin 5-HT1B receptor ligands. *Structure* **2014**, *22*, 1140−1151.
(194) Schmidt, D.; Bernat, V.; Brox, R.; Tschammer, N.; Kolb, P. Identifying modulators of CXC receptors 3 and 4 with tailored selectivity using multi-target docking. *ACS Chem. Biol.* **2015**, *10*, 715−724.
(195) Weiss, D. R.; Ahn, S.; Sassano, M. F.; Kleist, A.; Zhu, X.; Strachan, R.; Roth, B. L.; Lefkowitz, R. J.; Shoichet, B. K. Conformation guides molecular efficacy in docking screens of activated beta-2 adrenergic G protein coupled receptor. *ACS Chem. Biol.* **2013**, *8*, 1018−1026.
(196) Brogi, S.; Tafi, A.; Desaubry, L.; Nebigil, C. G. Discovery of GPCR ligands for probing signal transduction pathways. *Front. Pharmacol.* **2014**, *5*, 255.
(197) Mohr, K.; Schmitz, J.; Schrage, R.; Trankle, C.; Holzgrabe, U. Molecular alliance-from orthosteric and allosteric ligands to dualsteric/bitopic agonists at G protein coupled receptors. *Angew. Chem., Int. Ed.* **2013**, *52*, 508−516.
(198) Allegretti, M.; Cesta, M. C.; Locati, M. Allosteric modulation of chemoattractant receptors. *Front. Immunol.* **2016**, *7*, 170.
(199) Zarbock, A.; Allegretti, M.; Ley, K. Therapeutic inhibition of CXCR2 by Reparixin attenuates acute lung injury in mice. *Br. J. Pharmacol.* **2008**, *155*, 357−364.
(200) Lane, J. R.; Chubukov, P.; Liu, W.; Canals, M.; Cherezov, V.; Abagyan, R.; Stevens, R. C.; Katritch, V. Structure-based ligand discovery targeting orthosteric and allosteric pockets of dopamine receptors. *Mol. Pharmacol.* **2013**, *84*, 794−807.
(201) Fronik, P.; Gaiser, B. I.; Sejer Pedersen, D. Bitopic ligands and metastable binding sites: opportunities for G protein-coupled receptor (GPCR) medicinal chemistry. *J. Med. Chem.* **2017**, *60*, 4126.
(202) Bock, A.; Merten, N.; Schrage, R.; Dallanoce, C.; Batz, J.; Klockner, J.; Schmitz, J.; Matera, C.; Simon, K.; Kebig, A.; Peters, L.; Muller, A.; Schrobang-Ley, J.; Trankle, C.; Hoffmann, C.; De Amici, M.; Holzgrabe, U.; Kostenis, E.; Mohr, K. The allosteric vestibule of a seven transmembrane helical receptor controls G-protein coupling. *Nat. Commun.* **2012**, *3*, 1044.
(203) Silvano, E.; Millan, M. J.; Mannoury la Cour, C.; Han, Y.; Duan, L.; Griffin, S. A.; Luedtke, R. R.; Aloisi, G.; Rossi, M.; Zazzeroni, F.; Javitch, J. A.; Maggio, R. The tetrahydroisoquinoline derivative SB269,652 is an allosteric antagonist at dopamine D3 and D2 receptors. *Mol. Pharmacol.* **2010**, *78*, 925−934.
(204) Lane, J. R.; Donthamsetti, P.; Shonberg, J.; Draper-Joyce, C. J.; Dentry, S.; Michino, M.; Shi, L.; Lopez, L.; Scammells, P. J.; Capuano, B.; Sexton, P. M.; Javitch, J. A.; Christopoulos, A. A new mechanism of allostery in a G protein-coupled receptor dimer. *Nat. Chem. Biol.* **2014**, *10*, 745−752.
(205) Garnock-Jones, K. P. Brexpiprazole: a review in schizophrenia. *CNS Drugs* **2016**, *30*, 335−342.
(206) Sengupta, D.; Joshi, M.; Athale, C. A.; Chattopadhyay, A. What can simulations tell us about GPCRs: integrating the scales. *Methods Cell Biol.* **2016**, *132*, 429−452.
(207) Rodriguez, D.; Gutierrez-de-Teran, H. Computational approaches for ligand discovery and design in class-A G protein-coupled receptors. *Curr. Pharm. Des.* **2013**, *19*, 2216−2236.
(208) Kaczor, A. A.; Rutkowska, E.; Bartuzi, D.; Targowska-Duda, K. M.; Matosiuk, D.; Selent, J. Computational methods for studying G protein-coupled receptors (GPCRs). *Methods Cell Biol.* **2016**, *132*, 359−399.
(209) Ciancetta, A.; Sabbadin, D.; Federico, S.; Spalluto, G.; Moro, S. Advances in computational techniques to study GPCR-ligand recognition. *Trends Pharmacol. Sci.* **2015**, *36*, 878−890.
(210) Motlagh, H. N.; Wrabl, J. O.; Li, J.; Hilser, V. J. The ensemble nature of allostery. *Nature* **2014**, *508*, 331−339.
(211) Dror, R. O.; Pan, A. C.; Arlow, D. H.; Borhani, D. W.; Maragakis, P.; Shan, Y.; Xu, H.; Shaw, D. E. Pathway and mechanism of drug binding to G-protein-coupled receptors. *Proc. Natl. Acad. Sci. U. S. A.* **2011**, *108*, 13118−13123.

DOI: 10.1021/acs.jmedchem.6b01453
J. Med. Chem. 2018, 61, 1−46